Silver Clusters and Nanoalloys

Dissertation

zur Erlangung des Grades
des Doktors der Naturwissenschaften
der Naturwissenschaftlich-Technischen Fakultät III
Chemie, Pharmazie, Bio- und Werkstoffwissenschaften
der Universität des Saarlandes

von

M.Sc.-Phys Mohammad Molayem

Saarbrücken

November, 2011

Tag des Kolloquiums:
Dekan:
Berichterstatter:

Vorsitz:
Akad. Mitarbeiter:

Abstract

The focus of this thesis is on determination of putative global minimum structures of silver clusters, and copper-silver and nickel-silver bimetallic clusters by using a combination of embedded atom method and basin-hopping algorithm. Global minima of silver clusters with N=2 to 100 atoms are based on icosahedra, polyicosahedra, *fcc* truncated octahedra, and decahedra. The set of magic sizes and structural motifs of Ag clusters suggest an icosahedral growth pattern based on a combination of MIC/Mackay and TIC/Polyicosahedral growth. For Cu_mAg_n and Ni_mAg_n clusters, with N = m+n from 2 to 60, global minima are mainly icosahedron and polyicosahedron structures, with exception for some clusters of size N = 38 which are truncated octahedrons. Different theoretical measures such as bond order parameter and radial distances suggest that in both Cu–Ag and Ni–Ag nanoalloys core–shell structures with Ag atoms segregated to the surfaces are preferred. The two types of nanoalloys exhibit different energetical properties while they are very similar in structural properties.

Cluster, Nanoalloy, Copper, Nickel, Silver, Global Optimization, Structure, Properties

Zusammenfassung

Der Schwerpunkt dieser Arbeit liegt in der Bestimmung der Strukturen von Ag-Clustern und bimetallischen Kupfer-Silber und Nickel-Silber Clustern mit globalen Minima. Dabei wird eine Kombination von Embedded-Atom Methode und Basin-Hopping Algorithmus angewandt. Die globalen Minima von Silber-Clustern mit N = 2 bis 100 Atomen stellen Ikosaeder, Polyicosahedra, *fcc*-Oktaeder, und Dekaedern dar. Die magischen Zahlen und Strukturmotive der Ag-Clustern deuten auf ein ikosaedrisches Wachstumsmuster mit einer Kombination von MIC/Mackay- und TIC/Polyikosaeder-Wachstum. Für Cu_m Ag_n und Ni_m Ag_n-Cluster mit N = m + n von 2 bis 60 werden als globale Minima hauptsächlich Ikosaeder und Polyikosaeder. Die einsigen Ausnahme sind einige Cluster mit der Größe N = 38, die *fcc*-Oktaeder sind. Theoretische Größen wie Bindungsordnungparameter und radiale Abstände lassen vermuten, dass in beiden Cu–Ag und Ni–Ag Nanolegierungen Kern-Schale Strukturen mit Ag-Atome vorwiegend an der Oberflächen bevorzugt werden. Die beiden Typen von Nanolegierungen haben unterschiedliche energetischen Eigenschaften während sie sich sehr ähnlich in ihre Struktur sind.

Cluster, Nanoalloy, Kupfer, Nickel, Silber, globaler Optimierung, Struktur, Eigenschaften

Abstract

In the last two decades, a new field has developed explosively which is now known as nanoscience. The field addresses the phenomena that occur in systems of a few nanometers in size. The objects of this size are bridging blocks between single atoms or molecules and bulk materials. The huge interest in the field is mainly due to the unique and peculiar properties of these objects, which arise from their tiny sizes. Their properties thus vary dramatically with size, and this provides unique opportunity for inventing materials with precisely controlled properties. A main category of nano-objects is aggregates of atoms or molecules of nanometric sizes, known as clusters. Clusters, and specially metallic and bimetallic clusters, have attracted much interest because of their electronic, magnetic, optical, and catalytic properties and applications. All these properties of the metallic and bimetallic clusters may be controlled and tailored by adjusting their sizes, structures, morphologies, and even compositions. Unraveling and understanding the fundamental physical and chemical properties of metallic clusters requires computer simulations to implement state-of-the-art theoretical and computational approaches.

The computational studies documented in this thesis focus on the global optimization of silver clusters, and copper-silver and nickel-silver bimetallic clusters. We model the atomic interactions in the clusters by the realistic many-body embedded atom method, and search for the global total-energy minimum structures by basin-hopping algorithm. For Ag_N clusters with N = 2 to 100 atoms, we demonstrate that global minima of different sizes also have different structural motifs. These structures include icosahedra, polyicosahedra, *fcc* truncated octahedra, and decahedra. We determine all magic sizes of Ag clusters, and by analyzing these sizes and the corresponding structural motifs, we realize that the growth has an icosahedron pattern with islands of decahedron and truncated octahedron.

For Cu_mAg_n and Ni_mAg_n clusters with N = m+n from 2 to 60, we consider every combination of m and n. The global minima of both bimetallic clusters have mainly icosahedron and polyicosahedron structures, except a few clusters of size N = 38 which are truncated octahedrons. We have also examined the ordering of atoms in the Cu–Ag and Ni–Ag nanoalloys by using different theoretical measures such as bond order parameter, and radial distances. The results show that both nanoalloys prefer core–shell structures with Ag atoms segregated to the surfaces. Through a complete and careful analysis of the total energy, we determine the most

stable stoichiometries as functions of (m, n). We find in many cases that Ag-rich stoichiometries of the bimetallic clusters are energetically more favored. Finally, the comparison of the two types of nanoalloys shows that their energetical properties are different in many ways, although they have very similar structural properties.

Cluster, Nanoalloy, Copper, Nickel, Silver, Global Optimization, Structure, Properties

Zusammenfassung

In den letzten zwei Jahrzehnten hat sich mit enormer Geschwindigkeit das Forschungsfeld der Nanowissenschaften etabliert. In diesem Forschungsbereich werden Phänomene untersucht, die in Systemen von wenigen Nanometern entstehen. Objekte dieser Größe sind verbindende Elemente zwischen einzelnen Atomen oder Molekülen und Festkörper. Das große Interesse an diesem Forschungsgebiet ist hauptsächlich durch die einzigartigen und besonderen Eigenschaften dieser Objekte begründet. Diese Eigenschaften sind durch die winzige Größe der Objekte begründet. Kleine Veränderungen in der Größe führen daher zu drastischen Änderungen der Charakteristika. Dies bietet die einzigartige Möglichkeit Materialien mit präzise kontrollierbaren Eigenschaften zu entwerfen. Eine der Hauptkategorien der Nano-Objekte sind molekulare oder atomare Aggregate von nanometrischer Größe, genannt Nanocluster. Metallische und bimetallische Cluster haben aufgrund ihrer elektrischen, magnetischen, optischen und katalysischen Eigenschaften und Anwendungen großes Interesse geweckt. All diese Charakteristika von metallischen und bimetallischen Clustern können kontrolliert und angepasst werden durch eine entsprechende Änderung ihrer Größe, Struktur, Morphologie und sogar Komposition. Das Entschlüsseln und das Verständnis dieser physikalischen und chemischen Eigenschaften von metallischen Clustern benötigen modernste Computersimulationen.

In dem simulationstheoretischen Teil dieser Arbeit wird die globale Optimierung von Silber-Clustern sowie den bimetallischen Kupfer-Silber und Nickel-Silber-Clusertern behandelt. Es werden die atomaren Interaktionen in den Clustern mittels des realistischen vielteilchen Embedded-Atom-Methode modelliert und nach globalen Gesamtenergieminimalstrukturen mittels des Basin-Hopping Algorithmusses gesucht. Für Ag_N Cluster mit N = 2 bis 100 Atome wird demonstriert, dass globale Minima mit verschiedenen Größen verschiedene Strukturen haben. Die Strukturen umfassen Icosahedra, Polyicosahedra, *fcc* Truncated Octahedra und Decahedra. Es werden alle magischen Größen von Ag-Cluster bestimmt und durch die Analyse ihrer Größe sowie der zugehörigen Strukturen wird festgestellt, dass das Wachstum ein Icosahedron- Muster mit Decahedra- und Truncated Octahedra-Inseln aufweist.

Für Cu_mAg_n und Ni_mAg_n Cluster mit N = m+n von 2 bis 60 wird jede Kombination von m und n betrachtet. Die globalen Minima beider bimetallischen Cluster haben hauptsächlich Icosahedron- and Polyicosahedron-Strukturen, abgesehen von wenigen Clustern der Größe N = 38, welche Truncated Octahedra-Strukturen

aufweisen. Desweiteren wird die Anordnung der Atome in den Cu–Ag and Ni–Ag Nanoalloys mittels theoretischer Methoden wie Bond-Order-Parameter und radial Distanzen untersucht. Die Resultate zeigen, dass beide Nanoalloys Kern-Schele-Strukturen mit Ag-Atomen, welche sich an den Oberflächen absondern, bevorzugen. Durch eine vollständige und gründliche Analyse der Gesamtenergie werden die stabilsten Stöchiometrie als Funktion in m und n charakterisiert. In vielen Fällen stellt sich heraus, dass silberreiche Stöchiometrie von bimetallischen Clustern energetisch bevorzugt werden. Abschließend zeigt der Vergleich dieser beiden Typen von Nanoalloys, dass ihre energetischen Eigenschaften in vielerlei Hinsicht verschieden sind, wohingegen ihre strukturellen Eigenschaften sehr ähnlich sind.

Cluster, Nanoalloy, Kupfer, Nickel, Silber, globaler Optimierung, Struktur, Eigenschaften

Dedication

I would like to dedicate this thesis to my affectionate mother, *Fatemeh Molayem*, without whose caring support it would not have been possible. Also, in memory of my honorable father, *Habibollah*, for his patience and selfless love as always. I am deeply indebted to them for their continued encouragement and unwavering faith in me.

Acknowledgment

It would not have been possible to write this doctoral thesis without the help and support of the kind people around me, to only some of whom it is possible to give particular mention here.

I owe my deepest gratefulness to my supervisor, Prof. Dr. Michael Springborg, whose encouragement, supervision and tremendous support from the preliminary to the concluding level enabled me to develop an understanding of the subject. I would like to show my greatest appreciation to my second supervisor, Dr. Valeri G. Grigoryan, whose good advice and crucial contribution made him a backbone of our research and so to this thesis. I would also like to show my gratitude to Dr. Yi Dong whose support and friendship has been invaluable on both an academic and a personal level.

Words are not enough to thank Violina Spurk sincerely, who helped me in many ways. I am especially grateful for her great endless support after the devastating loss of my father and also her nice lessons of German (*Danke Schön Vili*). A special acknowledgment goes to my friend Dr. Michael Bauer for his various unconditional support which has been essential all these years.

I would like to acknowledge all of my current or past colleagues at Ak Springborg: Elisaveta Hristova, Sahar Abdalla, Jorge Vargas, Yong Pang, Nicolas Louis, Dr. Max Ramirez and Nathalie Atif. I would also like to thank our cheerful secretaries, Silvia Nagel and Ingelore Weidenfeld. I should also acknowledge Esfandiar Mohammadi and Melanie Manusch for their generous help.

My deepest gratitude goes to my family for their unflagging love and support throughout my life; this dissertation is simply impossible without them. I am deeply indebted to my father, *Habibollah Molayem*, for his care and love. He spared no effort to provide the best for me and never complained, in spite of all the hardship in his life. Although he is no longer with us, he is forever in my heart and in every second of my life. I can not ask for more from my dedicated mother, *Fatemeh Molayem*, as she is simply perfect. I have no suitable word that can fully describe her everlasting love to me. Mother, I love you.

Preface

The results of the studies documented in this thesis were published in the following papers.

I. M. Molayem, V. G. Grigoryan, and M. Springborg: "Theoretical Determination of the Most Stable Structures of Ni_mAg_n Bimetallic Nanoalloys", J. Phys. Chem. C **115** (2011) 7179-7192. Copyright (2011) American Chemical Society.

II. M. Molayem, V. G. Grigoryan, and M. Springborg: "Global Minimum Structures and Magic Clusters of Cu_mAg_n nanoalloys", J. Phys. Chem. C Just Accepted Manuscript, DOI: 10.1021/jp2050417. Copyright (2011) American Chemical Society.

The code for computing total energy (embedded atom method) was provided by Dr. Valeri G. Grigoryan. The basin-hopping code was downloaded from the website of Dr. David J. Wales and modified by Elisaveta Hristova. The analyses of results were done by using the ASE code provided by Prof. Dr. Michael Springborg. The code has been changed from monometallic to bimetallic case.

Contents

List of Figures

List of Tables

Chapter 1

Introduction

Human life has been affected significantly by metals and their alloys since 3500 B.C. They were first used as materials for very simple applications like making knives, and afterwards they also emerged in other areas of daily life such as the economy. The great impact of metals on human life started just after their unique properties and those of their alloys were discovered. Since then, living without metals has been almost impossible.

The field of nanoscience has emerged during the last few decades, since the encouraging lecture of Richard Feynman entitled 'There's Plenty of Room at the Bottom.' The field extends across many different sciences and interdisciplinary fields all dealing with sizes in the range of 10^{-9} meters. Nanoscale materials, consisting of countable particles below the thermodynamic limit, gain their novel properties from reduction of their dimensionality and the related nontrivial size effects. These peculiar properties of nanomaterials are tunable as their sizes are adjustable. The above facts promise a wide range of applications for nanoscale materials which spans from optical devices, sensors and catalysts to medicine and cosmetics.

Clusters are one of the very principle categories of nanoscale materials defined as "a group of similar or dissimilar atoms or molecules gathered together"[6]. The properties of clusters are easily manipulated and tailored by adjusting the number and also type of their atoms.

Extensive interest in metal clusters is driven by both fundamental and applied reasons. These types of clusters have been predicted to possess unique properties which may lead to advanced material, e.g., quantum dots, and also to novel photocatalysts and electrocatalysts. The catalytic properties of metal clusters, which

originate from high ratio of surface/volume atoms, are expected to have a great impact on many technological and industrial fields, such as energy, pharmaceutical, and petrochemical industries.

The field of cluster science has attracted the interest of many researchers since the early famous work of Faraday in the nineteenth century. But great progress in this field has only been possible since the development of modern experimental techniques like high resolution scanning electron microscopy (SEM), atomic force microscopy and mass spectroscopy. Two major difficulties are related to the experimental studies of nanoclusters. First, nanoclusters are supposedly made out of all elements of the periodic table and their combinations. Obviously it is impossible to experimentally examine all these clusters and find the one appropriate for a given purpose. Second, although experiments using very developed techniques provide us with precise information about nanoclusters, it is very difficult, if not impossible, to interpret the results without computational modeling. The development of powerful computers and also very efficient computational methods have now made it possible to simulate nanoclusters with very precise methods. This computational modeling can help to understand the results of the experiments. Precedent information provided by computational studies is also very important in the design and development of more specific and purposeful experiments.

A complete understanding of the properties of clusters relies on the knowledge of their geometric structures. But finding the global minimum structure of a cluster is a challenging task, due to the huge number of possible geometries which increases as an exponential function of the cluster size. The problem becomes even more intricate for alloy clusters, because in addition to the geometrically different isomers, we should also consider the topological isomers or *homotops*. Homotops are structures with similar geometries but different arrangements of atomic species.

As a result of these difficulties, even the fastest first principle methods are not able to locate the global minimum structures of clusters with more than a few atoms. Therefore, our aim in the studies documented in this thesis was to employ the Embedded Atom method and determine the putative global minimum structures of pure Ag clusters and bimetallic Cu–Ag and Ni–Ag nanoalloys. The embedded atom is a fast and precise semiempirical method which has been specially developed to model the atomic interactions in metals and alloys. For the global optimization of structures we used an efficient algorithm called Basin–Hopping. The considered

Ag clusters had 2 to 100 atoms, and the nanoalloys were all possible stoichiometries of sizes from 2 to 60 atoms. The putative global minimum structures were then thoroughly analyzed and the structural and energetical properties are reported here.

Chapter 2

Nanoclusters

The science of nano-objects dates back to the scientific works of Faraday on colloidal gold nanoparticles in the 1850's while their application is much older where they were used in decorations by Ancient Romans. But the revolution of Nanoscience was ignited by the encouraging lecture of Richard Feynman. Since then many physicists, chemists and other scientists have concentrated their attention on this new world. Among all possible nano-sized structures and systems, nanoclusters, or simply clusters, have been the focal point of this attention as they are expected to play the role of building blocks in many electronic, optical, magnetic, and even medical applications[1].

The most accepted and used description of nanoclusters defines them as aggregations of a countable number of atoms or molecules with a population of 10 to 10^6 [7]. Clusters are usually put in three different size categories, i.e., small, medium and large sizes. The main criterion for these definitions comes from the behavior of the cluster properties and the way they change with the sizes. Small clusters are usually defined as those whose properties strongly depend on their sizes and morphologies. The properties of medium clusters vary more smoothly with the number

[1]Beside the term 'nanocluster', we also have 'nanoparticle' which may be confusing. In fact there is still some ambiguity in definitions of these two terms in literature. But in a simple word we can consider clusters as systems with exactly defined structures and chemical compositions or stoichiometries, while nanoparticle refers to particles which are characterized less precisely and are often considered with their size distributions, i.e., their exact structures are not a concern in their studies.

of their particles, and even in some cases they show a gradual transition toward those of bulk materials. For large clusters, properties primarily resemble those of bulks. From a fundamental point of view, it is interesting to understand how the properties of clusters vary depending on their sizes or compositions, and also how they approach those of bulk materials. As an example for this interesting dependence on size, we can point to silver which is a good electric conductor in the bulk phase, but its clusters of defined sizes has transitions to insulators [8].

Atoms of all elements in the periodic table can theoretically cluster together at nanoscales. According to the types of particles in a cluster, it can belong to one of the following types (i) Metallic (ii) Semiconductor (iii) Van der Waals (iv) Heteroatomic (v) Molecular clusters and (vi) Cluster Molecules [9, 6]. Bonds in metallic clusters are of different natures, from non-directional delocalized to even covalent. Semiconductor clusters made of elements like carbon, silicon and germanium have covalent and strongly directional bonds. C_{60} fullerene is a typical example of this type. Atoms of Van der Waals or rare gas clusters bond to each other with weak van der Waals forces and interatomic attractions which are directly proportional to the atomic masses. Heteroatomic clusters are made of two (or more) different elements with (large) differences in electronegativity and therefore polarized electrostatic bonds. Among the well known heteroatomic clusters we can name sodium-chlorine, magnesium-oxygen, Cadmium-Sulfur, and Zinc-Oxygen. In molecular clusters, molecules bond to each other with different bonding phenomena such as van der Waals, dipole or even multipole interactions. Water, ammonia, methanol, and biomolecular clusters are examples of this category. Cluster molecules are stable symmetrical nanostructures assembled from clusters or molecular clusters. An example of cluster molecules is Fullerite, an assembly of multiple C_{60} fullerenes [10].

Metal clusters are as diverse as the type of metals in the periodic table, and therefore they have different bonding natures as following. Alkali and alkali earth metal clusters have metallic, delocalized and non-directional bonds with contributions primarily from the valance s orbitals. Metals with electrons of sp character in their valence shell, e.g., Aluminum, can build bonds with the involvement of both s and p orbitals. These bonds have covalent characters to some extent. Inclusion of valence d orbitals for transition metals causes higher directionality in bonds and also more covalency. The atomic electronic configuration of the coinage metal atoms such as Cu and Ag consists of *(n-1)* d^{10} ns orbitals. In an oversimplified view, the

filled d orbital has a resemblance to those of transition metals, although the half filled s orbital can be seen as analog of those of monovalent alkali metals.

2.1 Cluster Properties

The peculiarity of cluster properties is in their variability with not only the type but also the number of constituent atoms. Many properties of clusters change by size, e.g., ionization energy, cohesive and binding energy, electron affinity and melting temperature [11, 12]. As mentioned above, properties of a small cluster vary significantly and also not uniformly with a change in the number of the constituent particles. In medium sizes this behavior is smoothed to some extent, but they still differ significantly from those of the corresponding bulks. Large clusters have properties that vary smoothly with their sizes and show a convergence into those of bulk counterparts. Size dependent changes of cluster properties are known as cluster size effects (CSE). This unique trait of clusters is the main reason for the ever-growing interest in the field because it makes the production of materials with predefined properties possible.

In a very simple model developed for describing the effect of size, an N-atom cluster is approximated by a sphere of radius R (Spherical Cluster Approximation, SCA). The size effects are then described by simple scaling laws in the power of cluster nuclearity or its radius. Although these scaling laws work perfectly for large sizes, they show some deviations for small and even some medium sizes. This is related to the quantum size effects, electronic shell closure, surface effects, and also geometric shell closure in the clusters [9].

The gradual change of cluster properties provides another unique opportunity. In this view, cluster studies are necessary to find the limiting sizes where properties of clusters converge to those of bulks or molecules, and answer questions like 'Do all properties of a given cluster converge with the same gradient as those of bulks or molecules?'

Another result of size effects in clusters is their high ratio of surface/volume number of atoms. According to the spherical cluster approximation, even large clusters have a considerable number of their atoms on the surface, i.e., 20% of atoms in large clusters, 20%–86% in medium and more than 86% in small clusters [9]. This makes metal clusters, especially those of small and medium sizes, eligible

for catalytic applications as they have more low-coordinated atoms on their surfaces and therefore more active bonds.

The under-coordinated atoms on the surfaces make clusters very similar to the surfaces of solids, as surface reconstructions can take place in both types of systems in favor of building additional bonds and minimizing the surface energies[2]. Thus, clusters are also simple test bench to understand complex surface effects.

2.2 Cluster Structure and Magic Sizes

The preliminary and most important step in cluster science is the determination of the most favored structures. In atomic clusters these are structures related to the global minimum of the corresponding potential energy as a function of the coordinates of atoms or the so-called potential energy surface (PES). From a computational point of view, finding the global minimum structure of an N-atom cluster (A_N) is a very complicated problem, because the number of local minima on the PES increases exponentially with the number of atoms [13, 14, 15, 16]. For example, there are 1467 local minimum structures for the simple case of the 13-atom Lennard-Jones cluster and they increase to more than 10^{12} for the 55-atom case [17, 18, 19].

To reduce the complexity of the problem, two different theoretical models have been developed to find a general scheme which can help to predict the structural motifs of clusters in different size ranges, and also explain the *magic sizes*. Magic sizes are those nuclearity of clusters which show high peaks of abundance in mass spectra. One of the developed models is based on electronic and the other one on geometric shell closure.

According to the geometric shell model, structurally optimized clusters have compact quasi-spherical shapes. A way of building these structures was proposed by Mackay who suggested the Mackay icosahedra [20, 21]. An icosahedron (Ih) is a noncrystalline structure with 5-fold rotational axes. Surface energy is well optimized in these geometries as they only have closed-packed facets. But Ih is a strained structure, because intershell (radial) bonds are compressed and intrashell bonds are stretched. Therefore, icosahedra are favored only by small size clusters. Marks truncated decahedra are other possible noncrystalline compact structures with optimized surface energy. The strain reduces significantly in a marks truncated decahedron and

[2]Ligands can also be used to coordinate surface atoms of clusters and stabilize them.

becomes much smaller than that of an icosahedron. Therefore, intermediate cluster sizes can favor truncated decahedra. Both surface energy and the contribution of internal atoms to the binding energy of a cluster should be optimized in larger sizes. Thus, *fcc* truncated octahedron can be favored structures for the clusters in this size range. Experiments on rare gas and transition metal clusters have confirmed the validity of the geometrical shell closing model, but with different cross over sizes between Ih, decahedra, and truncated octahedra motifs [22, 23, 24].

The geometric shell model relates some of the magic sizes of a typical N-atom cluster (A_N) to closed geometrical shells. The model predicts that the geometric closed shell structures with k concentric shells are formed when the number of atoms can be written as

$$N(k) = \frac{1}{3}(10k^* + 15k^2 + 11k + 3). \tag{2.1}$$

It gives N = 13, 55, 147, ... as magic numbers with different structural motifs, i.e., icosahedra, decahedra and cubooctahedra.

The well known model in the framework of electronic shell closure is the spherical jellium model. In this model, a metal cluster is considered as a uniform, positively charged shpere. The electrons are constrained to move inside this cluster sphere subjected to an attractive mean field potential due to the ionic cores or nuclei. Two different simple forms of this potential are the infinitely deep spherical well and the harmonic well. Magic numbers found for each of these potentials are N = 2, 8, 18, 20, 34, 40, 58, ... for spherical well and N = 2, 8, 20, 40, 70, ... for harmonic well [7]. Electronic shell closure works very well in explaining the magic sizes measured in mass spectra of alkali metal clusters with up to 2000 atoms, and also those of small noble metal clusters [9, 21, 25, 26]. Many studies have shown that the electronic shell closing model works better for small sized clusters of a material, but at larger sizes it is the geometric shell model which can predict the correct magic sizes [21, 25, 26]. In many cases, however, both electronic and geometric shell effects are found important, while their interplay and dependence on the types and number of atoms are not trivial [27].

2.3 Bimetallic Clusters

Intermetallic compounds and alloys greatly extend the range of properties and applications of metallic systems. The idea of combining the flexibility afforded by

alloyed metals and their controllable structures and properties at a nanoscale has generated considerable interest in bimetallic and multimetallic alloy clusters or the so-called nanoalloys. The main reason for the ever growing interest in nanoalloys is the possibility of tuning their properties by adjusting not only their sizes but also the corresponding compositions and degrees of chemical ordering. The properties of nanoalloys are distinct from those of the pure elemental clusters and also those of corresponding bulk alloys [1, 7, 28, 29]. Well known examples are nanoalloys of iron and Ag which are immiscible in the bulk phase [30]. Nanoalloys have already found their applications in different fields such as catalysis [31, 32, 33], optoelectronics [34, 35], magnetic sensors or recording [36], and biodiagnostics [37].

Because of the presence of two types of atoms, the complexity of bimetallic nanoalloys is much higher than pure metallic clusters. In addition to different geometrical structures (geometrical isomers), homotops are also possible for bimetallic clusters. Homotops of an A_mB_n nanoalloy with a fixed number of atoms (N = m+n) and composition (m/n), are similar structures which differ only in the arrangements of A and B atoms [28, 38]. The number of homotops for a given structure of A_mB_n cluster is given by following formula:

$$^{N}P_{m,n} = \frac{N!}{m!\ n!} \tag{2.2}$$

There are, for example, 184756 homotops for an $A_{10}B_{10}$ cluster, if point group symmetries are ignored. If we remove the constraint of constant composition then the number of homotops for a given structure counts as 2^N. This means for a 20-atom nanoalloy we have 10^6 homotops [1].

Possible structures of nanoalloys are analogues to those of pure metal cluster, and they can take noncrystalline structures like icosahedra, decahedra and polyicosahedra (pIh) as well as crystalline structures such as *fcc* octahedra or truncated octahedra (TO). As explained before, compact noncrystalline structures are mainly formed with strains and therefore the large pure metal clusters do not favor these types of structures. But if the size mismatch between atomic species of a bimetallic cluster is large enough, and smaller atoms tend to form the inner part of the cluster, then the strain will be reduced and compact structures like icosahedra or polyicosahedra will be favored [39].

Atoms of bimetallic nanoalloys can be ordered with different patterns, and these affect the reactivity of clusters as the type of the surface atoms will differ. Nanoalloys

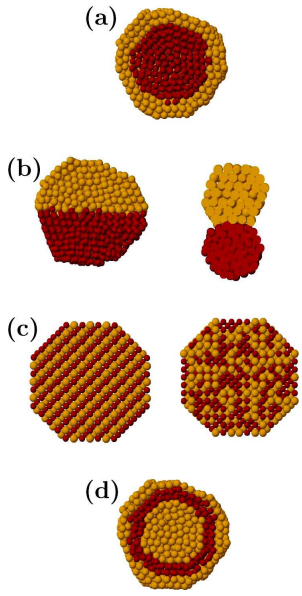

Figure 2.1: Schematics of four possible mixing patterns of bimetallic nanoalloys: (a) core–shell, (b) subcluster segregated, (c) mixed, and (d) three shell. Reprinted with permission from Ref. [1]. Copyright (2011) American Chemical Society.

have four distinguished mixing patterns: (a) core–shell, (b) subcluster segregated, (c) mixed, and (d) three shell (Fig. 2.1) [1]. In core–shell segregation, one type of atom forms the inner part of the cluster and the second species covers the formed core. This $A_{core}B_{shell}$ segregation has been found for various types of nanoalloys, e.g., the Au–Ag and Pt–Ru nanoalloys [40, 41]. A and B atoms are completely separated in subcluster segregation and have only one mixed interface. Atoms can also mix in an orderly way or randomly and form mixed nanoalloy. The random mixing, i.e., intermixing, is found for many nanoalloys such as Co–Rh and Ni–Al [42, 43]. And finally, atoms may form alternative shells in a multishell nanoalloy. This mixing has been seen in many theoretical [44, 45] as well as experimental studies [46].

Recently, it has been proposed that a set of factors are responsible for the degree of segregation/mixing and ordering of atoms in an A_mB_n bimetallic nanoalloy [1]. These factors are as follows: (a) if heteroatomic (A–B) bonds are stronger than homoatomic (A–A and B–B) bonds then mixing would be preferred. If otherwise, atoms will segregate and the core of the cluster will be taken by the species with the strongest homoatomic bonds; (b) the atoms of the element with lower surface energy segregate to the surface of the cluster to minimize the contribution of surface

energy and stabilize the structure; (c) in order to reduce the (compressive) strain, smaller atoms occupy the core of the cluster; (d) if the two species of atoms have large difference in electronegativity, then they would prefer a mixed structure to make the charge transfer more possible; (e) in supported or passivated clusters, the element which has stronger bonds with the support of ligand atoms will segregate to the surface; (f) electronic shell closing or electron spin interactions are also key factors in the preferred mixing pattern of some nanoalloys. It is noteworthy that an interplay of all these factors will determine the structure and ordering of atoms in a nanoalloy, and this interplay is in no way trivial.

As the last point it should be added that nanoalloys can also have magic compositions (m/n) beside those magic sizes (N = m+n). These magic compositions have higher stabilities in comparison to other clusters of the same or neighboring sizes which have different values of m and n. It turns out that the determination of the magic sizes or compositions of nanoalloys is not as straightforward as in pure clusters. This point will be discussed in the following sections in more detail.

2.4 Experimental Methods

Thus for we have described some principle characteristics of nanoclusters and nanoalloys mainly from a theoretical point of view. Nevertheless it was only after the development of new experimental techniques that scientists have been able to make progress in cluster science. This section outlines different techniques used in the three main stages of experimental studies of clusters: generation, detection/selection, and analysis.

2.4.1 Cluster Generation

Almost all typical methods for producing clusters consist of the following steps. First, a vapor from the desired material is produced, then atoms and molecules of the vapor condense to make the initial seeds of clusters (nucleation). In the growth stage, the seeds absorb more particles and transform into small clusters which in turn merge with each other in the coalescence processes and grow.

The medium of generation has very important effects on the behavior of clusters and also their response to analyses. Clusters are normally generated in molecular beams or gas phases, in isolated matrices, by deposition on surfaces or even in solid

phases. Clusters in molecular beams and gas phases are free and without any ligand or support. These are perfect for a complete analysis and understanding of cluster properties. Matrix isolated clusters are normally implanted into a condensed liquid, glassy, or crystalline phase of a rare gas or molecule. These clusters are suitable for spectroscopic analysis. To analyze the clusters by using surface microscopy techniques, they should be deposited as single clusters on an inert surface such as graphite [9, 6].

The most common method for generating gas phase clusters is the cluster molecular beam. One should first evaporate the target metal by using different techniques such as laser ablation, heavy ion sputtering, magnetron sputtering, or electric discharge. Then atoms of the generated plasma collide with a cold carrier rare gas and condensate to initialize the cluster generation by forming initial seeds. Clusters grow more by collisions and coalescence. Further cooling is done by a supersonic expansion of the mixture into a vacuum chamber [1, 9].

Clusters of volatile materials are generated by effusive sources. In these sources a low pressure vapor of the volatile liquid or solid is produced in an oven with a small aperture from which the vapor expands out and clusters form in the subsonic low flux.

Liquid metal ion source is another method for generating low melting metal clusters. In this source the tip of a needle is first wetted with the target metal and kept at temperatures above the melting point of the metal. Afterward a high voltage electric field is applied to the needle tip and detaches atoms of the metal. The clusters are initially hot and charged but they cool down by evaporating and breaking into small sizes.

2.4.2 Cluster Detection and Selection

After generating clusters one should also detect and separate them. Ionized clusters are detected and mass selected by mass spectroscopy techniques. By ionizing neutral clusters they can also be detected and selected in the same ways.

In ordinary mass spectrometers, homogeneous electric or magnetic fields interact with clusters in a beam and deflect them according to their charge/mass ratios and velocities. More sophisticated magnetic sector mass spectrometers have a sector magnetic field which selects the clusters of defined masses and then a sector electric field with an adjusted energy compensates the magnetic field. In Wien filters,

perpendicular homogeneous electric and magnetic fields act simultaneously on an accelerated ionized cluster beam. If the net force acting on a cluster becomes zero then it will not deflect and can be separated from others [9].

Clusters of different sizes are separated by time-of-flight mass spectrometers. Ionized clusters first accelerate in successive electric fields and then fly in a field-free tube. The mass/charge ratios of clusters determine their time of flight, i.e., distances they can travel inside the tube.

All methods explained above work fine for cluster ions. Detection and size selection of neutral clusters are done mostly by cluster beam deflection and re-neutralization of cluster ions. In the cluster beam deflection method a beam of neutral clusters collides with another beam of ionized rare gas atoms. Large clusters scatter at small angles because of the momentum conversion rule. Thus, clusters of different sizes can be separated. Size selected neutral clusters can also be generated by re-neutralizing ionized clusters. The re-neutralization is done with the following methods: (a) cluster anions absorb photons and decay their extra electrons, (b) they can collide with other atoms to detach their electron, (c) anions/cations of clusters can also exchange charge in collisions with more electronegative/electropositive atoms [9].

2.4.3 Cluster Analysis

Mass spectroscopy also provides information about the size and stability of clusters. At similar generation conditions, mass spectra of clusters show high peaks for cluster sizes with greater abundances. This has been associated with the higher stability of these clusters.

Light spectroscopy is used to probe high intensity cluster beams. For small metal clusters, absorption spectra is mainly measured in the range of ultra violet (UV) and infra red (IR) wavelengths. For beams with low concentrations of charged clusters, depletion spectrometers are the ideal probing devices in which the frequencies of a photoexcitation laser beam is scanned to find the UV-Visible absorption spectrum of clusters.

Structures, sizes and temperatures of rare gas or metal clusters are measured by diffraction experiments. The averaged effect of interactions between the electrons of an electron beam and the atoms of clusters manifest themselves in the diffraction patterns of scattered electrons. X-ray beams have also been applied for diffraction

experiments on surface deposited metallic clusters. Patterns of X-ray and electron diffraction experiments are very complicated and computational methods should be used to interpret the results.

Electron microscopy is widely used to determine the structure of a cluster. Different techniques of electron microscopy are employed in cluster studies; e.g., scanning (SEM), transition (TEM) or high resolution electron microscopy. Scanning tunneling microscopes (STM) use an electrically biased needle to scan and map the topography of the substrate which supports the clusters. Electrons tunnel from or to the needle when they scan the surface. In an operation mode of STM, the distance from the needle to the surface varies to keep electric current constant, but in the other mode the tip of the needle is fixed and the variation of current is measured [9].

2.5 Ag Nanoclusters and Ag-Based Nanoalloys

In our studies we focused on pure Ag clusters and nanoalloys made by mixing Ag with Cu (Ag–Cu) or Ni (Ag–Ni). A brief description of these clusters and a review of the available literature are given below. Further details will follow in the relevant chapters.

2.5.1 Ag Clusters

Pure solid Ag has extensive applications in the preparation of high-temperature superconductors, electrical, medical, and dental equipment, and photography films. Ag clusters have received the attention of scientists because of possible applications in electronic and optoelectronic devices, DNA markers and also catalytic processes [47, 48, 49, 50]. For example, Ag clusters exhibit a size-dependent insulating property, which is a result of the large gap between the highest occupied and lowest unoccupied molecular orbitals (HUMO-LUMO gap) [8].

The half-filled s orbital of Ag atom has encouraged the application of the spherical jellium model for Ag clusters. Many properties of Ag clusters are explained successfully by this model; to name a few, these are structures of their electronic energy spectrum measured by photoelectron spectroscopy [51]. Mass spectroscopy experiments indicate similar shell closure effects and stability patterns, as seen for alkali clusters, as well as for the clusters of Ag and two other coinage metals, Au and

Cu [52, 53]. Nevertheless, the simple jellium model ignores the *d*-orbital electrons while experiments and also first principle calculations emphasize the effects of these electrons on many properties of coinage metals and their significant contributions in the bonds [54, 55]. Even *s*–*d* hybridization is also seen for the clusters of coinage metals [56]. This hybridization is another reason for the interest in challenging studies of Ag clusters.

Experimental analyses of the frequencies and intensities of vibrational modes have suggested a planar trapezoidal structure for Ag_5 [57]. This is in contrast to the results of electron spin resonance spectroscopy (ESP) which have found the trigonal-bipyramid with Jahn-Teller distortion [58]. Xing et al. carried out trapped ion-electron diffraction experiments on Ag_N^+ clusters with $N \leq 55$. Structures with 5-fold symmetry were characterized at smaller sizes which evolved to icosahedral symmetry at $N = 55$ [59]. The exception was $N = 38$ for which DFT calculations have predicted a *fcc* truncated octahedral as the global minimum structure. A similar experimental technique has also shown that icosahedral motifs are the structures of the lowest energy isomer of Ag_N^+ clusters with $N = 19$ to 79 atoms [60]. Handschuh et al. analyzed the photoelectron spectra of Ag_N^- ($N \leq 21$) at different photon energies [61]. According to the pattern developed for the electronic shell of cationic Ag clusters, they found that up to $N = 16$, the clusters are nonspherical and for $N = 6$–8, the geometries are prolate.

Theoretical studies of neutral, cationic and anionic sliver clusters with $N = 5$–9 atoms have been performed by Huda et al., using the second-order many-body perturbation theory with a Hay-Wadt effective core potential [62, 63]. Their results showed that neutral clusters with up to 6 atoms favor planar two dimensional (2D) geometries, while charged clusters with more than 6 atoms prefer three dimensional (3D) structures. But, quantum chemical and *ab initio* calculations confirmed that the competitions between 2D and 3D structures are more pronounced for neutral Ag clusters rather than for those cationic clusters [64, 65, 66].

2.5.2 Cu–Ag Nanoalloys

Mixing two coinage metals with unfilled *s* orbitals into a bimetallic cluster should result in novel structural, magnetic, and catalytic effects. The interaction between the two free electrons and their influence on the structures are also very interesting. In fact a reason for interest in Cu–Ag (and also Ni–Ag) nanoalloys is the possible

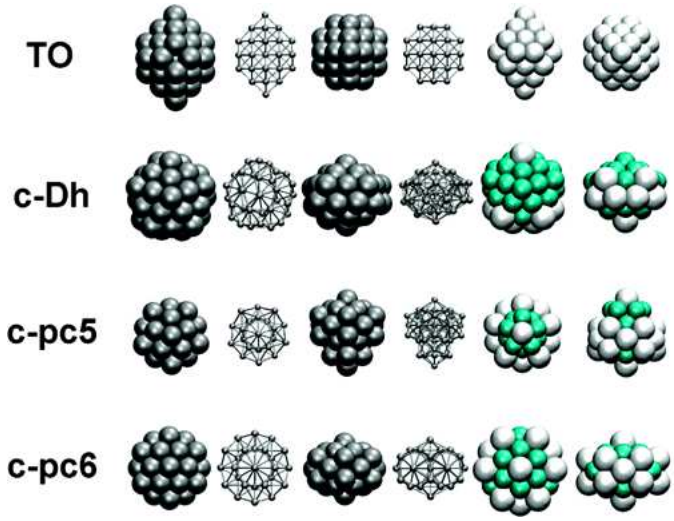

Figure 2.2: Examples of typical structures found for Cu–Ag nanoalloys: (first row) *fcc* truncated octahedron (TO), (second row) capped decahedron (c-Dh), (third row) capped fivefold pancake (c-pc5) and (fourth row) capped sixfold pancake (c-pc6). Reprinted with permission from [2]. Copyright (2011) American Chemical Society.

optical properties. These properties come from the surface plasmon and therefore depend on the type of surface atoms.

Experimental studies of Cu–Ag nanoclusters, produced in a mixed solution of Cu and Ag sulfate [67, 68] or by using thermal evaporation methods [69], have shown that $Cu_{shell}Ag_{core}$ is the preferred mixing pattern. In contrast, sequential deposition of Cu and Ag on an amorphous substrate resulted in a $Cu_{core}Ag_{shell}$ pattern [70]. The formation of core–shell structures is explained by properties of pure Cu and Ag atoms and comparing them with the conditions explained in the previous section (Sec. 2.3). The atomic radii for Cu, and Ag are 1.28 and 1.445 Å, respectively. Their bulk cohesive energies are 3.49, and 2.95 eV/atom, and the corresponding surface energies equal 113.9, and 78.0 meV/Å^2, respectively [1]. All these suggest that the formation of $Cu_{core}Ag_{shell}$ configurations should be more favored.

Janssens and co-workers used mass spectroscopy to analyze the stability of cationic $Cu_1Ag_n^+$ clusters and found clusters with n = 8, 20, 34, 40, and 58 to have particularly stable structures, which is in agreement with the predictions of the jellium model [71]. The interplay between the electronic shell closure, given by the jellium model and the geometric shell closure, have been studied theoretically by Barcaro

et al. for Cu–Ag nanoalloys with the size N = 40, a magic size according to the jellium model [2]. They found that although Cu–Ag nanoalloys of this size can adopt different morphologies, the capped 5-fold pancake (c-pc5) geometry, for which the geometric shell closure occurs, has the lowest total energy. The other possible morphologies were found to be capped decahedral (c-Dh) and capped 6-fold pancake (c-pc6).

By a capped pancake, we mean a structure consisting of pentagons (5-fold) or hexagons (6-fold) which is capped with two single atoms at each end of the symmetry axis. Accordingly, the c-pc5$_{34}$ structure (a 5-fold capped pancake with 34 atoms) contains layers of 1 + 5 + 1 + 5 + 10 + 5 + 1 + 5 + 1 atoms and the c-pc5$_{39}$ (a 5-fold capped pancake with 39 atoms) has 1 + 5 + 1 +10 + 5 + 10 + 1 + 5 + 1 atoms. Both of these structures are fragments of the 55-atom icosahedron structure (Ih$_{55}$). The c-pc6$_{40}$ (a 6-fold capped pancake with 40 atoms) structure with 1 + 6 + 6 + 1 + 12 + 1 + 6 + 6 + 1 atoms consists of six Ih$_{13}$ icosahedra, each pair of which has common atoms. The two atoms on the symmetry axis are shared by all the 13-atom icosahedra. Examples of these structures are shown in Fig. 2.2 taken from Ref. [2].

Parameter-free density functional theory (DFT) calculations determined a large gap between the highest occupied and the lowest unoccupied molecular orbitals of Cu–Ag nanoalloys with N = 34 and 40. The stabilities of these sizes are indications of jellium shell closure effects. Also the particular stability of c-pc5 Cu_7Ag_{27}, pIh Cu_8Ag_{30}, and c-pc5 $Cu_{13}Ag_{27}$ clusters was found through DFT studies [39, 72, 73]. Here pIh refers to polyicosahedron structures that are made of multi-interpenetrating Ih$_{13}$ motifs. The properties of Cu_7Ag_{27} clusters were also compared to Cu–Ag bulk alloys by using DFT calculations [74]. The hierarchy of the bond strengths was found to be a key factor in the determination of the global minimum structures.

The structural and vibrational properties of small cationic and neutral Cu_mAg_1 (m = 1 – 7) clusters have been thoroughly examined by Jiang et al. using DFT calculations [75]. Their results showed that three-dimensional geometries form at m $>$ 6 for neutral clusters, while for cationic ones it occurred already for m $>$ 5. In a recent study, some selected large sizes of Cu–Ag nanoalloys have been investigated by performing global optimizations in the framework of a model potential followed by DFT calculations [76]. The favored structures were found to be anti Mackay icosahedra for $Cu_{55}Ag_{72}$ and $Cu_{147}Ag_{132}$, and chiral icosahedra for $Cu_{309}Ag_{200}$ and

$Cu_{561}Ag_{312}$.

2.5.3 Ni–Ag Nanoalloys

A combination of one transition metal (Ni) and one coinage metal can also result in nanoalloys with peculiar properties. Bimetallic nanoalloys made of Ni and Ag are fundamentally interesting because of their unique optical properties which have been found to be distinct from those of pure Ni and Ag clusters [77, 78, 79, 80]. Possible magnetic applications have also been suggested for Ni–Ag nanoalloys based on their super-paramagnetic characteristics measured by Lee et al. [81].

If we consider the important factors which determine the ordering of atoms (see Sec. 2.3), then we should expect a core–shell pattern for the Ni–Ag nanoalloys. This prediction is based on the following facts: (a) the atomic radii of Ni and Ag have a noticeable difference (r_{Ni} = 1.245 Åand r_{Ag} = 1.445 Å), (b) the surface energy of Ni is much higher than that of Ag (149 and 78.0 meV/Å^2, respectively), (c) the cohesive energy of solid Ni lies 50% above that of solid Ag (4.44 eV/atom for Ni in comparison to 2.95 eV/atom for Ag). Moreover, Ni–Ag systems are immiscible even at high temperatures for almost all compositions [82, 83], while Ni nanoparticles were found to be miscible in an Ag matrix after a thermal annealing [84]. Previous experimental studies, using optical analysis and low energy ion spectroscopy, have confirmed the formation of $Ni_{core}Ag_{shell}$ configurations for selected sizes and compositions [79, 78]. In a mass spectroscopic analysis of Janssens and co-workers on Ni–Ag nanoalloys, 2D structures were not found of enhanced stability which indicates that three dimensional (3D) shell closures are favored even at small sizes [71]. DFT calculations have also been performed for very small sizes of Ni_mAg_n clusters with pre-chosen structures by Harb and co-workers [80, 85]. They found that for $N \leq 6$ Ag-rich compositions take mainly planar geometries while Ni-rich compositions take three dimensional geometries. Monte Carlo simulations of Segregation and shape transitions in Ni_mAg_{3m} bimetallic nanoclusters in the N = 55 to 309 size range showed that the most stable structures at low temperatures are icosahedral, and the clusters undergo a shape transition at high temperatures before the Ni core melts [83].

The growth pattern of Ni–Ag nanoalloys has been investigated by Baletto et al., using a molecular dynamics simulation in which 200–300 Ag atoms were deposited on a truncated octahedron core of 201 Ni atoms [86]. According to their results,

$Ni_{core}Ag_{shell}$ is the energetically most favored ordering of atoms. They also performed a global optimization of the clusters with N = 55 atoms, by using a genetic algorithm (GA) combined with the second-moment approximation to the tight-binding model (SMATB). The stable composition was found to be $Ni_{19}Ag_{36}$ with a non–icosahedral morphology.

Chapter 3

Computational Methods

In this chapter, the theoretical framework followed in this study is explained. After a short introductory part on the modeling of the clusters and their potential energy surfaces, we will discuss the employed potential model and global optimization algorithm.

3.1 Energy Potential Model and Potential Energy Surface

One challenge in the theoretical study of clusters is the determination of the cluster configurational energy as a function of the atomic coordinates, in order to build the corresponding potential energy surface (PES). The important parameters in choosing an energy model are the type and size of the clusters and also the physical and chemical properties in which we are interested. The complexity of interactions, even in clusters with few atoms, requires the employment of approximate methods. Although nowadays, the first principle methods are more feasible with high performance computer resources, they are still practicable only for modeling very small clusters. In this context semiempirical many-body potentials are reliable tools because they do not need huge computational resources of the first principle methods, while still keeping the many body nature of (metallic) bonding. Most of these potentials have free parameters which are fitted to the experimental data on material properties or to the results of *ab initio* calculations. Several semiempirical potentials have been developed for metallic systems, like second-moment approximation to the tight binding or Gupta [87, 88], glue [89], Sutton-Chen [90], effective-medium [91]

and embedded atom [92, 93] potentials. Although the accuracy of these models are not in the order of *ab initio* methods, with care attention they can be used reliably for cluster structure optimization.

Along with the above facts, a two step methodology has also been recently proposed and used by many authors [73], where first a semiempirical potential is used to build a database of most probably stable structures for a cluster, and then they are relaxed further by more accurate methods. As the first step of this methodology is the purpose of this study, we have used the embedded atom model to calculate the energies of nanoclusters. This model is described in detail in the following section.

Once the PES of a cluster is built, one should find its deepest minimum. As already mentioned in Sec. 2.2, the number of minima for a pure N-atom cluster has an exponential growth with size (N), and the problem becomes even more complicated for the bimetallic nanoalloys where one should also consider the homotops (see Sec. 2.3). If we consider a part of a PES, it can be one of the following types: single-minimum with weak noises, single-funnel with multiple local minima, or a rough PES which has multiple funnels. An ideal search algorithm should be efficient in (a) finding the local minimum related to each point on the PES, and (b) hopping between all funnels. Various algorithms have been developed and employed for exploring the PES of nanoclusters by considering the above facts. These are the genetic algorithm (GA), simulated annealing, quantum annealing, and the basin-hopping algorithm (BH). Among these algorithms, GA and BH have been found to be more efficient and successful in locating even very difficult global minima [7]. In the studies documented here, we have employed the BH algorithm and it is explained in detail in the following.

3.2 Embedded Atom Model

The embedded atom model (EAM) was originally developed by Daw and Baskes for metals, based on the formalism of density functional theory [92, 93]. The main assumption of this method was taken from the preceding quasi-atom model of Scott and Zaremba [94]. According to the quasi-atom model, the energy of a host system with an impurity is a functional of the electron density of the host system without the impurity and a function of the impurity position and charge. Employing the same concept in the EAM, the cohesive energy of a metal can be accounted for

by embedding an atom in the local electron density induced by neighboring atoms. The embedding energy of this atom has a functional form of the electron density provided by the other (host) atoms at its position. The effect of pairwise interactions of atoms is also included in the EAM by considering short-ranged pair potentials. Therefore, the total energy of an N-atom system takes the following form [93]

$$E = \sum_{i=1}^{N} \left[F_i(\rho_i^h) + \frac{1}{2} \sum_{j=1,(i\neq j)}^{N} \Phi_{ij}(r_{ij}) \right]. \tag{3.1}$$

$\Phi_{ij}(r_{ij})$ in Eq. 3.1 represents the short-range pair interactions between atoms i and j with an interatomic distance of r_{ij}, and $F_i(\rho_i^h)$ is the embedding energy of atom i embedded in the host of other atoms. Here, ρ_i^h is the local electron density provided by other atoms at the position of atom i. This local density is calculated as the superposition of spherically averaged atomic electron densities ($\rho_j^a(r_{ij})$) provided by all other atoms:

$$\rho_i^h = \sum_{j=1,(j\neq i)}^{N} \rho_j^a(r_{ij}). \tag{3.2}$$

The parameters of the embedding functions and pair potentials should be determined by fitting to the experimental data of the corresponding bulk systems, such as the heat of solution, elastic constants, and sublimation and vacancy-formation energies. An important advantage of the EAM is that the embedding functions are universal and depend only on the local electron densities in the vicinity of each atom, but not on the source and type of the atoms which provide it. Therefore, the same set of functions can be used to determine the energy of an atom in both pure and alloyed metals. This prevents the need for building new functions for alloyed systems.

Each of the pair (A–A, B–B, and A–B) interaction functions should change monotonically and vanish beyond certain distances while they should also be continuous and differentiable within these domains. To satisfy these conditions, cutoff distances are considered for both homoatomic and heteroatomic interactions. The interaction functions are also extrapolated for distances quite larger than their specific cutoff. This guarantees their continuity and differentiability. In the studies documented here, the value of cutoff distances for Cu–Cu, Ni–Ni and Ag–Ag were equal to 4.95 Å, 4.80 Å, and 5.55 Å, respectively.

Foiles et al. have shown that heteroatomic (A–B) interaction functions can be approximated by a geometric mean of the pure pair interactions [95], i.e.,

$$\Phi_{AB}(r) = \sqrt{\Phi_{AA}(r) \cdot \Phi_{BB}(r)}. \tag{3.3}$$

Further, a cutoff distance equal to the minimum value of the corresponding homoatomic interaction cutoffs was found a reasonable choice for the heteroatomic interactions, because these types of interactions vanish even at smaller distances.

It is worth pointing out that the EAM potential has been applied successfully to various metallic systems [92, 93, 95, 96]. Also metallic clusters have been studied with EAM and the results showed a good agreement with the available experimental data [3, 4, 97, 98, 99, 100].

3.3 Global Optimization: Basin Hopping Algorithm

The basin-hopping (BH) approach is basically similar to the Monte Carlo minimization algorithm of Li and Scheraga [101], and the conformational search method developed by Baysal and Meirovitch [102]. The BH was developed by Wales et al. [103]. The algorithm uses typical features of a PES, i.e., a large potential energy gradient and the low possible transition state energies or rearrangement barriers [104, 105], and transforms the highly complex PES into a modified PES with a staircase-like shape formed by basins. The staircase-like surface is built by performing the following transformation [105, 106]

$$\tilde{\mathrm{E}}(\vec{\mathrm{X}}) = \min\{\mathrm{E}(\vec{\mathrm{X}})\}. \tag{3.4}$$

Here, $\vec{\mathrm{X}}$ is a 3N dimensional vector containing all coordinates of N atoms in the system and $\tilde{\mathrm{E}}(\vec{\mathrm{X}})$ is the energy obtained after a local optimization starting from the initial structure $\vec{\mathrm{X}}$. This transformation of the PES lowers the barriers between different funnels but does not change the levels of minima. One should then search all basins of the transformed surface and find the deepest which corresponds to the global minimum structure of the system. This search is normally done by performing a canonical Monte Carlo simulation at a constant T.

The whole procedure can be summarized as follows. First, one considers an initial (random) structure and determines the local minimum of the corresponding funnel. This funnel will be marked by its local minimum from now on. Then, the algorithm jumps into another funnel by slight changes in the coordinates of the atoms, and repeats the local optimization to locate the related local minimum. This procedure is implemented in a Monte Carlo loop to search all funnels of the PES. In each step of Monte Carlo, the new structure is accepted when it has a lower energy in

comparison with the previous one, and if not, it will be accepted with a probability calculated by exp[(E_{old}-E_{new})/k_BT]. E_{old} and E_{new} are energies of the old and new structures, respectively. This conditional acceptance of the structures with higher energies allows the system to jump over barriers and hop between the funnels at a thermal energy of k_BT (in units of binding energy of the cluster dimer). T is just an imaginary temperature and should be adjusted to improve the efficiency of simulations. In our calculations, 5000 Monte Carlo iterations were performed for each cluster at T = 0.8.

The other adjustable parameters are the degree of perturbation or the maximum change of any Cartesian coordinate of the structure in each Monte Carlo iteration (STEP), and the tolerance on the binding energy of each atom (ASTEP) below which an angular step is also done for that atom. This means, if the binding energy of any atom is smaller than that of the most tightly bound atom multiplied by the ASTEP then that atom is randomly replaced on the sphere of radius equal to that of the atom furthest from the center of mass of the cluster. We found the best values of the STEP and ASTEP parameters to be 0.4 and 0.36, respectively. Another important parameter of Monte Carlo is the acceptance ratio which determines the number of accepted trials. Large values of acceptance ratio decreases the possibility of finding the real global minimum, and its small values make the optimization very slow. The best common value for this parameter is 0.5, which means 50% of all trials are accepted. To keep this acceptance ratio, the value of STEP is adjusted during the simulation.

The BH algorithm has been able to identify the global minimum structures for many different types of systems including pure Lennard-Jones clusters [105], clusters of transition and noble metals [107], and also binary clusters [108, 109, 110, 111]. Moreover, the BH has successfully located the difficult putative global minima of Lennard-Jones clusters at sizes 38, 75, 76, 77, and 98.

3.4 Analyses of Results

We utilize different analytical tools to extract physical/chemical insight from the putative global minimum structures found in our studies. These analyses consider either the structural or energetic properties of the nanoclusters. In this section we explain these analytical tools. It is noteworthy that our results make long listings

of total energies and atomic positions as functions of size, N, and/or composition, (m, n).

3.4.1 Energetic Analysis

There are many indicators for structural stability of nanoclusters and nanoalloys. The simplest one is the binding energy per atom E(N)/N. A more sophisticated measure of the relative stability of clusters is the second difference in the energy of a cluster, Δ_2(N), or the so called stability function. Δ_2(N) for a pure cluster of size N is given by

$$\Delta_2(\mathrm{N}) = \mathrm{E}(\mathrm{N}+1) + \mathrm{E}(\mathrm{N}-1) - 2\mathrm{E}(\mathrm{N}), \tag{3.5}$$

where E(N) is the energy of the N-atom cluster. The clusters which show peaks in Δ_2 are called magic sizes or clusters and are supposedly more stable in comparison to the neighboring sizes. The peaks in Δ_2(N) have also been correlated to those seen in the mass spectra of clusters [112, 113]. This correlation can be explained in the framework of the quasi-equilibrium model proposed by de Heer and his coworkers [114]. According to this model, the intensity of a cluster with N+1 atoms in a beam is given as $\mathrm{I_{N+1}} = \mathrm{I_N}\exp(\frac{\Delta_2 \mathrm{E_b(N)}}{\mathrm{kT}})$. $\mathrm{E_b}$ is the binding energy of the N-atom cluster and $\Delta_2\mathrm{E_b}$(N) is its second derivative. Obviously, if the N-atom cluster has a high value of $\Delta_2\mathrm{E_b}$(N) in comparison to its neighbors then it is also expected to have a high abundance peak in the mass spectra.

When it comes to the bimetallic nanoalloys, the concept of the stability function turns out to be more complicated, because here we should decide to compare which clusters with each other. There are different ways to define the stability function for a given N-atom nanoalloy with a (m, n) composition. We can compare clusters with the same size but different compositions (stoichiometries) using [115]

$$^{\mathrm{N}}\Delta_2 = \mathrm{E}(\mathrm{m}-1,\mathrm{n}+1) + \mathrm{E}(\mathrm{m}+1,\mathrm{n}-1) - 2\mathrm{E}(\mathrm{m},\mathrm{n}). \tag{3.6}$$

Here, E(m,n) is the total energy of the $\mathrm{A_mB_n}$ nanoalloy. We may fix the number of one sort of atoms, m or n, and compare clusters of nearby sizes with the same m or n. With this choice we come up with

$$^{\mathrm{n}}\Delta_2 = \mathrm{E}(\mathrm{m}+1,\mathrm{n}) + \mathrm{E}(\mathrm{m}-1,\mathrm{n}) - 2\mathrm{E}(\mathrm{m},\mathrm{n}) \tag{3.7}$$

and

$$^{\mathrm{m}}\Delta_2 = \mathrm{E}(\mathrm{m},\mathrm{n}+1) + \mathrm{E}(\mathrm{m},\mathrm{n}-1) - 2\mathrm{E}(\mathrm{m},\mathrm{n}). \tag{3.8}$$

The last possibility is to vary both m and n. That results in

$$^{mn}\Delta_2^{(1)} = E(m, n+1) + E(m-1, n) - 2E(m, n), \tag{3.9}$$

and

$$^{mn}\Delta_2^{(2)} = E(m+1, n) + E(m, n-1) - 2E(m, n). \tag{3.10}$$

We should calculate the Δ_2 functions for the global minimum structures of pure and alloyed Ag clusters to determine the magic sizes and/or compositions.

Although the number of total-energy minima for a given small cluster is limited and therefore the energy gap between two successive geometrical isomers is relatively large, for larger sizes these energy differences becomes very small. Large gaps in the energies of two next-lying isomers of a cluster can be interpreted as the relative thermal stability of the lower-lying isomer. In our analyses, we calculate the energy differences between the two lowest-lying (first and second) isomers ($E_{N.2} - E_{N.1}$) of pure and also bimetallic clusters, and plot the results versus the total number of atoms (N) or the composition (m or n for alloyed clusters). The peaks in these graphs correspond to the clusters with thermally stable lower isomers.

To compare the relative stability of nanoalloys with different compositions but of the same size, we should calculate their excess energies E_{exc} with respect to the pure reference clusters. The excess energy of A_mB_n nanoalloy is defined as [39, 1]

$$E_{exc} = E(m, n) - m\frac{E(A_N)}{N} - n\frac{E(B_N)}{N}. \tag{3.11}$$

In Eq. 3.11, $E(A_N)$ and $E(B_N)$ are the energies of the pure A and B clusters with N = m+n atoms, respectively. We choose the global minimum structures of the pure nanoclusters as references. With this choice, the excess energy is zero for pure clusters, and it will be negative if mixing of the atoms is preferred in the nanoalloys. The most stable cluster of a given size has the lowest value of the excess energy in comparison to all other compositions. Here, the high values of E_{exc} for pure A and B clusters does not mean that they are unstable. In our analyses we plot the excess energy of the Cu_mAg_n and Ni_mAg_n nanoalloys versus m.

3.4.2 Structural Analysis

The similarities or differences between the structures of two given clusters are important, because two similar clusters possibly have the same structures and accordingly

some similar properties. The similarity function is a quantitative measure for the similarity of two given clusters [3, 4]. To calculate the similarity function for two N-atom clusters, we should first determine the radial distance of each atom in the first cluster using

$$r_i = |\vec{R_i} - \vec{R_0}|, \tag{3.12}$$

where $\vec{R_i}$ is the vector position of atom i and $\vec{R_0}$ is the geometric center of the cluster given by

$$\vec{R_0} = \frac{1}{N}\sum_{j=1}^{N}\vec{R_j}. \tag{3.13}$$

The same quantity r_i' is calculated for the atoms of the second clusters. The two sets of $\{r_i\}$ and $\{r_i'\}$ are then sorted in increasing order. The similarity function is now given by

$$S = \frac{1}{1+\frac{q}{u_l}} \tag{3.14}$$

with $u_l = 1$ Å. In Eq. 3.14, q is defined as

$$q = [\frac{1}{n}\sum_{i=1}^{n}(r_i - r_i')^2]^{1/2}. \tag{3.15}$$

S will approach one if the two clusters are similar.

We can also use the similarity function to study the growth patterns of nanoclusters. First, we should calculate the similarity function of clusters with N-1 and N atoms. To do so, all N possible cases of removing one atom from the N-atom cluster are considered and their similarity functions are determined in comparison with the cluster with N-1 atoms. We take the highest value as the similarity function of the two clusters, and plot this quantity for a range of cluster sizes. A sudden drop in the similarity function of a given N-atom cluster corresponds to an irregular growth.

It is convenient to analyze the mixing patterns and chemical orderings in nanoalloys by means of the bond order parameter [116]. For an A_mB_n nanoalloy, this parameter is defined as:

$$\sigma = \frac{N_{A-A} + N_{B-B} - N_{A-B}}{N_{A-A} + N_{B-B} + N_{A-B}} \tag{3.16}$$

where N_{ij} (i, j = A, B) is the number of nearest neighbor i–j bonds. σ should be positive if phase separation (segregation) takes place in the nanoalloy. It is almost zero when disordered mixing occurs, and negative when mixed and onion-like phases both exist.

The mixing energy is another quantitative measure for characterizing the mixing propensity of atomic species in a nanoalloy [28, 38]. This quantity is used to study the (structural and energetical) effects due to the substitution of some atoms in a pure cluster with other types of atoms. The mixing energy of an A_mB_n nanoalloy with a given configuration and total energy of $E(m, n)$ is defined as:

$$E_{mix} = E(m, n) - [E(A_m/A_mA_n) + E(B_n/B_mB_n)] \tag{3.17}$$

where $E(A_m/A_mA_n)$ is the total energy of a structure made by considering the m A atoms fixed at their positions as in the A_mB_n nanoalloy, but the n B atoms substituted with A atoms. These n A atoms do not contribute with their interatomic interactions to the total energy, but they are felt by the m A atoms whose energy is calculated. E_{mix} is clearly large and negative for clusters with mixed phases of chemical ordering. Based on the mixing energy we can also calculate the mixing coefficient M:

$$M = \frac{E_{mix}}{E(m, n)} \times 100\%. \tag{3.18}$$

The mixing coefficient gives the degree of contribution of the mixing energy in the total energy.

Chapter 4

Pure Ag Nanoclusters

4.1 Introduction

Theoretical studies of the static polarizabilities and optical absorption spectra of Ag_N clusters (with N = 2–8) have been carried out by Idrobo et al., using time-dependent DFT calculations [117]. They found that the static polarizabilities of clusters with less than seven atoms exhibit even-odd oscillations, but for both Ag_7 and Ag_8 they have close values which are noticeably lower. This behavior was interpreted as the effect of structural transition from 2D to 3D at N = 7. According to DFT simulations, layered structures dominate for Ag_N clusters with $9 \leq N < 16$, but for $N > 16$ quasi-spherical compact structures are more favored [118]. This shape evolution causes great changes in the cohesive energies, ionization potentials, and polarizabilities of the clusters. In another study of Ag clusters at sizes smaller than 13 atoms, Lee and co-workers used both DFT and *ab initio* calculations and explained the structural change from 2D to 3D at N = 7 in terms of a large energy gap between $4d$ and $5s$ orbitals of Ag which forbids hybridization [119].

Global optimization by using genetic algorithms and Gupta potential have predicted the global minimum structures of Ag clusters at sizes N = 6, 7, 12, 13, 14, 19, 38, 55, and 75 atoms [120]. The results showed that Ag clusters prefer icosahedral structures at all these sizes except at N = 38 and 75, for which *fcc* truncated octahedral and decahedral structures, respectively, are the global minima. Zhao et al. combined GA with the minimal parameter tight-binding potential to search the PES of Ag clusters with up to 21 atoms [27]. According to their results, the icosahedral growth pattern starts from N = 11. Magic sizes were found at N = 2, 8, 14, 18, and

20, for which electron shell closure is possible.

Two versions of Gupta potential with different parameterizations were implemented in the *aufbau/abbau* global optimization algorithm to determine the structures of Ag clusters with N $\leq$ 150 atoms [5]. In the same study, two versions of EAM potential were also used with the same optimization algorithm to locate the stable structures of sizes 2 to 60. Different potentials gave different structures as the global minimum of a given size, and it was attributed with an interchange in the order of energetic low-laying structures (isomers). The clusters growth was characterized as decahedral with islands of icosahedral and truncated octahedral. In global optimization of Ag_N clusters with N$\leq$80, Shao et al. employed a random tunneling algorithm and two different, Gupta and Sutton-Chen, potentials [121]. Lowest-energy structures determined by the two potentials were different, especially at small sizes (N = 15–47). The structures optimized by Gupta potential were highly strained with a general tendency toward disorder motifs, whereas structures given by Sutton-Chen had less strain and favored more ordered geometries. Molecular dynamics simulations of Ag clusters were also performed, using many-body potentials of Rosato, Guillopé, and Legrand (RGL) [122]. In the growth process of clusters with less than 100 atoms, icosahedral (Ih) and truncated decahedral motifs were always recovered, while various structures competed for the clusters at larger sizes of about 150.

4.2 Results and Discussion

In this section we will report the results of our study on the Ag_N clusters with N = 2 to 100 atoms. To check the validity of our approach, first we compare the dimer bond length calculated by using EAM (2.4433 Å) with the experimental value (2.53 Å) and find them in agreement [123, 124]. It is also in agreement with the value given by DFT calculations (2.49 Å) [117].

4.2.1 Structural Properties

Fig. 4.1 presents the geometries of the lowest-energy isomers found for some selected sizes of Ag clusters, and table 4.1 lists all the symmetry point groups of the three low-energy isomers of all considered sizes. For N = 6 and 7, our putative global minima (GM) are the octahedron and pentagonal bipyramid, respectively, and for N = 12, 13, 14, and 19 the GM are based on variants of the icosahedral structure.

All these are in agreement with the previous experimental and theoretical studies [5, 60, 120]. But some discrepancies are also seen when we compare our results for N = 4–6 with the planar structures determined by DFT calculations [118]. The reason for this contrast is that the DFT methods consider all many-body interactions simultaneously, while the model potentials which all contain a pair-interaction term have a tendency toward close packing.

Our results show that many types of disordered structures are the global minima morphologies for clusters of N = 20 to 37 atoms, which are mainly formed by multi-interpenetrating 13-atom icosahedra. But at N = 38 we find the *fcc* truncated octahedron as the lowest-energy configurations, again in agreement with all other available studies [5, 120, 107]. The structure of Ag_{39} is the capped 5-fold pancake (c-pc5) which makes a part of the 55-atom icosahedra (Ih_{55}). This geometry is the base motif for N = 40–54, where extra atoms add to its surface and then at N = 55 the complete icosahedra Ih_{55} forms as the global minimum structure. The Ih_{55} structure has also been detected in experiments [60].

From size N = 56 to 74, atoms are added to the surfaces of the Ih_{55}, until the formation of the decahedron at N = 75. Interestingly, the global minimum of Ag cluster with N = 76, 81, 82, 83 atoms are a cut of *fcc* crystalline structure, and for N = 77 the GM has a disorder motif. The structures of lowest-energy isomers for N = 78 to 80 are made by the 75-atom decahedron with extra atoms added to the surfaces. In contrast, the lowest-energy isomers of N = 85–98 have a completed Ih_{55} and extra atoms added to the surfaces with a trend for completing the new shell of atoms. We find interesting exceptions for N = 96, 99, and 100, for which we have located uncompleted decahedra as the global minima.

Although the comparison between the symmetry point groups of neutral and ionized clusters are not always an accurate test, it is still helpful. Combined experimental/theoretical studies have indicated the preferences of the first and third lowest-energy isomers of the Ag_{19}^{+} clusters for the icosahedra structures with C_s and D_{5h} symmetry point groups [60]. We also found also the same, but with a reversed order of point groups (Table 4.1). The icosahedra that we found for neutral Ag_{55}, has also been measured in experiments for both cationic and anionic clusters of Ag_{55} [60, 125].

We find that our results for the structures and symmetries of Ag clusters are very similar to those determined by Gupta and specially the EAM potentials combined

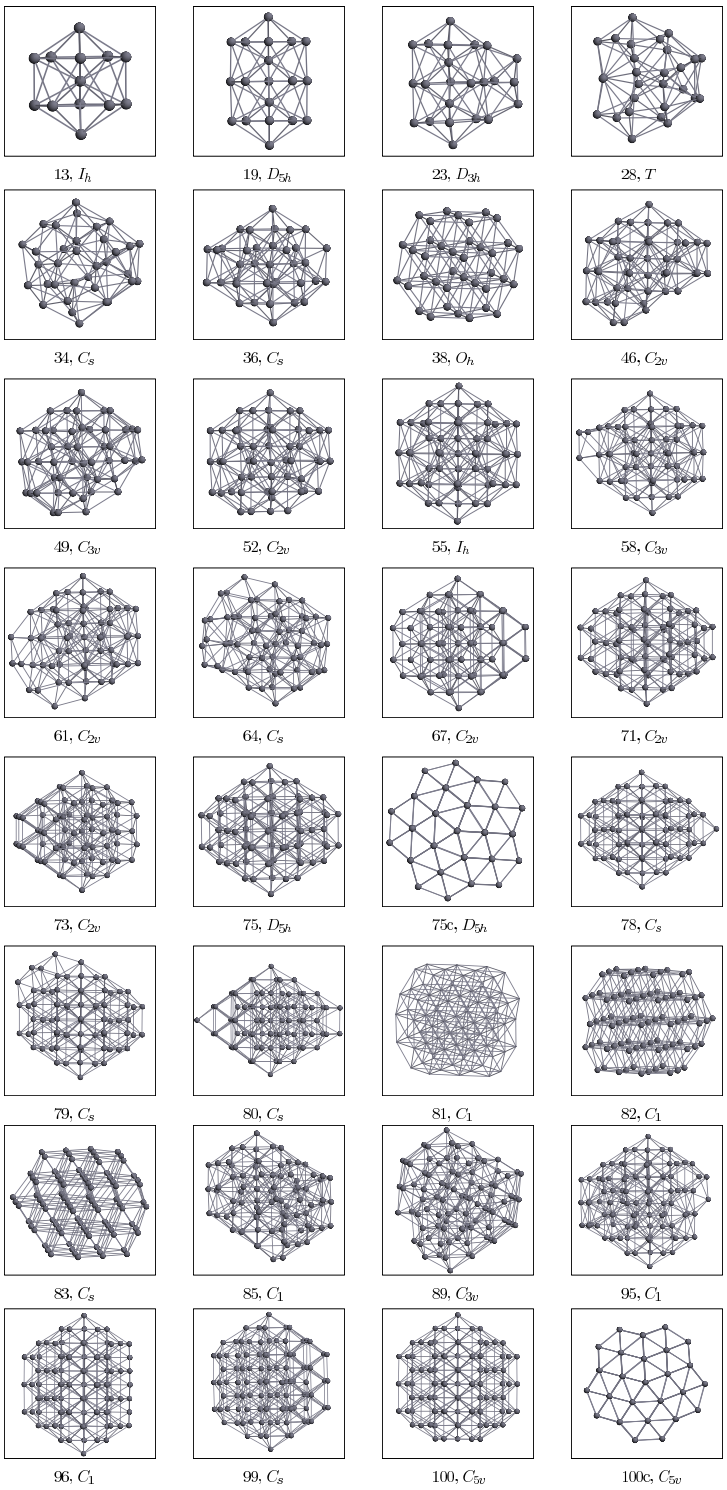

Figure 4.1: Structures and symmetries of the global minimum structures of some selected Ag_N clusters with N = 2 to 100 atoms. The structures are determined by using the EAM potential and basin-hopping algorithm.

with the *aufbau/abbau* algorithm [5]. The noticeable differences are as follows. At N = 23, the symmetries of Ag clusters in our study are D_{3h}, D_{3h} and C_2, in order of the first to the third lowest-energy isomers. But the combination of the EAM and the *aufbau/abbau* has given this set of symmetries as D_{3h}, C_2 and C_s. We find the other noticeable difference for the third isomer of Ag_{38} where, according to our results, it is a structure with C_s symmetry but the *aufbau/abbau* gives a C_{5h}.

As we are going to consider the nanoalloys of Ag with Cu and Ni in the next chapters, it may be useful to compare the symmetries of Ag clusters with those of the Cu and Ni clusters. We compare our results with those Cu and Ni clusters which were determined with the same version of EAM potential but different optimization algorithms [4, 3]. Our results show that the structures of the lowest-energy isomer of Ag clusters and their symmetries at N = 13, 19, 23, 28, 38, 55 and 75 are completely similar to those of Cu and Ni. The differences for these sizes appear for the second and third isomers. The second and third isomers of Ag_{13} and Ni_{13} have all C_s symmetry, whereas for Cu_{13} they are D_{5h} and O_h, respectively. We find the second noticeable difference for the third isomers of N = 19, where both structures of Ag and Ni are with C_s symmetry and that of Cu has C_1. At N = 38, again the second isomers of Ag and Ni have the same symmetries, i.e., C_{5v}, but the Cu cluster structure has C_5. For the third isomers of this size, N = 38, the symmetries point groups are C_s, C_{5v} and C_5 for Ag, Ni and Cu clusters, respectively. Only the third isomer of 55-atom Ag cluster has a different symmetry point group which is C_1, while those of Cu and Ni are both C_s. The clusters of sizes N $\geq$ 80 show more identical symmetry point groups only if we consider the Ag and Ni clusters.

To compare the similarity of the clusters of these three metals more quantitatively, we employ the concept of similarity function introduced in Sec. 3.4.2. Before proceeding with this comparison, we should mention that the coordinates of atoms in the Cu and Ni clusters have been scaled with respect to their lattice constants in order to compensate for the differences in bond lengths. Figs. 4.2 and 4.3 show the similarity functions for Ag compared with Cu and Ni clusters of sizes N = 2 to 100. The structures of Cu and Ni clusters are taken from Refs. [3] and [4]. The general behavior and the values of the similarity functions imply that the shape of Ag clusters resemble more Cu clusters. The Ag and Cu clusters at small sizes show higher values of similarity functions, while for Ag and Ni they are considerably smaller. But for sizes N $>$ 81, the similar structures are realized more often for the

Ag and Ni clusters than for Ag and Cu.

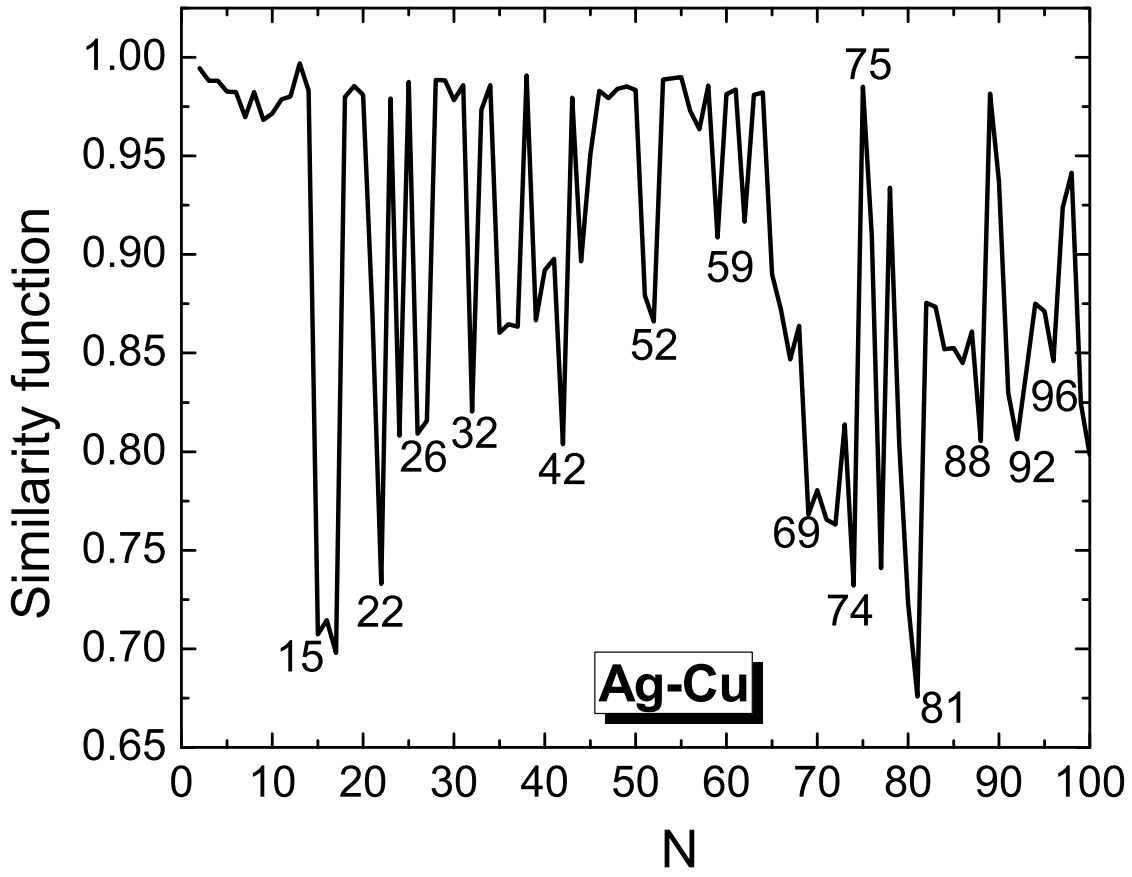

Figure 4.2: The similarity function of Ag_N clusters with N = 2–100 atoms compared to Cu_N clusters. The structures of Cu clusters have also been defined by the EAM potential which was implemented in the *aufbau/abbau* global optimization algorithm [3].

It is known that the types and ranges of the potentials, used in modeling the interactions between atoms in a cluster, can affect the determined structures [126]. To investigate this effect in our calculations, we have shown the similarity functions of the global minimum structures of Ag clusters determined by the EAM and Gupta potentials in Fig. 4.4. The structures of the latter clusters are taken from Ref. [5]. The results show that all clusters determined by the two methods are only similar at small sizes of $N < 15$. After this size, although many similar clusters are seen, the number of structurally different clusters increases considerably. This dissimilarity of the clusters increases even for larger clusters with $N > 80$. We should also note

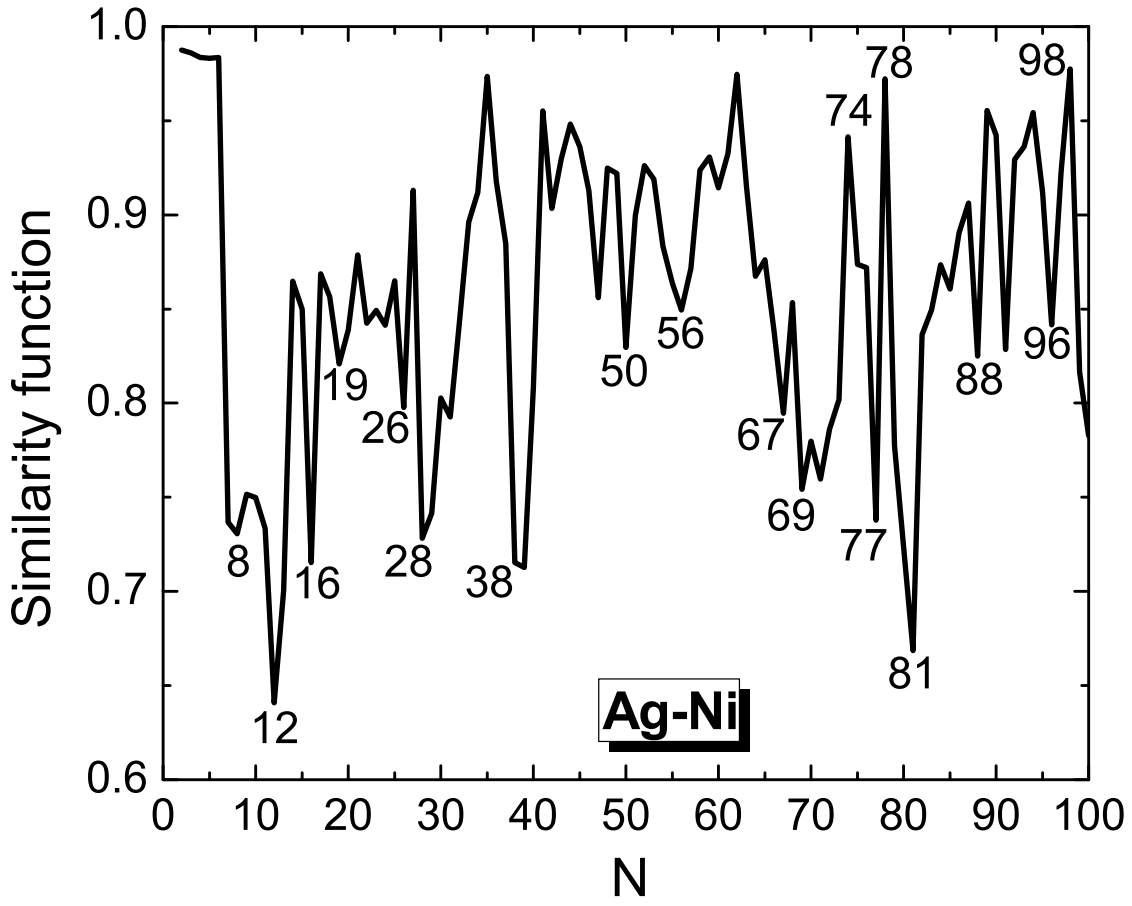

Figure 4.3: The similarity function of Ag_N clusters with N = 2–100 atoms compared to Ni_N clusters. The structures of Ni clusters have also been determined by the EAM potential which was implemented in the *aufbau/abbau* global optimization algorithm [4].

that the two sets of the putative global minima were determined by different global optimizations. This can also be a cause of some dissimilarities, especially at large sizes where locating the global minima is more challenging.

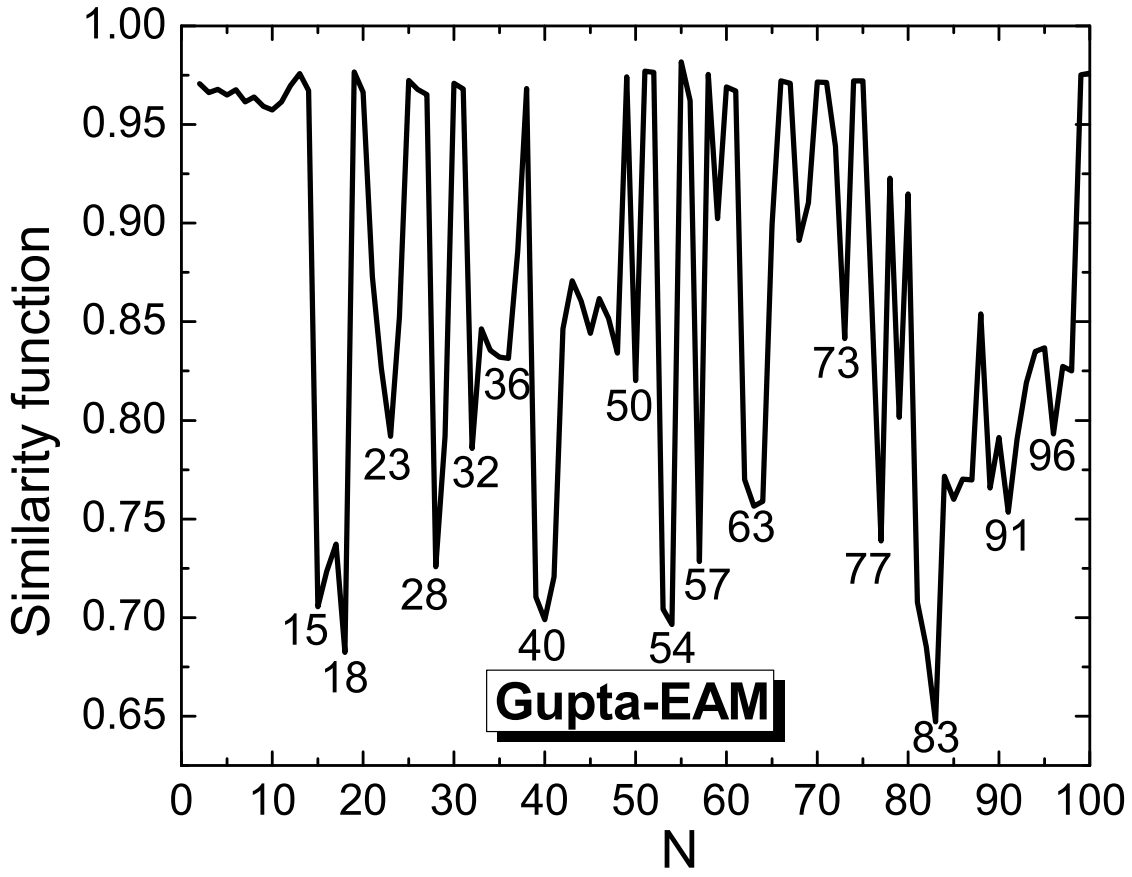

Figure 4.4: The similarity function obtained when comparing the global minimum structures of Ag_N determined by the EAM potential implemented in the BH global optimization algorithm (in this study) and by the Gupta potential implemented in *aufbau/abbau* in Ref. [5].

4.2.2 Energetic Properties

In this section we consider and analyze the energetic properties of Ag clusters. Fig. 4.5 shows the binding energy per atom ($E_b = -\frac{E_N}{N}$) for the three lowest-energy isomers of Ag clusters. At sizes smaller than N = 19, the binding energy of three isomers is completely separated, but as the size increases the differences become

negligible. For all three isomers we find some features at some particular sizes, e.g., N = 13, 19, 55, and 75.

The unsmooth behavior of binding energy per atom suggests that some clusters may exist which are more stable than others. We have identified these clusters by calculating the stability functions of the putative global minima of Ag clusters using Eq. 3.5. The results are depicted in Fig. 4.6 and the most stable clusters, or the so-called magic sizes, are marked with their number of atoms. According to Fig. 4.6, the most pronounced peak is found for Ag_{75} and further peaks are seen for many other sizes, i.e., N = 13, 19, 23, 28, 38, 46, 49, 55, 64, 71, 78, 80, and 89. The stability of clusters with 13, 19, 55, and 75 atoms are in agreement with the small kink (slightly higher values) which we found for their binding energies per atom.

We identify the magic sizes of different types of structures which include decahedral (N = 75 and 71), icosahedral (N = 13, 19, 23 and 55) and also *fcc* truncated octahedral (N = 38). Additionally, our results contrast those of the previous studies which did not find stability peaks for clusters of N = 23 and 28 sizes.

In comparison to the stability function of Ni clusters, the Ag clusters with N = 39, 77, 79, and 95, atoms are not magic sizes, while these sizes of Ni clusters have enhanced stabilities. On the other hand, the magic sizes of Ag_N with N = 38, 78, 80, and 96 were not identified particularly stable for Ni clusters [4]. For Cu clusters, N = 92 and 95 correspond to magic clusters, while they are not stable for Ag [3]. But the case is inverse for N = 38, 43, 78, 89, and 96. If we compare the Ag and Au clusters, their stability functions are even far away from each other and have many more differences [127].

The (thermal) stability of Ag clusters can also be examined by calculating the energy differences between the first and second lowest-energy isomers. This quantity is plotted in Fig. 4.7 for all considered Ag_N clusters versus the total number of atoms (N). The stable clusters are recognized by high peaks and many of them are marked by their sizes.

In Fig. 4.7 many clusters with high values of the stability function (Fig. 4.6) show to also be thermally stable. But we notice some differences. For instance, according to Fig. 4.7 the Ag_{38} cluster is not stable anymore, whereas Ag_{36}, Ag_{39}, Ag_{95} and Ag_{97} are now given thermally stable. In comparison with previous results for Ag clusters modeled by using Gupta potential [5], we see many similarities in the results of the two methods for the energy difference between the two lowest-laying isomers.

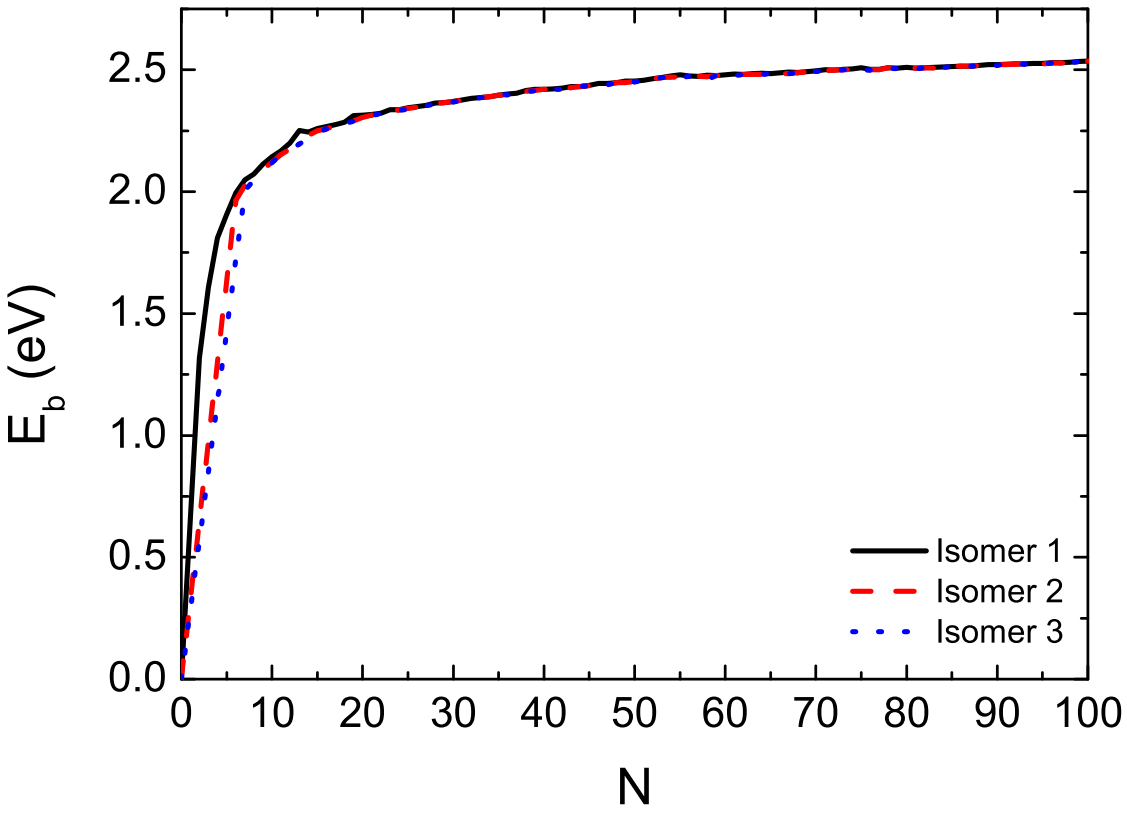

Figure 4.5: Binding energy per atoms of three lowest-energy isomers of Ag_N clusters (with N = 2 to 100) vs the number of atoms.

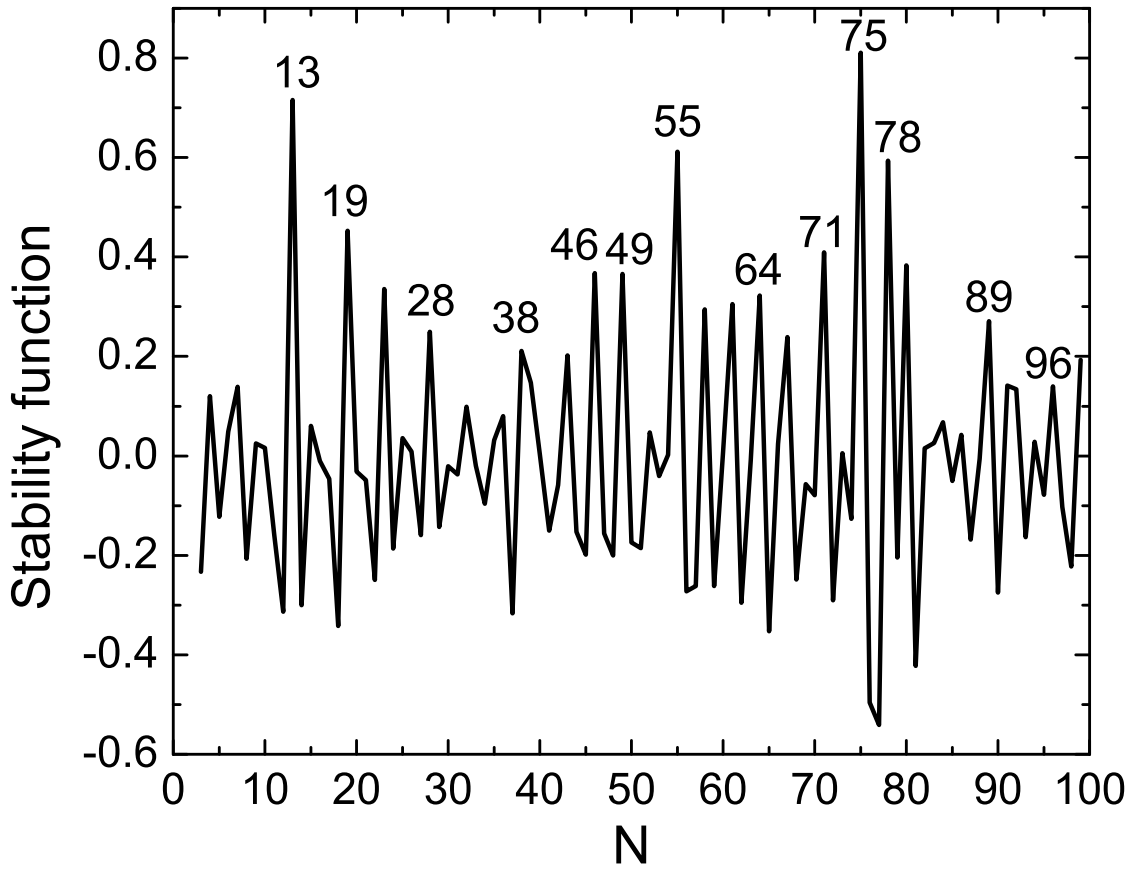

Figure 4.6: Stability function of Ag_N clusters with N = 2–100 atoms. Clusters of enhanced stability are singled out with high peaks. The sizes of magic clusters are denoted on related peaks.

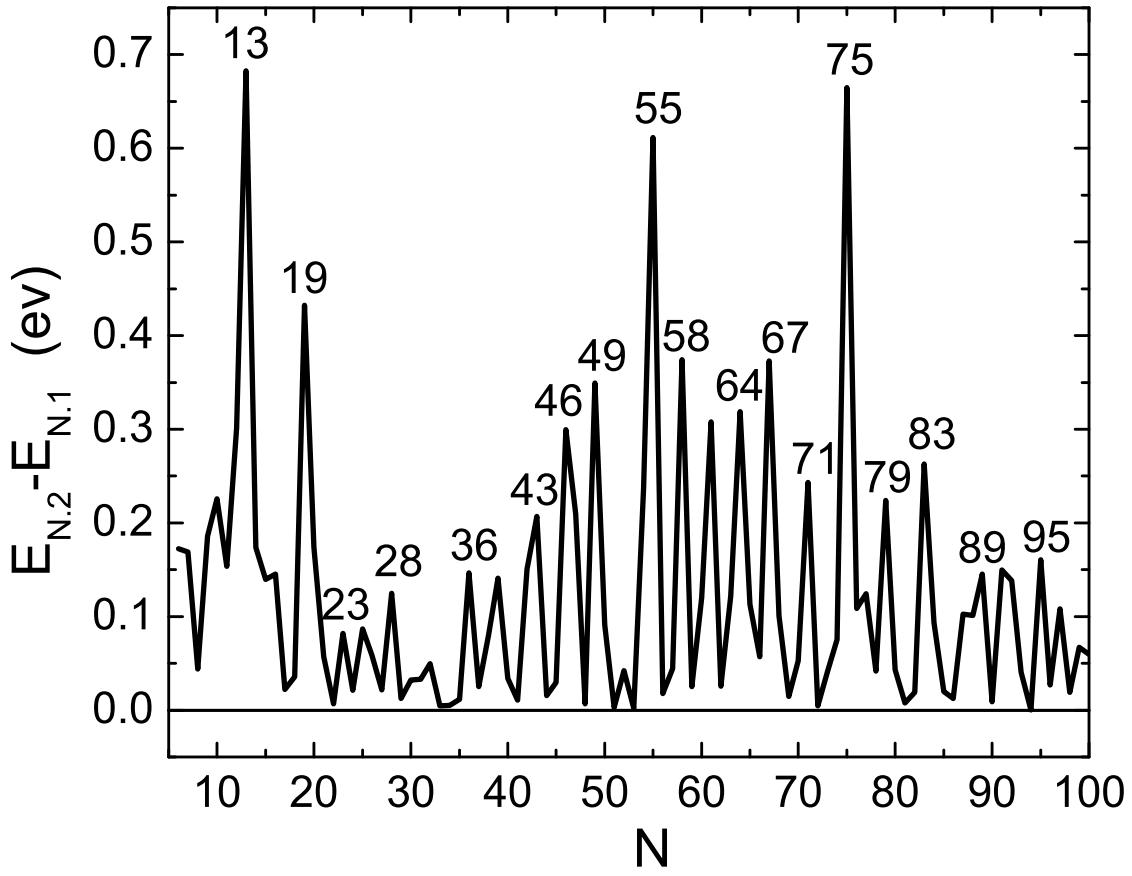

Figure 4.7: Differences between the energies of first and second lowest-lying isomers of Ag clusters vs the total number of atoms (N).

The interesting differences are the enhanced stability of the Ag_{38}, Ag_{63} and Ag_{90} clusters optimized by the Gupta potential, which we do not find in the results of EAM. Moreover, Ag_{28} and Ag_{36} are determined thermally stable by EAM but not the Gupta potential. The Ag_{38} cluster, which is stable according to the stability function but not the isomers energy differences, is shown to have two lowest-lying isomers with very closed values of total energy. For this size the second isomer also has a symmetric structure, i.e., a 5-fold c-pc5_{39} with one uncapped side.

4.2.3 Growth Patterns

An important issue in the study of nanoclusters is understanding the way that they grow in size, and finding if the addition of one atom to the cluster with N-1 atoms can result in the N-atom cluster without causing large structural changes. Here we consider the growth process from a static point of view and neglect the dynamic and kinetic effects, although they are very important in experiments.

The structures of magic clusters provide us with basic information about the growth pattern. But first we should explain the two possible icosahedral growth patterns, because the majority of structures which we have found are icosahedra. In the first pattern of icosahedral growth, MIC/Mackay, new atoms are added to the top of the edges and vertices of the first Mackay icosahedron Ih_{13} [128, 129, 126, 130, 131]. The addition of more atoms in this way results ultimately in the second Mackay icosahedron, i.e., Ih_{55}. In the second growth pattern, TIC/Polyicosahedral or face-capping, new surface atoms sit on top of the atoms at the center of each face (T sites) [129]. This growth leads to the a rhombic tricontahedron for the 45-atom cluster. The structures formed in the TIC/Polyicosahedral growth have shorter average bond lengths and thus higher strain energies. Therefore, they are only expected to be favored at small sizes.

Martin et al. developed the umbrella model to explain the above icosahedral shell filling [132]. According to this model, the magic sizes are realized for N = 19, 24, 28, 32, 36, 39, 43, 46, 49, and 55 if the clusters grow by covering the Ih_{13} and following the MIC/Mackay pattern. But when the TIC growth dominates, then the expected magic sizes are N = 19, 23, 26, 29, 32, and 34.

The set of our magic sizes for the Ag clusters (Figs. 4.7 and 4.6) show that they grow first according to the TIC pattern from N = 13 to N = 26. Then, they follow the MIC/Polyicosahedral growth which ends to the formation of the second

complete icosahedron found at N = 55. Here, we find an exception for N = 38 which has *fcc* truncated octahedron structure. For clusters of sizes N = 56 to 71, the set of magic sizes coincide with those expected for a TIC growth, i.e., N = 58, 61, 64, 67, and 71 [128]. At larger sizes (N$\geq$ 71), the stable clusters given by the energy differences of the first and second isomers agree with the MIC pattern (N = 71, 83 and 92). These continuous changes between different types of icosahedral growth, and also the structures that we have recognized, suggest that Ag clusters grow mainly by forming icosahedral motifs but with islands of decahedral and octahedral structures. By islands we mean those few clusters which have different structures, i.e., decahedra and octahedra instead of icosahedra.

The competition between MIC and TIC patterns, and also between icosahedral, polyicosahedral, decahedral and even octahedral structures are tokens of a complicated growth for the silver clusters. To understand these effects more, we should determine and analyze the minimum coordination number of atoms in the Ag clusters. The value of minimum coordination number for a given cluster indicates whether the new atom is added to the surface or inner regions. The low values of the coordination number, i.e., 3 or 4, are due to the addition of the new atoms to the surfaces of the clusters, while the higher values, 5 or 6, indicate that atoms are added to the inner parts. We plot this quantity for the Ag clusters versus their sizes (N) in Fig. 4.8. As illustrated there, the minimum coordination number drops specially after those sizes which have symmetric structures, i.e., at N = 14, 20, 39, 56, and 76. This shows that for these clusters the growth continues by adding the new atoms to the surfaces of smaller symmetric clusters. It is completely in agreement with the structures that we found for these clusters. The same behavior is also found for many other sizes such as N = 15–17, 20–22, 24, 40, 41, 72, 76, 80, 81, and 96. High coordination numbers are given for clusters with N = 25–39, 51–55, 58–61, 66–71, 82–95, and 98–100 atoms. Most of these clusters do not have symmetric structures.

Not surprisingly, our results for the minimum coordination number of the Ag clusters are similar to those of the same clusters which were modeled by the Gupta potential [5]. Moreover, the minimum coordination number of Ag clusters more resembles that of the Ni than Cu clusters, while the latter type takes higher coordination numbers and shows a growth mainly from the inner parts of structures [3, 4].

Getting an insight into the cluster growth is also possible by calculating the

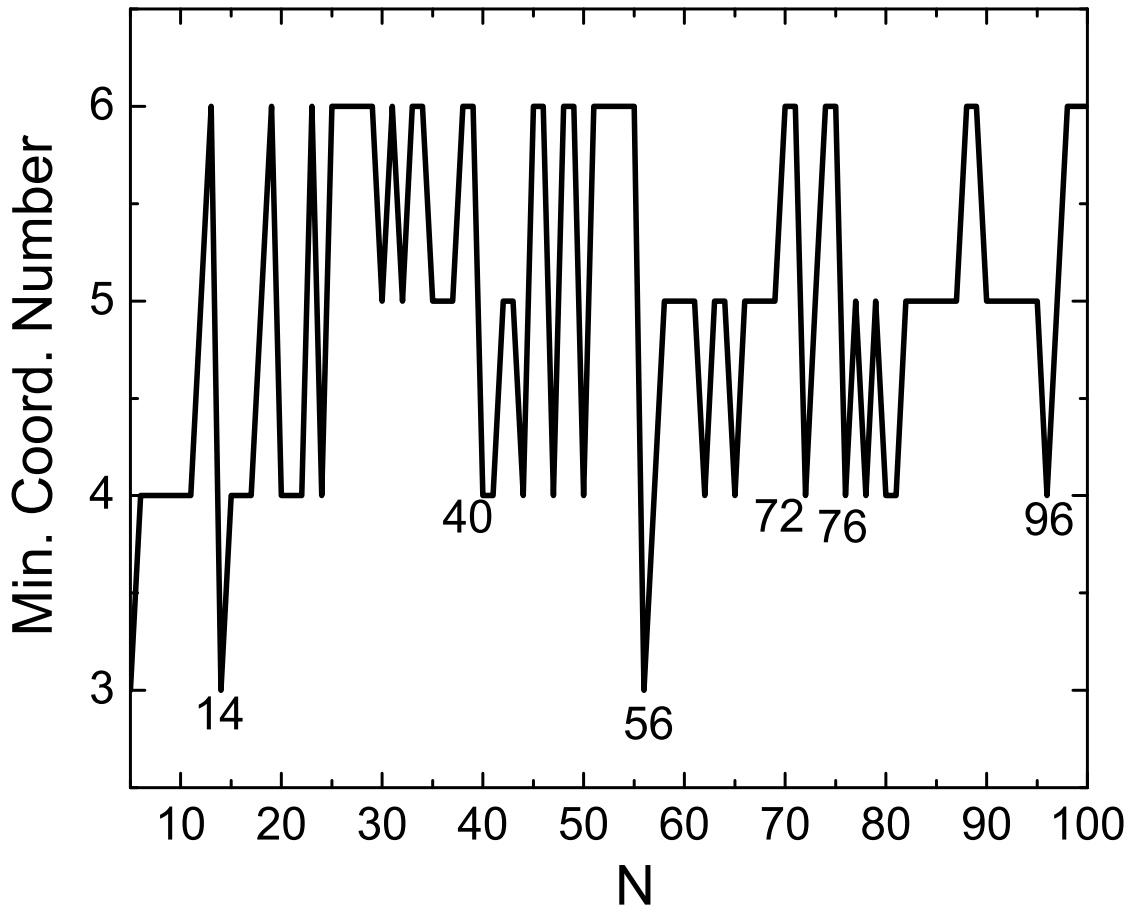

Figure 4.8: The Minimum coordination number for the GM of Ag clusters vs the number of atoms (N).

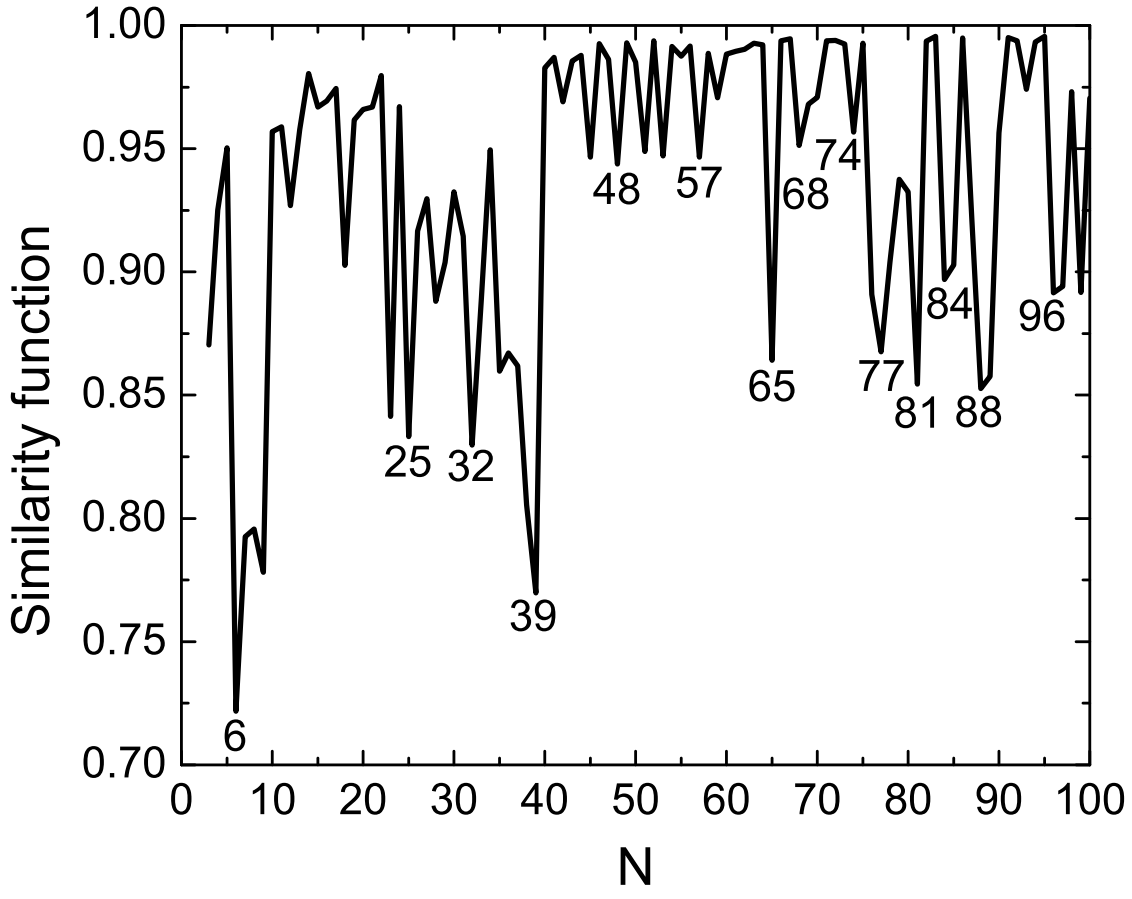

Figure 4.9: The similarity functions of Ag clusters with N and N-1 atoms. This shows the structural changes during the growth procedure.

similarity function for the clusters with N and N-1 atoms (see Sec. 3.4.2). Fig. 4.9 depicts these functions for the Ag_N clusters of sizes N = 3 to 100. Irregular growth and sudden structural changes are apparent for many clusters in the low values of their similarity functions. This happens more frequently for $N < 39$ and $N > 65$. The reason for the smoother growth in the size range of N = 11 to 22 is that all these structures are based on variants of Ih_{13}. We correlate the drops in the similarity functions of 23- and 25-atom clusters to the changes in the growth pattern from TIC to MIC. The other sizes for which clusters grow more smoothly include N = 40–64 and N = 75. The first region is dominated by icosahedral structures and the second with decahedral.

N	N.1	N.2	N.3	N	N.1	N.2	N.3	N	N.1	N.2	N.3
2	$D_{\infty h}$			35	C_s	D_3	C_{2v}	68	C_1	C_1	C_s
3	D_{3h}			36	C_s	C_1	C_2	69	C_1	C_1	C_1
4	T_d			37	C_s	C_{3v}	C_2	70	C_s	C_1	C_1
5	D_{3h}			38	O_h	C_{5v}	C_s	71	C_{2v}	C_5	C_{5v}
6	O_h	C_{2v}		39	C_{5v}	C_5	C_{4v}	72	C_s	C_1	C_1
7	D_{5h}	C_{3v}	C_2	40	C_s	C_s	C_1	73	C_{2v}	C_s	C_S
8	D_{2d}	C_s	D_{3d}	41	C_s	C_s	C_1	74	C_{5v}	C_1	C_s
9	C_{2v}	D_{3h}	C_{2v}	42	C_s	C_1	C_{2v}	75	D_{5h}	C_s	C_s
10	C_{3v}	C_2	C_{2v}	43	C_s	C_s	C_1	76	C_1	C_s	C_1
11	C_{2v}	C_2	C_2	44	C_1	C_1	C_s	77	C_s	C_1	C_{2v}
12	C_{5v}	D_{2d}	C_1	45	C_s	C_1	C_1	78	C_s	C_1	C_s
13	I_h	C_s	C_s	46	C_{2v}	C_s	C_1	79	C_s	C_1	C_1
14	C_{3v}	C_{2v}	C_1	47	C_1	C_1	C_1	80	C_s	C_1	C_s
15	C_{2v}	D_{6d}	C_{2v}	48	C_s	C_s	C_1	81	C_1	C_s	C_1
16	C_s	C_s	C_1	49	C_{3v}	C_s	C_s	82	C_1	C_s	C_s
17	C_2	C_s	C_s	50	C_s	C_s	C_s	83	C_s	C_1	C_1
18	C_s	C_{5v}	C_s	51	C_s	C_s	C_1	84	C_s	C_1	C_s
19	D_{5h}	C_1	C_s	52	C_{2v}	C_{3v}	C_s	85	C_1	C_1	C_1
20	C_{2v}	C_s	D_{3d}	53	C_{2v}	D_{5d}	C_{2v}	86	C_s	C_1	C_1
21	C_1	C_{2v}	C_s	54	C_{5v}	I_h	C_{2v}	87	C_s	C_1	C_2
22	C_1	C_s	C_s	55	I_h	C_s	C_1	88	C_s	C_1	C_1
23	D_{3h}	D_{3h}	C_2	56	C_{3v}	C_s	C_s	89	C_{3v}	C_s	C_1
24	C_{2v}	C_s	D_3	57	C_s	C_s	C_s	90	C_s	C_1	C_1
25	C_3	C_s	C_1	58	C_{3v}	C_s	C_1	91	C_s	C_s	C_1
26	C_1	T_d	C_{2v}	59	C_{2v}	C_1	C_1	92	C_{3v}	C_1	C_1
27	C_s	C_s	C_2	60	C_s	C_s	C_s	93	C_1	C_1	C_1
28	T	C_1	C_{3v}	61	C_{2v}	C_1	C_1	94	C_1	C_1	C_1
29	C_3	C_{2v}	C_2	62	C_1	C_1	C_1	95	C_1	C_1	C_1
30	C_s	C_{2v}	C_1	63	C_1	C_1	C_s	96	C_1	C_1	C_s
31	C_3	C_{2v}	C_s	64	C_s	C_1	C_1	97	C_1	C_1	C_1
32	C_{2v}	D_3	C_1	65	C_{2v}	C_1	C_s	98	C_s	C_1	C_1
33	C_2	C_s	C_s	66	C_s	C_1	C_1	99	C_s	C_{2v}	C_1
34	C_s	C_s	C_s	67	C_{2v}	C_s	C_s	100	C_{5v}	C_1	C_s

Table 4.1: Symmetry point groups of three lower-energy isomers of Ag_N clusters. N.i (i = 1,2 and3) points to the *i'th* isomer.

Chapter 5

Cu–Ag Nanoalloys

5.1 Introduction

Theoretical investigations of the global energy minimum structures of Cu–Ag nanoalloys have mostly been performed by using the Gupta potential or the second moment approximation to the tight binding (SMATB) method [2, 39, 133, 134]. All these studies have considered the clusters with N = 34, 38, 40 [2, 39, 133], and in one case the N = 98 atoms [134]. The global optimization method of all these studies was the genetic algorithms (GA) and the only exception is the one performed by Barcaro et al. [2], in which the authors used three different algorithms, i.e., the basin-hopping (BH), the energy-landscape paving, and the parallel excitable walkers algorithm, to determine the structures of the global total-energy minima. The predicted global minimum structures in all of these studies were core–shell polyicosahedra. The results suggested the Cu_7Ag_{27} cluster to be the most stable stoichiometry of size N = 34. This is the only stoichiometry of the size for which a complete pentagonal bipyramid can form by the seven Cu atoms in the core and a single layer of Ag atoms covers it as the shell.

Rossi et al. [39] and Rapallo et al. [133] investigated different stoichiometries of Cu–Ag nanoalloys of size N = 38 and determined Cu_8Ag_{30} as the most stable cluster. On the other hand, Cu_9Ag_{29} has the highest stability for this size, according to the results of Núñez and Johnston [134]. In the studies of Barcaro et al. and also Ferrando et al. [2, 73], the global minimum (GM) structures of Cu–Ag clusters with N = 40 were found of different motifs including capped decahedral (c-Dh) and 5- or 6-fold pancakes (c-pc5 or c-pc6). The enhanced stability of c-pc5 $Cu_{13}Ag_{27}$ was

determined by comparing the excess energies of all clusters of the size.

For N = 98, different types of icosahedron structures, such as incomplete anti-Mackay, Mackay, and poly-icosahedron, have been identified as the GM of the Cu–Ag nanoalloys [134], whereas Leary tetrahedra were predicted as the GM structures of palladium-platinum and platinum-aluminum clusters with the same number of atoms [135, 136].

Baletto et al. performed molecular dynamic simulations for deposition of Ag on a core made of Cu atoms. They found that at intermediate to high temperatures (300–600 K) the structures have a perfect core–shell ordering of atoms [137, 138]. The authors have also reported that a face–centered cubic core of Ag can result in the formation of Ag–Cu–Ag multishell structures at different temperatures, but deposition on Ih cores gives only core–shell structures [139].

Lattice gas models have also been used in numerical studies of large Cu–Ag clusters with some hundreds to thousands of atoms. Segregation isotherms were determined for cuboctahedral and icosahedral lattices [140, 141]. The Monte Carlo simulations with the same lattice-gas model for the Cu–Ag nanoalloys showed various stages of segregation phases for different Ag concentrations [142].

5.2 Results and Discussion

From the literature review given in Secs. 2.5 and 5.1 we see that computational studies of Cu–Ag nanoalloys have only been done for very few selected sizes. In our studies we performed an exhaustive search for the GM structures of all stoichiometries of Cu_mAg_n nanoclusters with N = m+n = 2 to 60. This required more than 1800 calculations from which many took more than 10 days. The results of this cumbersome research are presented in the following two sections. In some parts of the analysis we only choose the more interesting cluster sizes from the long listings of total energies and structures that have been obtained and discuss them more precisely. These sizes are N = 34, 38, 39, 55, and 60. The interest in the clusters with 34, 39, and 55 atoms is due to the symmetric structures which have been found for some stoichiometries of these clusters. We select 38-atom clusters because there are three different motifs for the global minima, i.e., pIh, c-pc5_{39}, and truncated octahedron. The largest size of our study, N = 60, should also be of interest and is therefore selected.

5.2.1 Structural Properties of Cu–Ag Nanoalloys

Structural Motifs

Our results for the GM structures of Cu–Ag clusters contain different types of icosahedral motifs, which include the 13-atom icosahedron (Ih_{13}), the 19-atom double icosahedron (Ih_{19}), the 34- and 39-atom capped 5-fold pancakes (c-pc5_{34} and c-pc5_{39}, respectively), the 6-fold pancake with 40 atoms, the Ih_{55}, and the pIh structures.

In Fig. 5.1, we show some putative GM structures of Cu_mAg_n clusters. For N = 13, the GM of all possible stoichiometries are Ih_{13}, but in many cases they have been deformed from the perfect shape of an icosahedron due to the differences in the bond lengths (Ag–Ag > Cu–Ag > Cu–Cu). The GM of larger clusters are then based on this Ih_{13} structure, where new atoms are placed on the T sites, i.e., the top center of the triangular faces formed by the atoms of the inner shell. This results in the second icosahedron for the clusters of size N = 19. After this size, new Ih_{13} icosahedra form on the sides of a central Ih_{19}. The GM of clusters with 23 < N < 34 are mainly different variants of the pIh, although for many clusters of this size range we can also identify the formation of a part of the c-pc5_{34} structure. At N = 34, the putative GM of the clusters with m = 5 to 15 Cu atoms have the c-pc5_{34} structures. These structures also have distortions because of the difference in bond lengths. Various polyicosahedra are the GM of other clusters of this size.

Some larger Cu–Ag clusters (N > 34) are also formed by the addition of new atoms to the 5-fold pancake geometry. These extra atoms reduce the symmetry of the structures and change them to the pIh. Interestingly, for 38-atom clusters the GM structures have three different motifs. First, for Ag- and some Cu-rich stoichiometries, i.e., m = 1, 2 and m = 31 to 34, they are c-pc5_{39}. But for those stoichiometries of 38-atom Cu–Ag nanoalloys which have more Cu atoms, i.e., m = 35–37, we find *fcc* truncated octahedron (TO) structures. The pIh is the structure of all other stoichiometries of size N = 38. Even for these clusters, a segment of the 5-fold geometry seems to be formed as the global minimum structures, but the extra atoms and also the core–shell preference have caused many structural changes which result in the polyicosahedra motifs. This is also the case for the Cu_6Ag_{32} cluster, for which a more symmetric structure was predicted in other studies [39, 133].

The GM of many Cu–Ag nanoalloys of size N = 39 have the c-pc5_{39} structure. These include the Ag-rich (m = 1–3) or Cu-rich (m = 24–38) clusters. The GM of

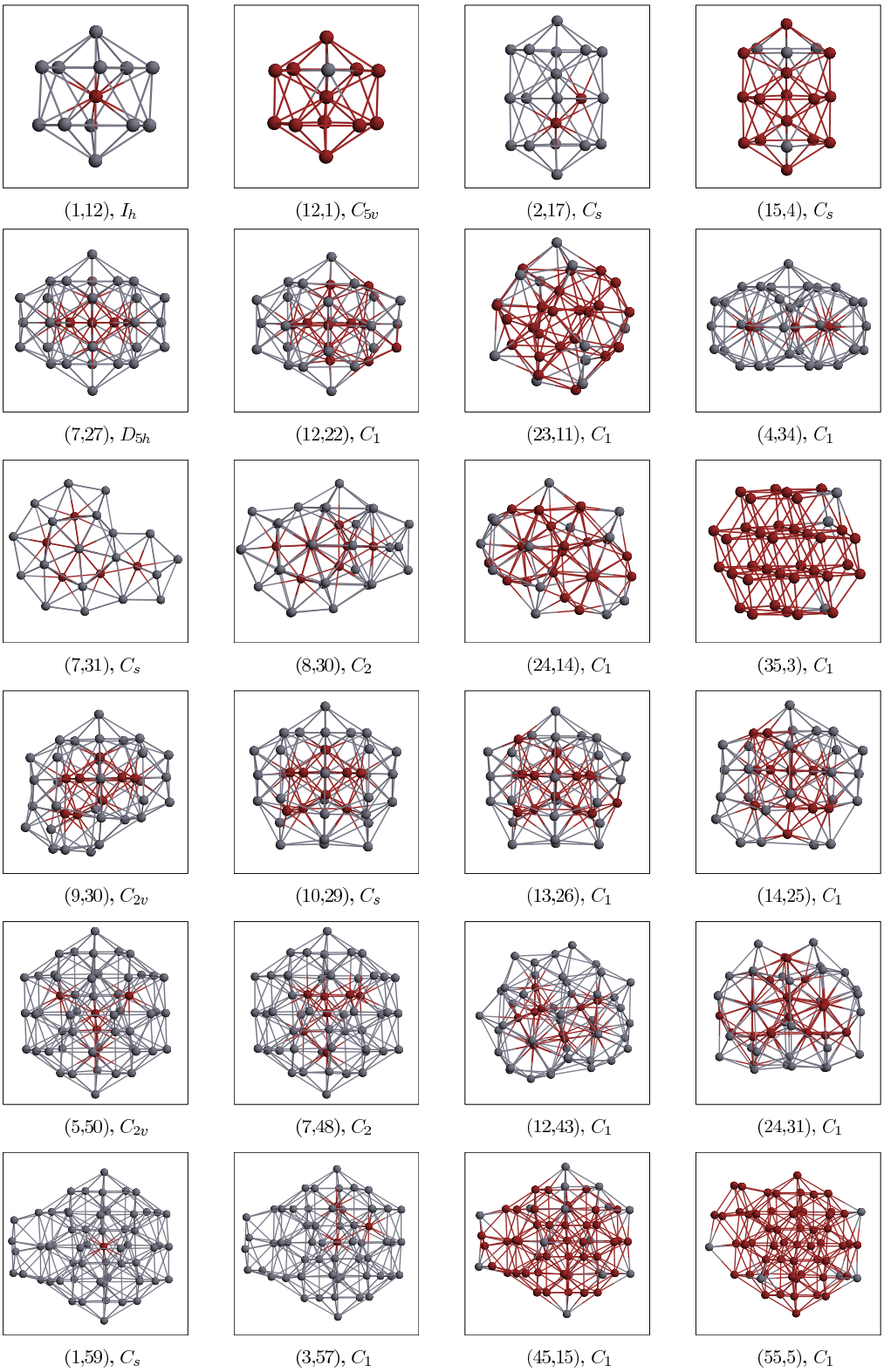

Figure 5.1: Structures of selected Cu_mAg_n nanoalloys with different compositions (m, n). Dark red and gray spheres represent Cu and Ag atoms, respectively.

Cu_6Ag_{33} has a completely different structure, where we find a c-pc6_{40} which is not capped from one side along the symmetry axis. Although we expected a preference for the c-pc6_{40} geometry at size N = 40, we find it in just one case, i.e., for $Cu_{33}Ag_7$. The structure of those nanoalloys of this size which have m = 1–3 or m = 28–39 Cu atoms are the c-pc5_{39} with one extra atom on the surface, and the GM of other cases are all different variants of pIh. The c-cp5_{39} forms the main part of the GM structures of many Cu- or Ag-rich clusters with 41 to 50 atoms. For these nanoalloys, the addition of extra atoms to the pancake structures follows in a way that the Ih_{55} is formed for N = 55. Although the structures of other stoichiometries of this size range have pIh motifs, in many cases an incomplete part of the c-pc6_{40} can be identified. In fact, the formation of a complete pancake is prevented by the tendency towards the core–shell ordering of atoms and also the presence of additional atoms.

For the Cu–Ag clusters of sizes N = 51, 52, 53, and 54 we find the incomplete Ih_{55} very often, and specially for stoichiometries which are rich in one type of the atoms. The clusters with this type of structures include those with m = 1–6 and m = 42–50 of size N = 51, m = 1–9 and m = 34–51 of N = 52. For N = 53 and 54 the number of clusters with this type of structure increases, where for the first size they include stoichiometries with m = 1–8 and m = 32–52, and for the latter size they are m = 1–8 and m = 25–53. We identify all other clusters of these sizes as the pIh structures.

Not surprisingly, the GM structures for many 55-atom nanoalloys are Ih_{55}. For the Ag-rich clusters we find the GM of those clusters with m = 1–9 to be Ih_{55}. By increasing the number Cu atoms, the structural distortion increases and causes the pIh structures to be more favored for the GM of $10 < m < 27$. If the number of Cu atoms increases more then the Ih_{55} appears again as the putative GM of compositions with $m > 27$. Many clusters with N = 56 to 60 atoms take the Ih_{55} as the main part of their GM structures. These are stoichiometries which contain more Cu or Ag atoms. In the other cases, the putative global minima have different motifs of the pIh.

Bond order Parameter And Radial Distances

As the next step in analyzing the structural properties of Cu–Ag nanoalloys, we should employ the concept of the bond order parameter to investigate the ordering of atoms more quantitatively. This parameter was introduced in Sec. 3.4.2 and here

we discuss the corresponding results. Fig. 5.2 depicts the bond order parameter (σ) and the number of different types of nearest neighbor bonds versus the number of Cu atoms (m) for Cu–Ag nanoalloys of sizes N = 34, 38, 39, 55, and 60 atoms. The positive values for σ in all cases are indications for the segregation of one species to the surface and the formation of core–shell structures. The $Cu_{core}Ag_{shell}$ ordering is also inferred from the number of different types of bonds. Fig. 5.2 shows the number of Ag–Ag bonds to decrease and becomes zero even for the clusters with a considerable number of Ag atoms. This implies that the Ag atoms separate on the surface of the Cu core and do not have a trend for building homoatomic bonds. In contrast, the number of Cu–Cu bonds does not vanish, even when the number of Cu atoms is very small, suggesting that even a small number of Cu atoms localize to form a core. This is also in agreement with the tendency to maximize the number of the stronger Cu–Cu bonds. As expected, Fig. 5.2 shows the maximum number of Cu–Ag bonds for the clusters with approximately equal numbers of Cu and Ag atoms.

A comparison between Cu–Ag and Ni–Ag clusters is also useful. As we will see in Sec. 6.2.1 and is also reported in Ref. [143], the bond order parameters in the latter clusters are very similar to those of Cu–Ag shown in Fig. 5.2. It is interesting when we notice that Cu and Ag atoms have more similar atomic radii, cohesive energies, and surface energies than Ni and Ag. But these close similarities do not take a mixed ordering for the Cu–Ag nanoalloys and the segregation is still preferred.

The core–shell ordering of atoms should also be obvious in the radial distances of the atoms from the center of the clusters. To check this, we calculate the radial distance of each atom in a cluster by using

$$r_i = |\vec{R}_i - \vec{R}_0|, \qquad i = 1, 2, \cdots, N \tag{5.1}$$

with

$$\vec{R}_0 = \frac{1}{N}\sum_{i=1}^{N}\vec{R}_i \tag{5.2}$$

being the center of the cluster of interest. The ratio between the average radial distances of the Cu and Ag atoms in a cluster indicates the type has segregated towards the surface. This ratio, which is defined as

$$r(m, n) = \frac{\langle r_{Cu}\rangle}{\langle r_{Ag}\rangle}, \tag{5.3}$$

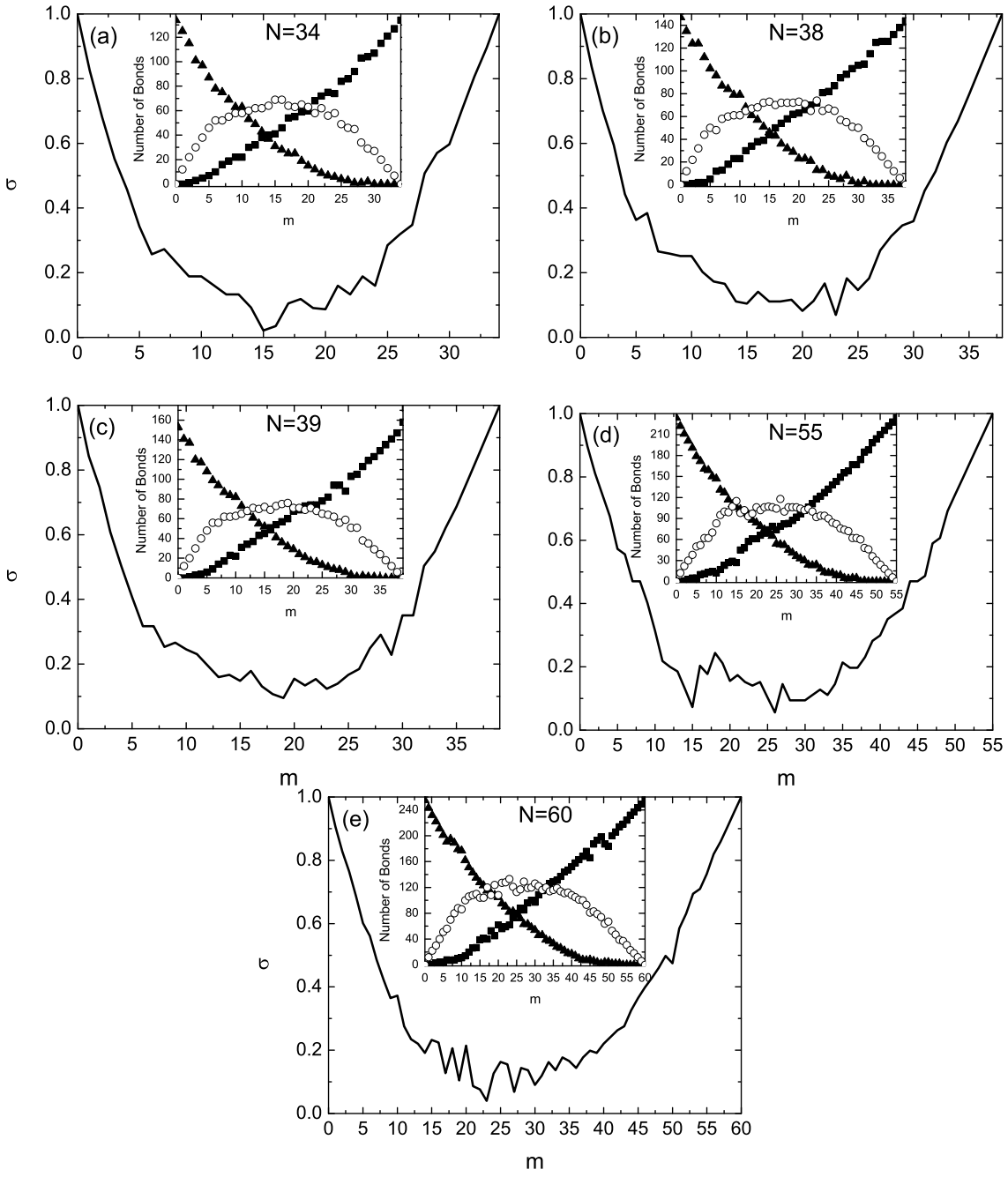

Figure 5.2: The bond order parameter of Cu–Ag clusters as a function of composition (number of Cu atoms, m) for the global minima of five selected sizes (N = 34, 38, 39, 55, and 60). The insert figures show the number of the three possible types of bonds vs m. Solid squares and triangles refer to the numbers of Cu–Cu and Ag–Ag bonds, respectively, whereas open circles are for the number of Cu–Ag bonds.

has values smaller than 1 when we have a $Cu_{core}Ag_{shell}$ ordering, whereas it is larger than 1 for $Ag_{core}Cu_{shell}$ and close to 1 for the mixed or multishell structures. We show this ratio for all Cu–Ag clusters considered in our study in Fig. 5.3. According to this figure, the ratio is always smaller than 1 and emphasizes on the $Cu_{core}Ag_{shell}$ ordering of atoms in all of the clusters. Finally, if we compare the Cu–Ag and Ni–Ag nanoalloys to each other (see Sec. 6.2.1 and Ref. [143]), it turns out that the ratios of average radial distances are almost identical for both cases.

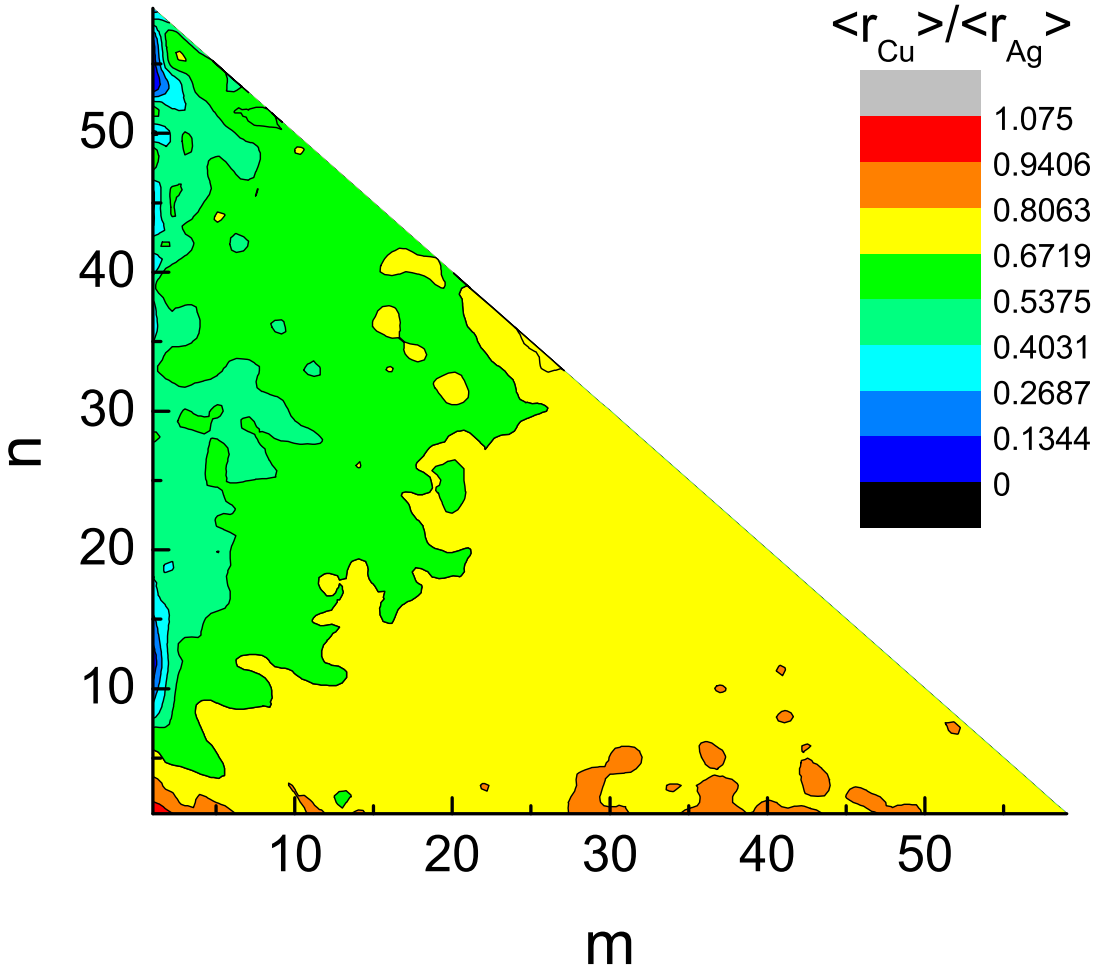

Figure 5.3: The ratio of average radial distance of the Cu and Ag atoms in the Cu_mAg_n clusters as a function of (m, n) for N = m+n from 2 to 60.

5.2.2 Energetic Properties of Cu–Ag Nanoalloys

Binding Energy

In this section, we discuss the energetic properties of the clusters. From the total energy we can easily determine the binding energy per atom, i.e., $E_b = -\frac{E(m,n)}{N}$. Here E(m, n) denotes the energy of an N-atom nanoalloy with m A-type (Cu) and n B-type (Ag) atoms. E_b is shown in Fig. 5.4 as a function of (m, n). When we keep the stoichiometry constant, i.e., fixed values of $\frac{m}{m+n}$, the binding energy per atom increases with the size. This is seen by considering intersecting straight lines, each of which passes through one color-region of the E_b graph. We also see that clusters of a given size have larger binding energy per atom when the number of their Cu atoms, m, is larger.

To consider the effect of size, Fig. 5.5 depicts the binding energy per atom as a function of N and for a fixed number of Cu (m) or Ag (n) atoms. In all curves of the binding energies, local maxima are seen for some sizes such as N = 13, 19, 23, and 55 which have icosahedra structures. E_b is almost constant for clusters with N > 20 and m = 4, 5, or 6 (Fig. 5.5a). But we do not find the same behavior for the clusters with a fixed number of Ag atoms (Fig. 5.5b). If we compare the two panels of the figure, we find that the substitution of a single Ag atom with a Cu atom in a cluster causes the binding energy to change more. The larger values of E_b for the clusters with more Cu atoms can be explained by the higher number of Cu–Cu bonds which are also stronger than both Ag–Ag and Cu–Ag bonds.

Stability Function

The rough binding energy per atom of the Cu–Ag clusters implies that there may exist some clusters which are particularly stable. To identify these magic clusters, we calculate different variants of the stability functions defined by Eqs. 3.6 to 3.10, and plot the results versus the number of Cu atoms (m). Fig. 5.6 presents ${}^{N}\Delta_2$ for clusters of sizes N = 34, 38, 39, 55, and 60. All the magic clusters with N = 34 are 5-fold c-pc5_{34} structures and include those with m = 7, 11, 13, 17, 19, and 22 Cu atoms. The stability of the Cu_7Ag_{27} cluster is in agreement with the results of previous studies [39]. The most stable cluster of the size N = 38 corresponds to the Cu_8Ag_{30} which is a pIh. The enhanced stability of this stoichiometry is also in agreement with other available results [39, 72]. Although the 38-atom magic clusters

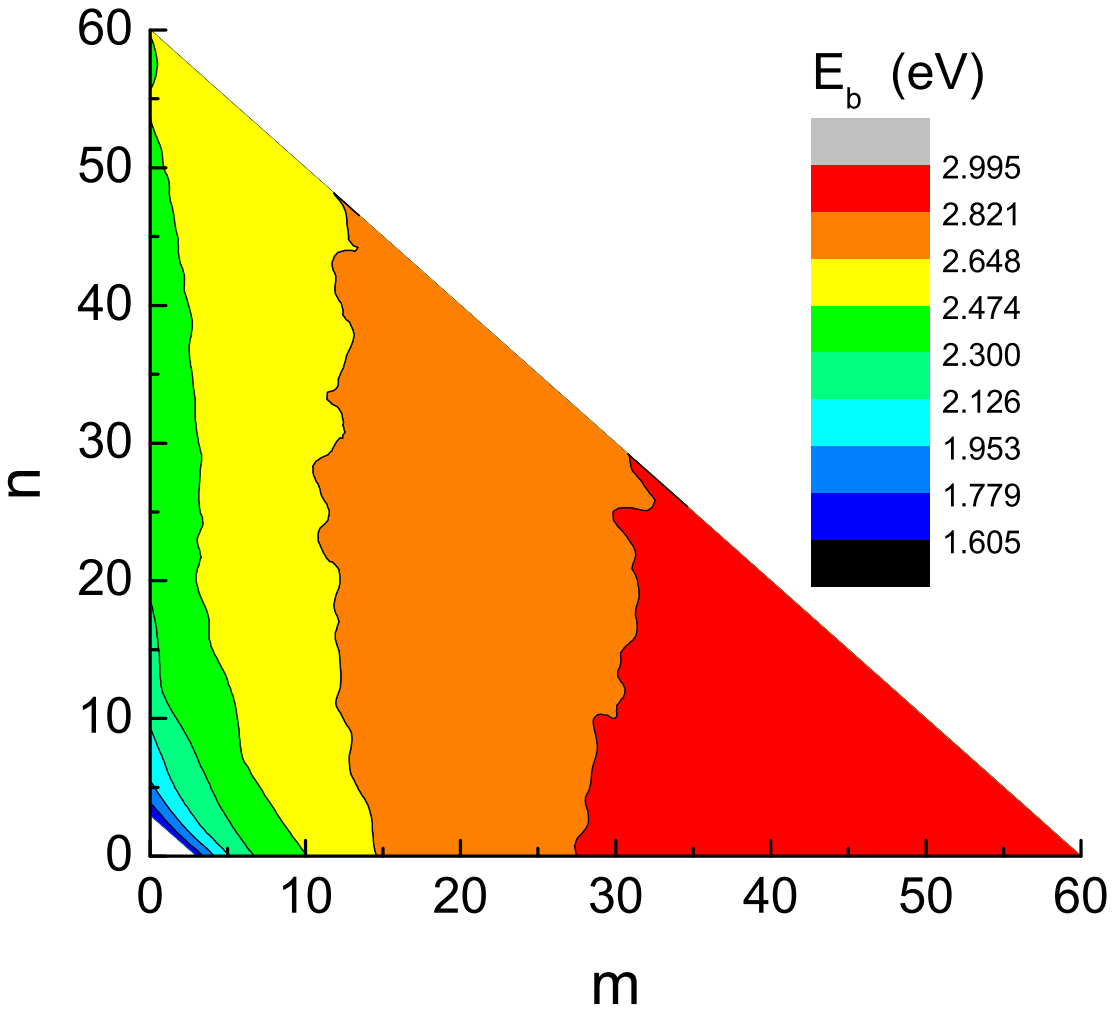

Figure 5.4: Binding energy per atom of the Cu_mAg_n nanoclusters vs m and n for N = m+n from 2 to 60.

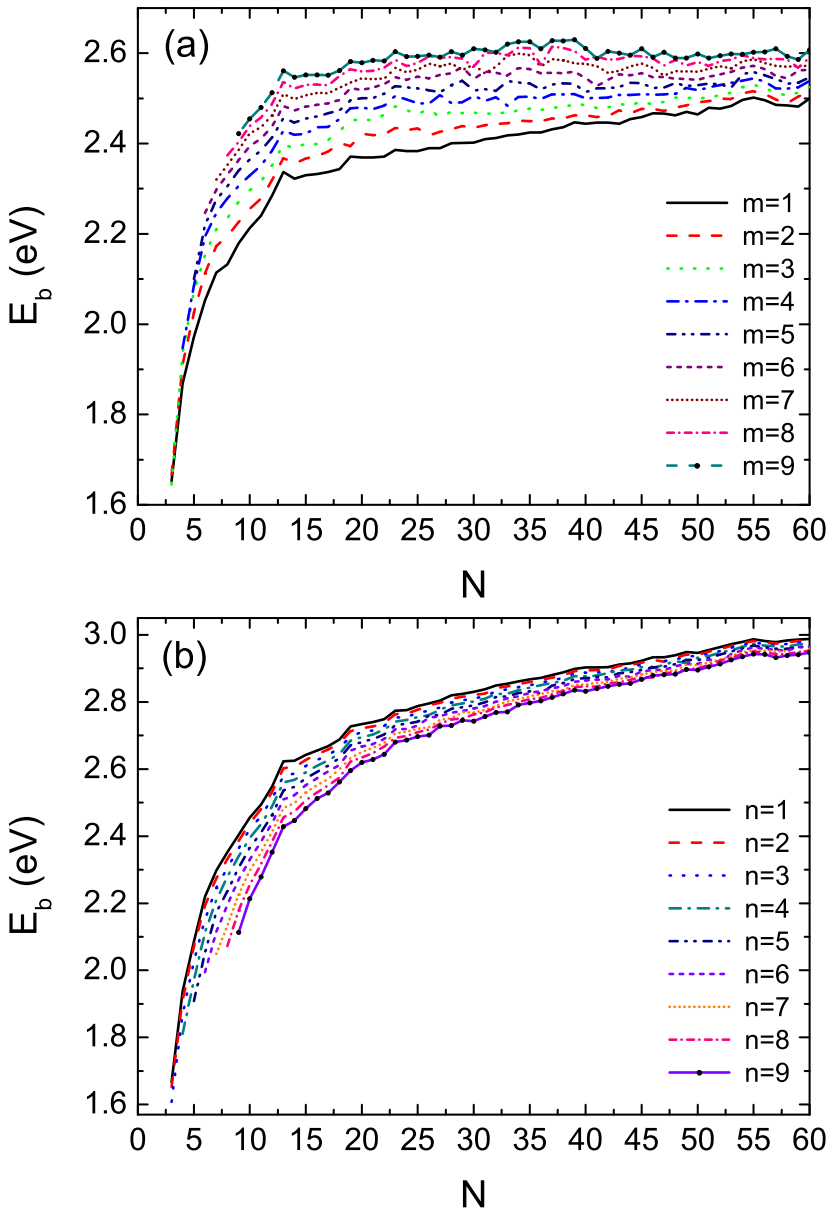

Figure 5.5: Binding energy per atom of the Cu–Ag nanoalloys with (a) fixed number of Cu atoms and (b) fixed number of Ag atoms vs the cluster size (N).

are all pIh, there are two exceptions, i.e., Cu_1Ag_{37} and $Cu_{32}Ag_6$, which have c-pc5_{39} structures with one vacant site each.

According to Fig. 5.6c, the most stable cluster with 39 atoms is the pIh Cu_9Ag_{30}. In fact this structure consists of a c-pc5_{34} with five extra atoms on the surface. Other stoichiometries of size N = 39, which have enhanced stabilities and also symmetric geometries, are Cu_1Ag_{38}, Cu_6Ag_{32}, and $Cu_{24}Ag_{13}$.

Although many of the 55-atom clusters have symmetric structures, the highest stability is seen for a core–shell pIh, i.e., $Cu_{12}Ag_{43}$. The sharp peak for this composition is explained by the fact that both GMs of $Cu_{11}Ag_{44}$ and $Cu_{13}Ag_{42}$ have Cu atoms which are segregated to the surface. This increases the contribution of the surface energies and causes these structures to be less favored. There are also three other pIh's determined to be particularly stable, which include those with m = 10, 20, and 24.

The peaks in Fig. 5.6e suggest that the addition of a single atom can cause a noticeable change in the stability of the Ag-rich nanoalloys with 60 atoms. Most of the magic clusters for this size have pIh structures, such as $Cu_{12}Ag_{48}$ and $Cu_{17}Ag_{43}$, but three stoichiometries with m = 1, 4, and 6 Cu atoms have an Ih_{55} core which is covered by five extra atoms on the last shell.

Figs. 5.7 to 5.10 show the stable clusters determined by using other definitions of the stability functions for four selected sizes. Here we will compare the results of these different definitions. Many of the particularly stable nanoalloys given by ${}^{N}\Delta_2$ are also among the magic sizes determined by other Δ_2 functions. Both ${}^{m}\Delta_2$ and ${}^{mn}\Delta_2^{(2)}$ show that the most stable 34-atom cluster is $Cu_{17}Ag_{17}$. This nanoalloy and Cu_2Ag_{32} have enhanced stability according to all forms of the Δ_2 functions.

If we calculate ${}^{n}\Delta_2$ and ${}^{m}\Delta_2$ for the clusters of size N = 38, again the pIh Cu_8Ag_{30} is given as a magic composition. But the most stable clusters determined by each of other definitions of the stability function are as following: ${}^{n}\Delta_2$ gives Cu_1Ag_{37} (c-pc5_{39}), ${}^{m}\Delta_2$ gives Cu_8Ag_{30} (pIh), ${}^{mn}\Delta_2^{(1)}$ gives Cu_7Ag_{31} (c-pc5_{39}), and ${}^{mn}\Delta_2^{(2)}$ gives $Cu_{18}Ag_{20}$. There is just one composition, i.e., (m, n) = (12, 26), which is stable according to all of the Δ functions. These results show that the predicted magic clusters for N = 38 depend sensitively on the way in which the Δ_2 functions are defined.

For N = 39, the pIh Cu_9Ag_{30} is the most stable cluster according to ${}^{N}\Delta_2$ and ${}^{n}\Delta_2$, and it is also the only magic composition suggested by all forms of the stability

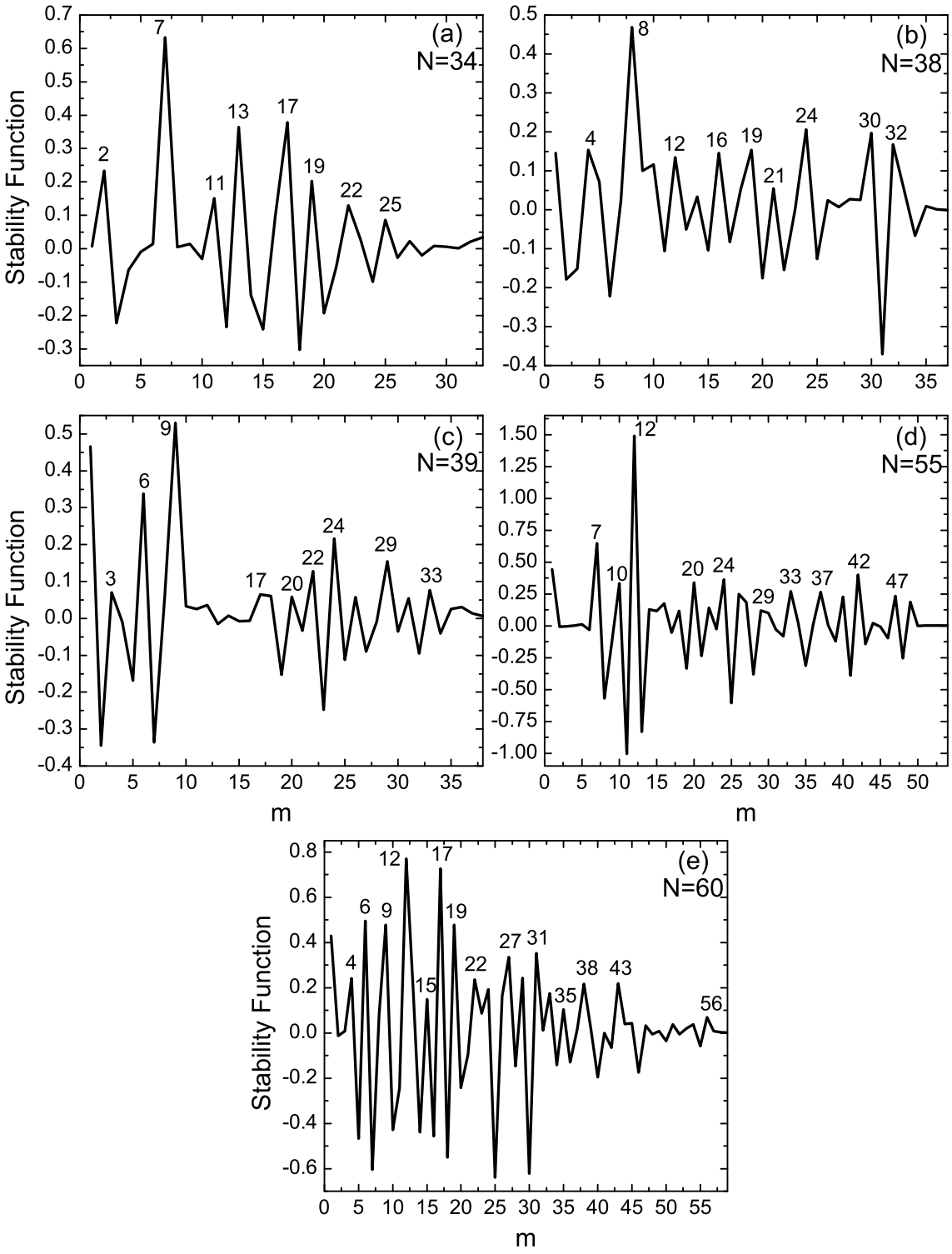

Figure 5.6: Stability function according to ${}^{N}\Delta_2$ (Eq. 3.6) for selected sizes of Cu–Ag nanoalloys vs number of Cu atoms (m).

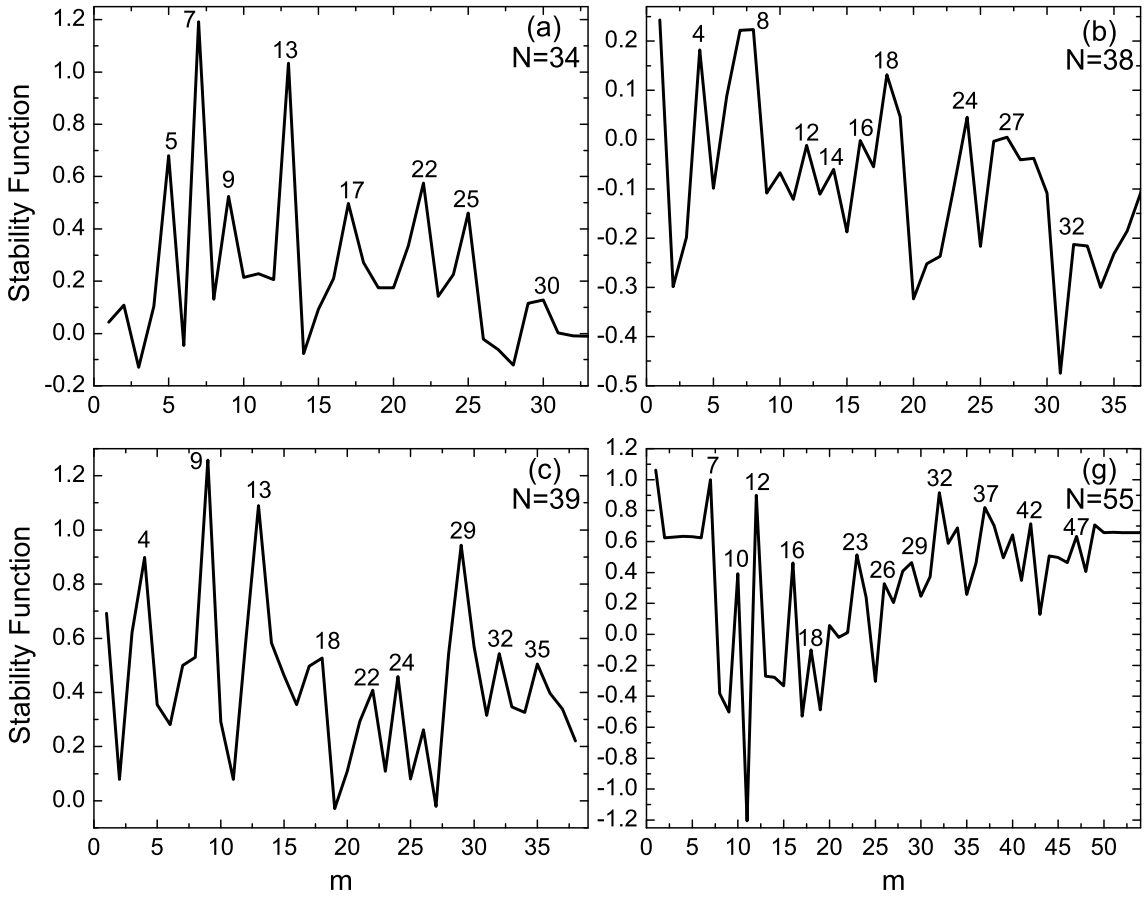

Figure 5.7: Stability function according to ${}^{n}\Delta_2$ (Eq. 3.7) for four sizes of Cu–Ag nanoalloys vs number of Cu atoms (m).

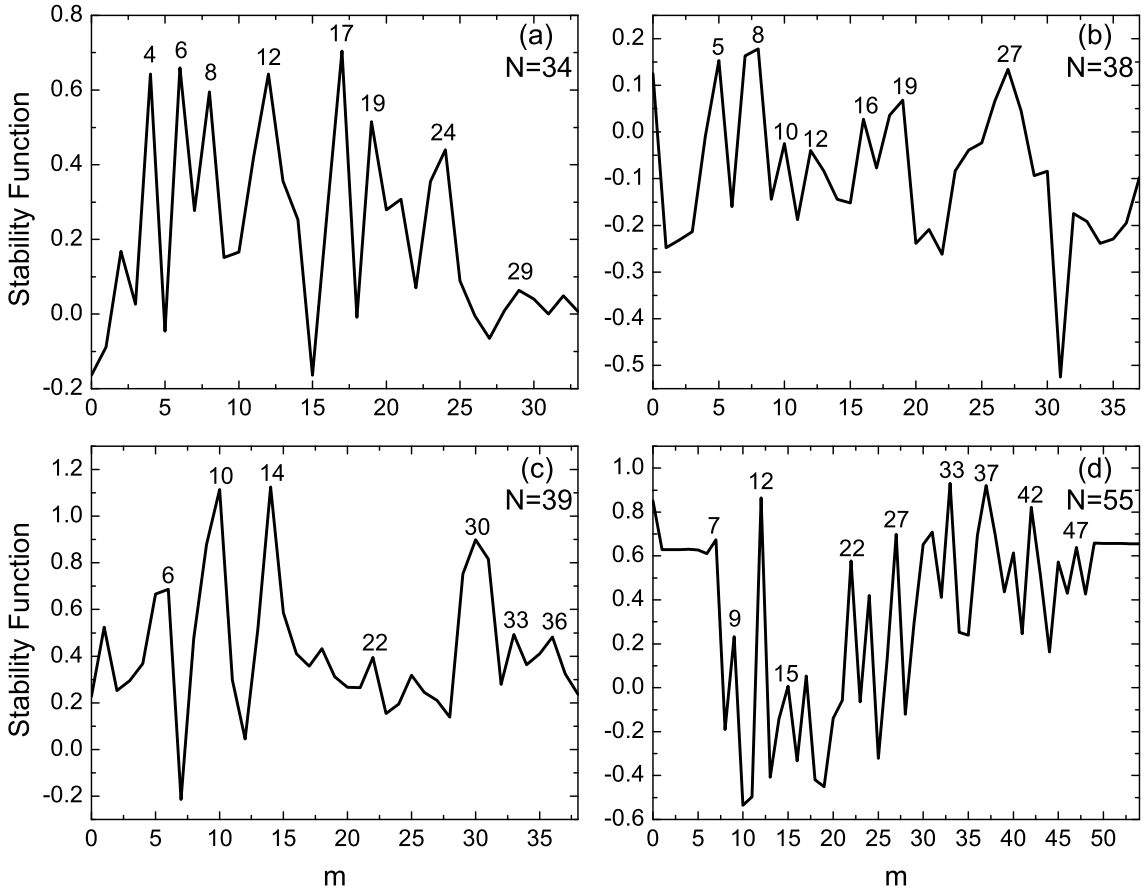

Figure 5.8: Stability function according to ${}^{m}\Delta_2$ (Eq. 3.8) for selected sizes of Cu–Ag nanoalloys vs number of Cu atoms (m).

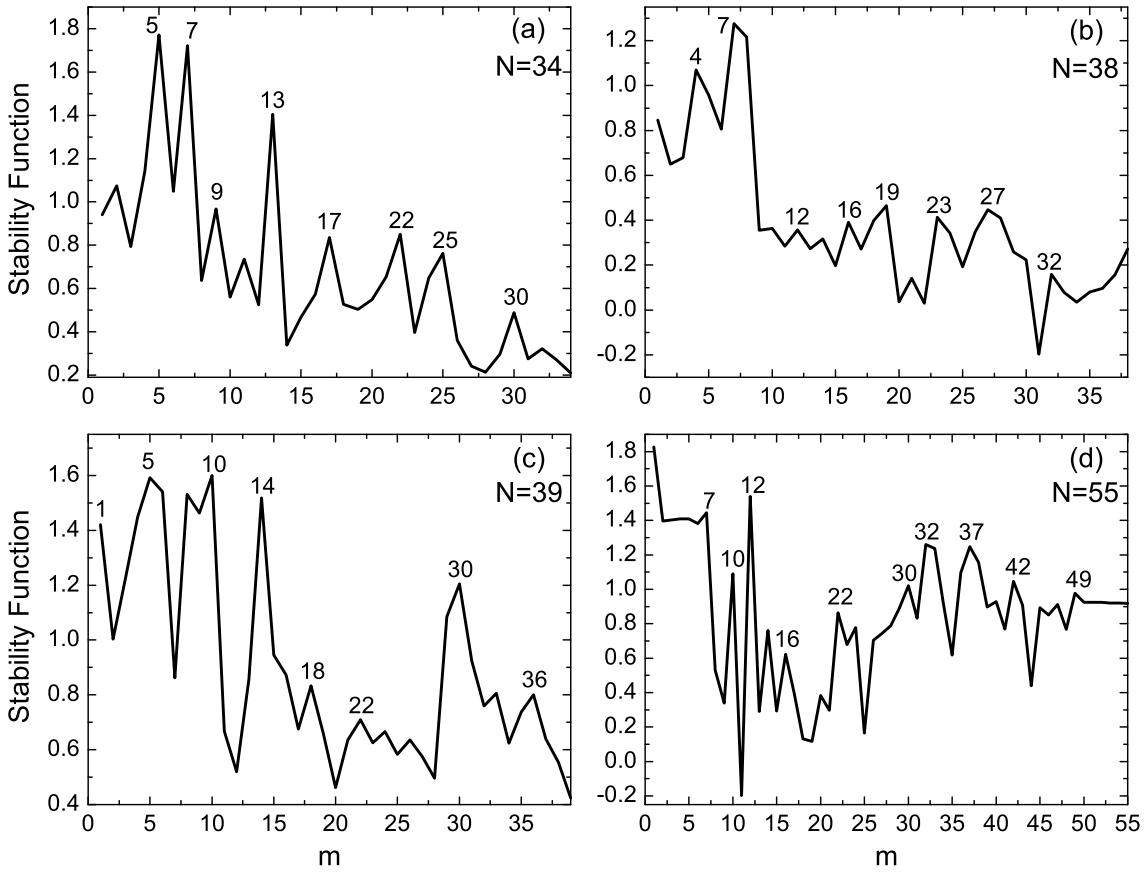

Figure 5.9: Stability function according to ${}^{\mathrm{mn}}\Delta_2^{(1)}$ (Eq. 3.9) for four sizes of Cu–Ag nanoalloys vs number of Cu atoms (m).

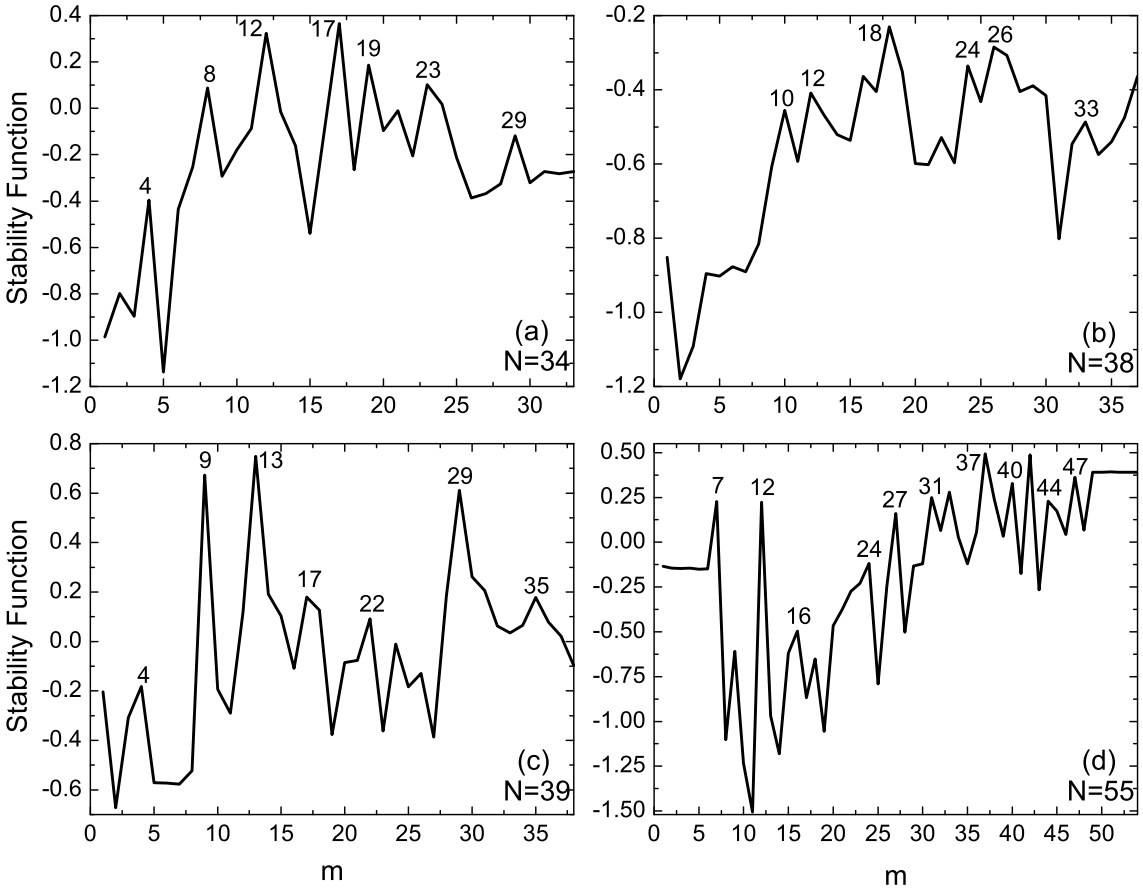

Figure 5.10: Stability function according to ${}^{\mathrm{mn}}\Delta_2^{(2)}$ (Eq. 3.10) for selected sizes of Cu–Ag nanoalloys vs number of Cu atoms (m).

functions. $Cu_{14}Ag_{25}$, $Cu_{10}Ag_{29}$, and $Cu_{13}Ag_{26}$ are other stoichiometries determined as the most stable ones by ${}^{m}\Delta_2$, ${}^{mn}\Delta_2^{(1)}$, and ${}^{mn}\Delta_2^{(2)}$, respectively.

Many clusters of size N = 55 are seen to be energetically favored, as we can identify their corresponding peaks in Figs. 5.6–5.10. This shows that these clusters are stable, independent of the definition of the stability function. As examples of these clusters, we notice those with m = 7, 12, 42, and 47 Cu atoms. Interestingly, all these clusters have Ih_{55} structures with only one exception which is the pIh $Cu_{12}Ag_{43}$.

Excess Energy

The above stable clusters were all determined in comparison with the clusters of similar or neighboring sizes. Now we will employ the concept of excess energy (see Sec. 3.4.1) and compare all clusters of the same size and find the stable stoichiometry. For this, we have calculated the excess energy (E_{exc}) of all Cu–Ag nanoalloys considered in our study by using Eq. 3.11. The results for E_{exc}/N are shown as a contour graph in Fig. 5.11 versus the number of Cu (m) and Ag (n) atoms. For almost all stoichiometries and sizes the excess energy per atom is negative. This points to the fact that mixing is favored by Cu–Ag clusters. The most negative values of E_{exc}/N correspond to those stoichiometries with m$\simeq$6–15 and n$\simeq$17–30. This indicates that the most stable clusters are found in this range of compositions.

For a more specific and detailed analysis, the excess energies of five selected sizes are shown in Fig. 5.12 versus the number of Cu atoms. From this figure we can immediately infer that the excess energies, in all cases, have a minimum for Ag-rich clusters and there is no size dependence for this behavior. Another effect that we see in E_{exc} of the selected clusters is its oscillatory behavior for some compositions. The only reason which explains this is the small structural changes of the corresponding clusters.

Fig. 5.12a emphasizes the enhanced stability of c-pc5_{34} Cu_7Ag_{27} by showing that it also has the minimum value of the excess energy. $Cu_{10}Ag_{28}$ as well as Cu_9Ag_{29} are given stability by E_{exc} (Fig. 5.12b). These two 38-atom clusters have pIh structures. For N = 39, Cu_9Ag_{30} is the only cluster which has the lowest value of the excess energy and this shows the enhanced stability of this composition.

According to the excess energies, the stable cluster of size N = 55 is $Cu_{20}Ag_{35}$

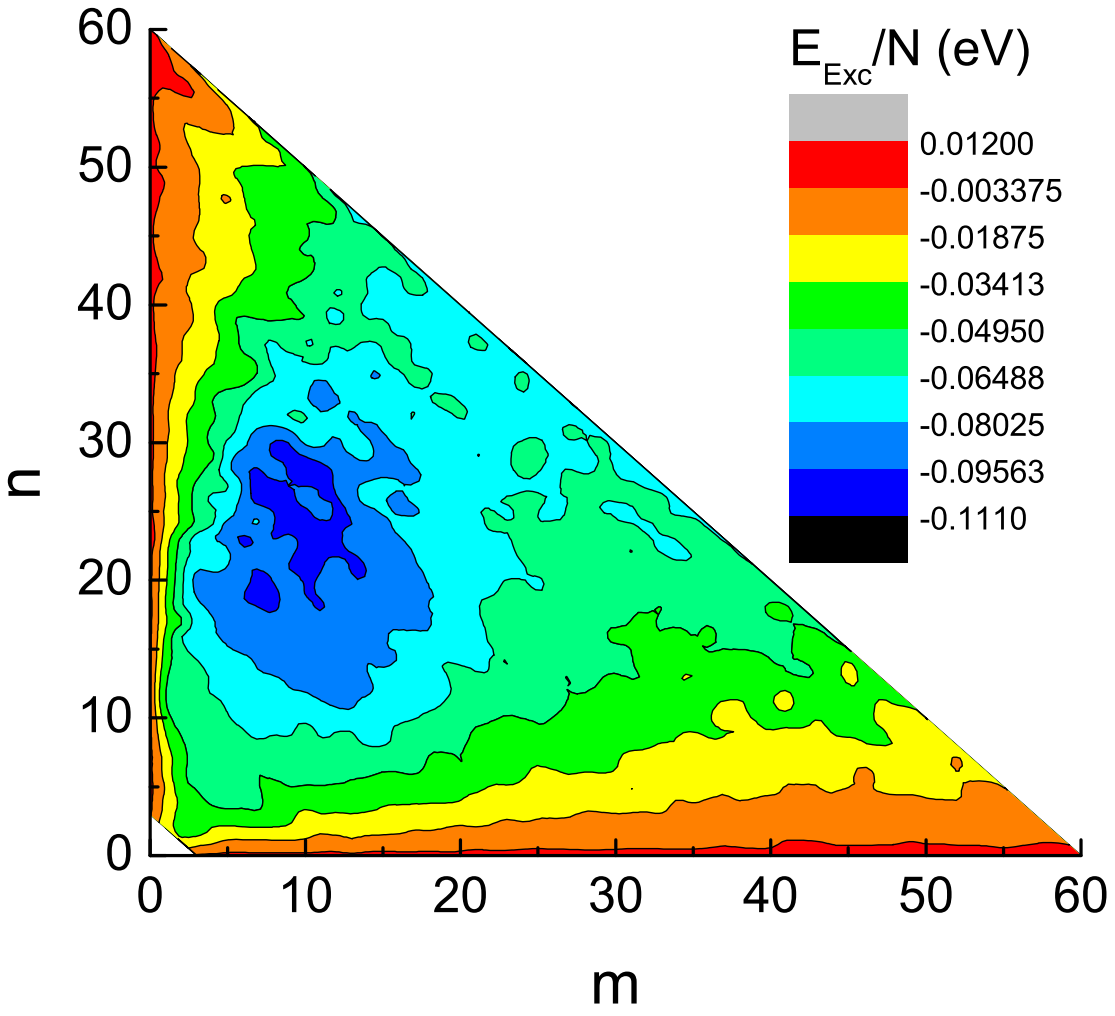

Figure 5.11: The excess energy per atom for Cu_mAg_n clusters as a function of (m, n) for N = m+n from 2 to 60.

with a pIh structure. But this is not found of enhanced stability when using the concept of stability functions. If we compare the excess energy of size N = 55 with those of smaller clusters, then it turns out that for the latter cases just one or two clusters have very low values of E_{exc} while for N = 55, a whole range of different compositions can have low excess energies (Fig. 5.12). The excess energy of clusters with 60 atoms also has the same behavior. But the lowest value of E_{exc} for N = 60 is found for $Cu_{22}Ag_{38}$ which has a pIh structure with many Cu atoms segregated to the surface.

Isomers Energy Difference

To determine the thermally stable Cu–Ag nanoalloys, we calculate the energy difference between the first and second lowest-lying isomers ($\Delta E_{isom} = E_{N.2} - E_{N.1}$, Sec. 3.4.1). Fig. 5.13 shows this quantity versus the number of Cu atoms (m) for five selected sizes, i.e., N = 34, 38, 39, 55, and 60.

The results confirm the enhanced thermal stability of many stoichiometries of size N = 34 which were also among the particular stable clusters determined by other measures. Examples are the (7, 27), (13, 21), (16, 18) and (22, 12) clusters with c-$pc5_{34}$ structures. But the case is different for $Cu_{10}Ag_{24}$ (c-$pc5_{34}$) and $Cu_{28}Ag_6$ (pIh) which are given just as thermally stable clusters. In contrast, some compositions of size N = 34, determined as particularly stable clusters by other criteria, do not have thermal stability. The examples are those with m = 5, 9, and 30.

There are many particularly stable Cu–Ag clusters of size N = 38 that we find are also thermally stable. In contrast, two clusters, Cu_9Ag_{29} and $Cu_{15}Ag_{23}$, have thermal stability, while we did not identify them as being particularly stable by using other criteria. Some clusters of this size show degenerate first and second isomers. As an example of this kind we notice the Cu_4Ag_{30} cluster.

The repetition of some energetically favored stoichiometries in the results of thermal stability measurement is also seen for sizes N = 39, 55 and 60. But for N = 39, we have two magic $Cu_{32}Ag_7$ and $Cu_{35}Ag_4$ clusters which are not thermally stable. The same is also seen for $Cu_{15}Ag_{40}$, $Cu_{32}Ag_{23}$, and $Cu_{33}Ag_{22}$ with 55-atoms which have very small or almost zero energy gaps between their first and second lowest-lying isomers. This contrasts with their enhanced stability according to the Δ_2 functions. We notice that the lowest energy isomers of those stoichiometries of size 55 with 7, 12, 42, and 47 Cu atoms, which exhibit high peaks in all Δ_2 functions,

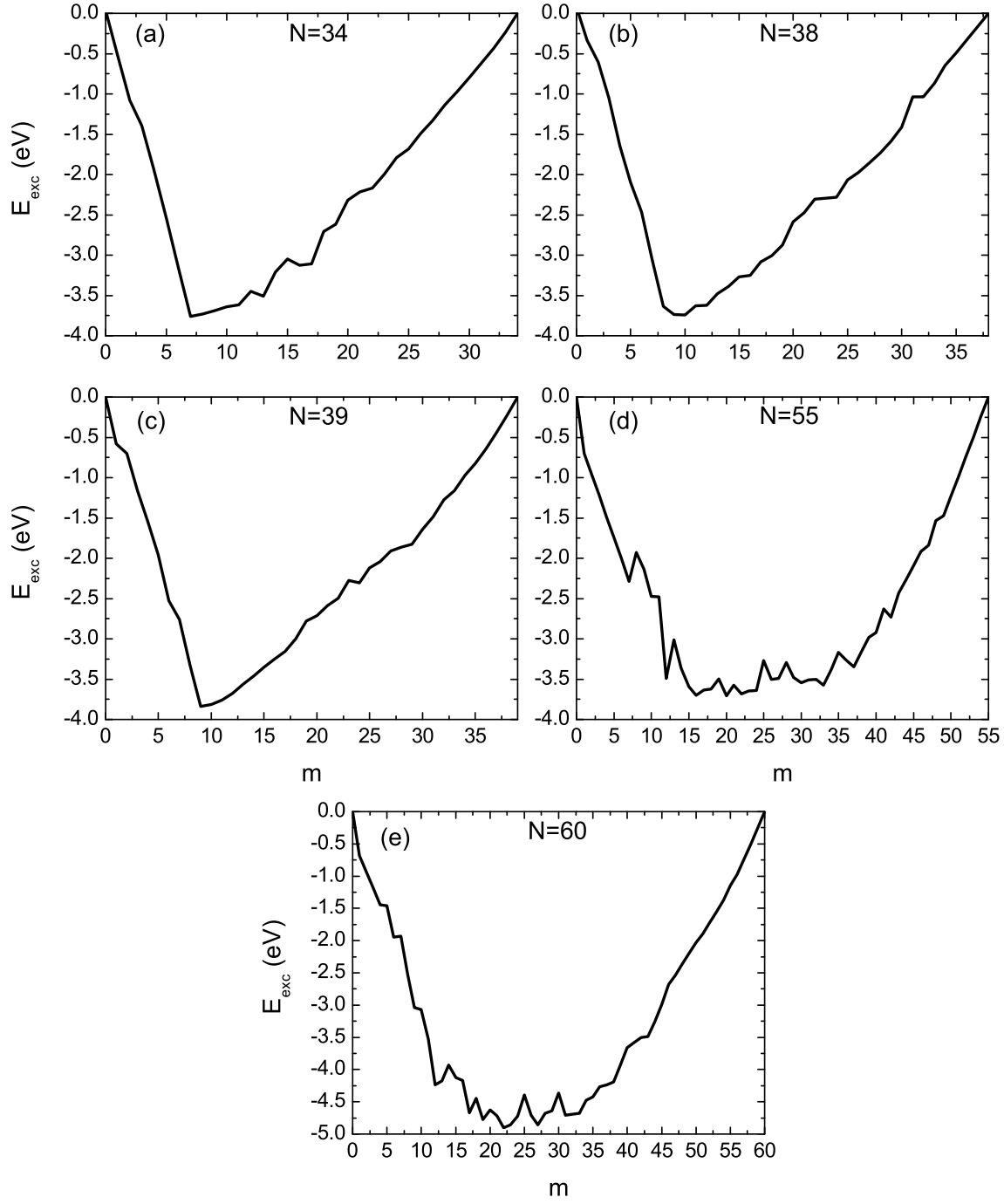

Figure 5.12: The excess energy of the Cu–Ag nanoalloys for some selected sizes (N = 34, 38, 39, 55, and 60) vs number of Cu atoms (m).

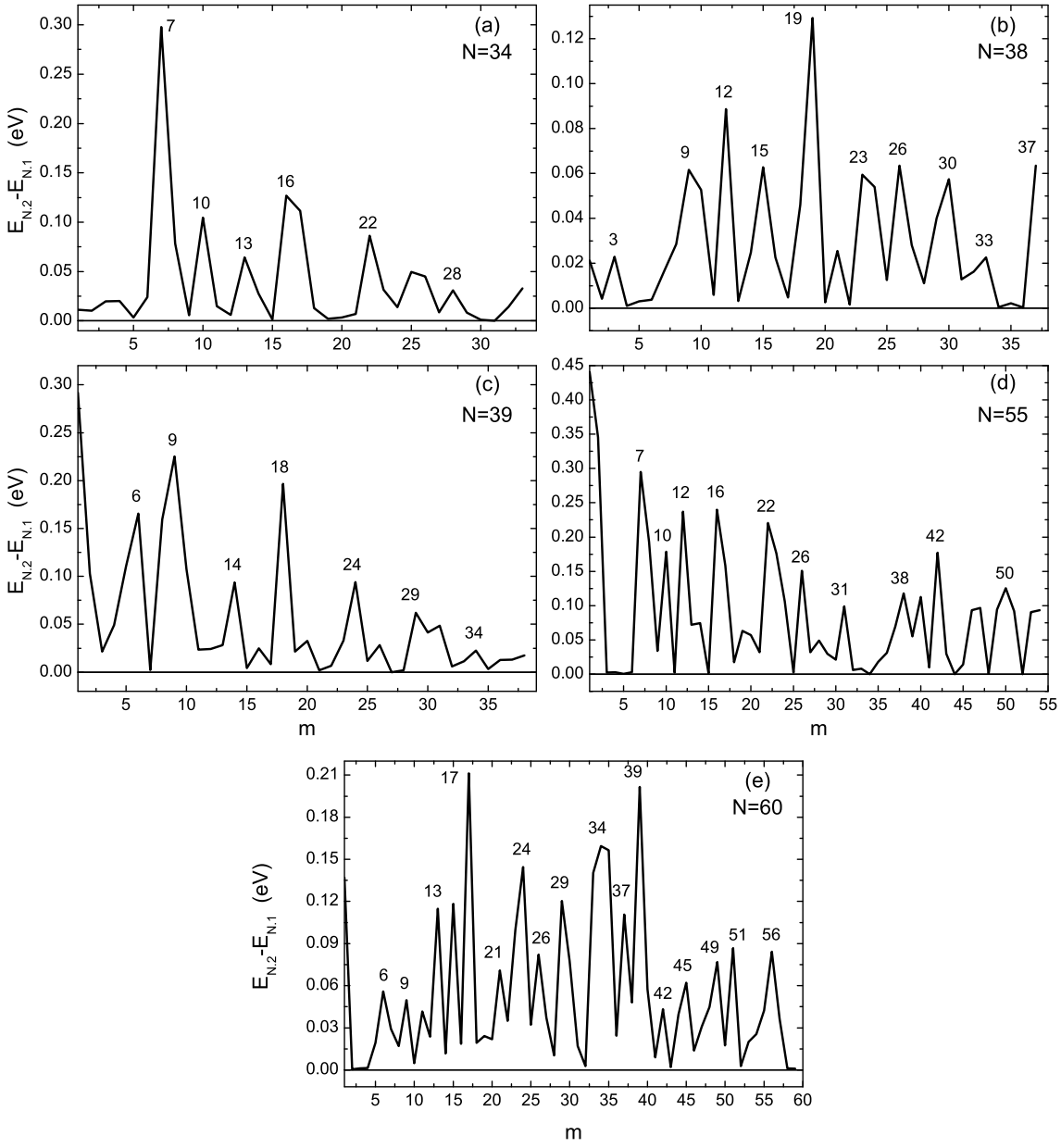

Figure 5.13: Energy difference between the first and second stable isomers of selected sizes of Cu–Ag nanoalloys vs number of Cu atoms (m).

have also relatively large energy gaps with their corresponding second isomers. This is an indication of their thermal stability. According to Fig. 5.13e, the following clusters are found thermally stable for N = 60: (m, n) = (13, 47), (24, 36), (26, 34), (34, 26), (37, 23), (39, 21), (42, 18), (45, 15), (49, 11), and (51, 9). These are all pIh structures, except the last three cases which consist of an Ih_{55} motif with five extra atoms added to the T sites above the last shell of atoms. Finally, one should also notice that, in all cases, there are many clusters for which the first and second isomers are essentially energetically degenerate. This suggests the possibility of interchanging the energetic orders of these isomers.

Before proceeding, in table 5.1 we summarize the energetically favorable stoichiometries determined by all stability measures for every size of Cu–Ag clusters considered in the current study. The diversity of the results for each size signifies the difficulties in determining the stable nanoalloys. According to table 5.1, some of the clusters are frequently identified as being energetically favored. The flowing cases are found stable by at least five criteria, (m, n) = (3, 2), (1, 11), (6, 23), (12, 39), and (9, 48). We also find 16 stoichiometries identified as being of enhanced stability by four measures, i.e., (2, 1), (3, 1), (5, 1), (4, 4), (1, 8), (1, 9), (1, 10), (1, 13), (1, 14), (1, 15), (2, 18), (3, 20), (3, 23), (7, 27), (8, 29), and (10, 44).

Mixing Energy and Coefficient

Mixing two different types of pure clusters and forming a bimetallic cluster should result in energetical and structural effects. One way to study these effects is to determine the mixing coefficients (M) and energies (E_{mix}) introduced in Sec. 3.4.2. We have calculated these values for all Cu–Ag nanoalloys considered in our study. The results are shown in Fig. 5.14. The segregation of Ag atoms to the surface of clusters is clearly reflected in the values of M, where we find very few stoichiometries which have values of M larger than 30%. On the contrary, for most of the clusters M is smaller than 12%, and even in Ag- and Cu-rich compositions it drops to less than 6%.

As expected, E_{mix} shows the same pattern as M. According to Fig. 5.14, when Ag or Cu atoms are added to a pure cluster, E_{mix} becomes deeply negative. However, negatively large values of E_{mix} are for Ag-rich clusters, which indicate the stabilizing effect of the Cu atoms when added to these stoichiometries. But, a similar effect is not seen when Ag atoms are added to those Cu-rich clusters. An explanation for

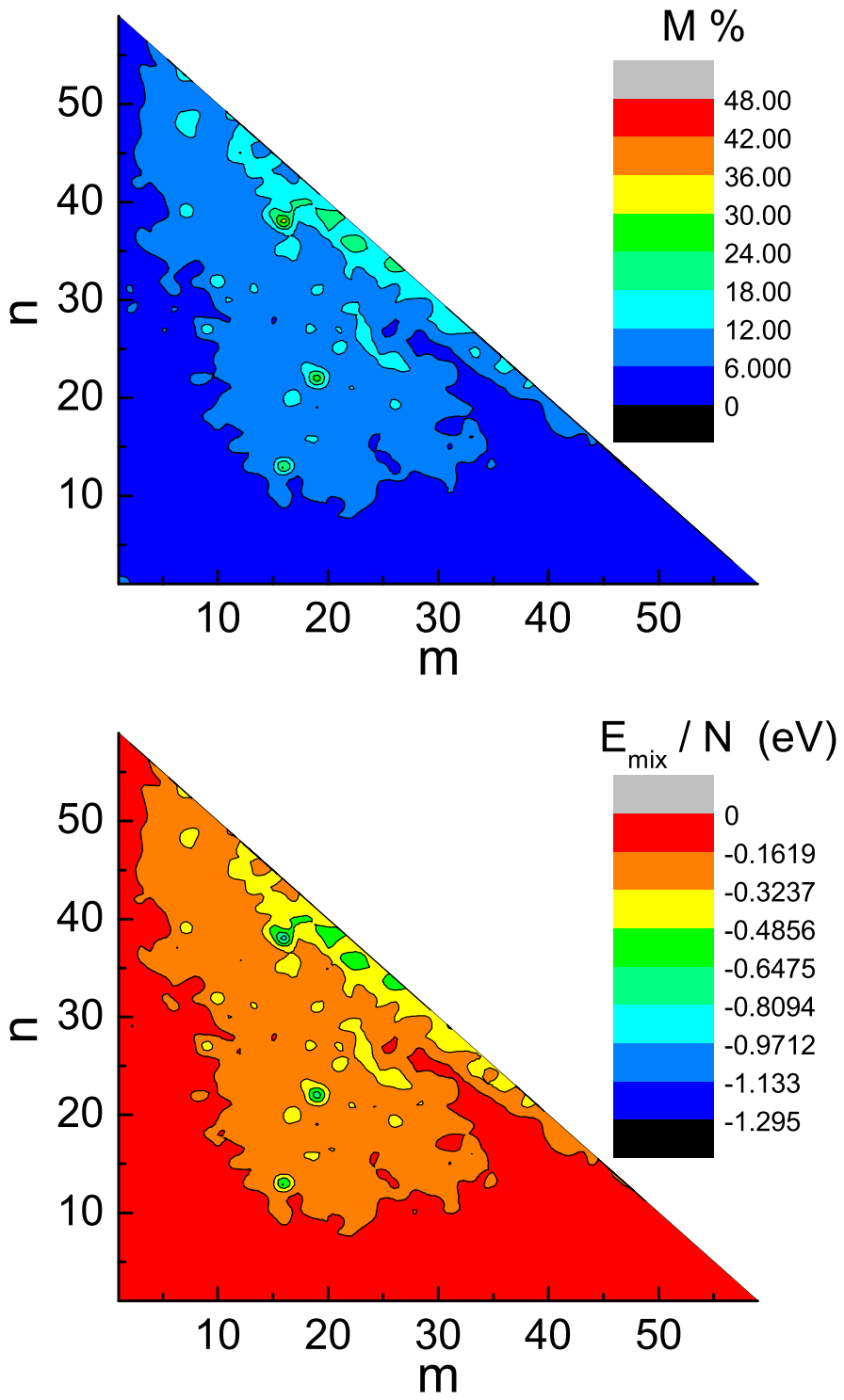

Figure 5.14: Mixing coefficients M (upper part) and mixing energy per atom (lower part) for Cu_mAg_n clusters as a function of (m, n) for N = m+n from 2 to 60.

N	$^{N}\Delta_2$	$^{n}\Delta_2$	$^{m}\Delta_2$	$^{mn}\Delta_2^{(1)}$	$^{mn}\Delta_2^{(2)}$	ΔE_{isom}	E_{exc}	N	$^{N}\Delta_2$	$^{n}\Delta_2$	$^{m}\Delta_2$	$^{mn}\Delta_2^{(1)}$	$^{mn}\Delta_2^{(2)}$	ΔE_{isom}	E_{exc}
2							(1, 1)	32	(8, 24)	(11, 21)	(4, 28)	(4, 28)	(11, 21)	(7, 25)	(11, 21)
3	(2, 1)	(1, 2)	(2, 1)	(1, 2)	(2, 1)		(2, 1)	33	(5, 28)	(13, 20)	(5, 28)	(5, 28)	(7, 26)	(17, 16)	(7, 26)
4	(3, 1)	(3, 1)	(3, 1)	(1, 3)	(3, 1)		(2, 2)	34	(7, 27)	(7, 27)	(17, 17)	(5, 29)	(17, 17)	(7, 27)	(7, 27)
5	(3, 2)	(3, 2)	(3, 2)	(1, 4)	(3, 2)		(3, 2)	35	(7, 28)	(7, 28)	(8, 27)	(7, 28)	(9, 26)	(10, 25)	(9, 26)
6	(2, 4)	(5, 1)	(5, 1)	(1, 5)	(5, 1)	(5, 1)	(2, 4)	36	(9, 27)	(33, 3)	(30, 6)	(6, 30)	(30, 6)	(20, 16)	(12, 24)
7	(2, 5)	(2, 5)	(1, 6)	(1, 6)	(5, 2)	(1, 6)	(2, 5)	37	(8, 29)	(9, 28)	(8, 29)	(9, 28)	(8, 29)	(8, 29)	(9, 28)
8	(2, 6)	(4, 4)	(4, 4)	(2, 6)	(7, 1)	(4, 4)	(4, 4)	38	(8, 30)	(1, 37)	(8, 30)	(7, 31)	(18, 20)	(19, 19)	(10, 28)
9	(1, 8)	(1, 8)	(3, 6)	(1, 8)	(7, 2)	(1, 8)	(4, 5)	39	(9, 30)	(9, 30)	(14, 25)	(10, 29)	(13, 26)	(1, 38)	(9, 30)
10	(1, 9)	(1, 9)	(7, 3)	(1, 9)	(7, 3)	(1, 9)	(5, 5)	40	(7, 33)	(12, 28)	(11, 29)	(11, 29)	(12, 28)	(13, 27)	(12, 28)
11	(1, 10)	(1, 10)	(9, 2)	(1, 10)	(9, 2)	(1, 10)	(5, 6)	41	(8, 33)	(15, 26)	(30, 11)	(7, 34)	(29, 12)	(21, 20)	(12, 29)
12	(1, 11)	(1, 11)	(1, 11)	(1, 11)	(9, 3)	(1, 11)	(4, 8)	42	(31, 11)	(12, 30)	(17, 25)	(12, 30)	(17, 25)	(16, 26)	(12, 30)
13	(1, 12)	(1, 12)	(12, 1)	(1, 12)	(12, 1)	(12, 1)	(3, 10)	43	(15, 28)	(11, 32)	(10, 33)	(2, 41)	(15, 28)	(2, 41)	(15, 28)
14	(1, 13)	(1, 13)	(4, 10)	(1, 13)	(10, 4)	(1, 13)	(4, 10)	44	(11, 33)	(8, 36)	(22, 22)	(8, 36)	(22, 22)	(21, 23)	(11, 33)
15	(1, 14)	(1, 14)	(3, 12)	(1, 14)	(14, 1)	(1, 14)	(5, 10)	45	(11, 34)	(13, 32)	(14, 31)	(13, 32)	(13, 32)	(11, 34)	(11, 34)
16	(1, 15)	(1, 15)	(4, 12)	(1, 15)	(7, 9)	(1, 15)	(7, 9)	46	(31, 15)	(1, 45)	(37, 9)	(1, 45)	(33, 13)	(37, 9)	(15, 31)
17	(2, 15)	(2, 15)	(5, 12)	(1, 16)	(15, 2)	(8, 9)	(5, 12)	47	(17, 30)	(20, 27)	(9, 38)	(13, 34)	(30, 17)	(13, 34)	(13, 34)
18	(2, 16)	(1, 17)	(2, 16)	(2, 16)	(8, 10)	(16, 2)	(8, 10)	48	(30, 18)	(8, 40)	(8, 40)	(8, 40)	(16, 32)	(21, 27)	(14, 34)
19	(1, 18)	(11, 8)	(18, 1)	(1, 18)	(18, 1)	(1, 18)	(4, 15)	49	(18, 31)	(36, 13)	(37, 12)	(12, 37)	(33, 16)	(47, 2)	(14, 35)
20	(2, 18)	(3, 17)	(2, 18)	(1, 19)	(2, 18)	(2, 18)	(7, 13)	50	(21, 29)	(18, 32)	(19, 31)	(18, 32)	(17, 33)	(32, 18)	(19, 31)
21	(2, 19)	(9, 12)	(9, 12)	(1, 20)	(20, 1)	(3, 18)	(6, 15)	51	(12, 39)	(12, 39)	(12, 39)	(12, 39)	(12, 39)	(30, 21)	(22, 29)
22	(3, 19)	(3, 19)	(3, 19)	(1, 21)	(18, 4)	(11, 11)	(6, 16)	52	(15, 37)	(4, 48)	(31, 21)	(31, 21)	(4, 48)	(30, 22)	(22, 30)
23	(3, 20)	(3, 20)	(12, 11)	(3, 20)	(13, 10)	(3, 20)	(7, 16)	53	(17, 36)	(17, 36)	(19, 34)	(17, 36)	(19, 34)	(22, 31)	(21, 32)
24	(3, 21)	(3, 21)	(3, 21)	(1, 23)	(19, 5)	(6, 18)	(5, 19)	54	(10, 44)	(10, 44)	(10, 44)	(6, 48)	(10, 44)	(1, 53)	(16, 38)
25	(10, 15)	(10, 15)	(2, 23)	(2, 23)	(10, 15)	(2, 23)	(6, 19)	55	(12, 43)	(1, 54)	(33, 22)	(1, 54)	(37, 18)	(1, 54)	(20, 35)
26	(3, 23)	(8, 18)	(3, 23)	(3, 23)	(8, 18)	(3, 23)	(7, 19)	56	(44, 12)	(12, 44)	(14, 42)	(12, 44)	(44, 12)	(18, 38)	(18, 38)
27	(4, 23)	(18, 9)	(4, 23)	(4, 23)	(18, 9)	(7, 20)	(8, 19)	57	(15, 42)	(9, 48)	(9, 48)	(9, 48)	(9, 48)	(9, 48)	(19, 38)
28	(3, 25)	(6, 22)	(7, 21)	(3, 25)	(27, 1)	(6, 22)	(7, 21)	58	(13, 45)	(15, 43)	(16, 42)	(15, 43)	(13, 45)	(8, 50)	(23, 35)
29	(6, 23)	(5, 24)	(6, 23)	(5, 24)	(6, 23)	(6, 23)	(6, 23)	59	(13, 46)	(6, 53)	(6, 53)	(7, 52)	(6, 53)	(23, 36)	(20, 39)
30	(7, 23)	(13, 17)	(7, 23)	(4, 26)	(13, 17)	(10, 20)	(9, 21)	60	(12, 48)					(17, 43)	(22, 38)
31	(6, 25)	(6, 25)	(8, 23)	(6, 25)	(8, 23)	(5, 26)	(8, 23)								

Table 5.1: The most stable compositions, (m, n), of the Cu–Ag nanoalloys within the size range of N = 2–60. These compositions are defined by all of the proposed stability criteria, i.e., the stability functions (Eqs. 3.6 to 3.10), as well as the first and second isomers energy difference, and the excess energy (Eq. 3.11).

this effect can be found in the different strengths of homoatomic and heteroatomic bonds, where we have Cu–Cu > Cu–Ag > Ag–Ag.

Chapter 6

Ni–Ag Nanoalloys

Before we proceed, first we will give a brief review of other available studies of Ni–Ag clusters in the next section (Sec. 6.1). The results of our exhaustive investigations are then discussed in the following section (Sec. 6.2).

6.1 Introduction

Many authors have used model potentials for interatomic interactions to study relatively large Ni–Ag nanoalloys. For instance, Rossi et al. used the second-moment approximation to the tight–binding model (SMATB) and the genetic algorithms (GA) to determine the low-energy structures of Ni_mAg_n with N = m+n = 34, 38, and 45 [39]. The most stable structures were reoptimized afterwards in DFT calculations. The results showed that, for a given size, the composition which has a perfect core–shell pIh structure is the most stable one. For N = 34, they identified Ni_7Ag_{27}, and for N = 38 the Ni_8Ag_{30} cluster, where both have perfect core–shell pIh structures, and correspond to the most stable compositions. The most stable composition size N = 45 was (m, n) = (13, 32), which had an anti-Mackay icosahedron structure. They also studied the melting point of Ag nanoalloys and found that bimetallic pIh structures have higher melting points than the pure Ag clusters of the same size. The global minima of Ni–Ag clusters with 34 atoms have also been investigated by Ferrando et al., using an empirical potential [73]. The putative global minima were subsequently reoptimized by using DFT calculations. The enhanced stability of Ni_7Ag_{27} with a 5-fold pancake geometry was again confirmed. Rapallo et al. have also studied nanoalloys of size-mismatched metals at sizes N =

34 and 38, by using SMATB and the GA algorithm [133]. The enhanced stability of the Ni_7Ag_{27} cluster is also approved in their analyses. But for the 38-atomic, they found three different compositions to be stable, i.e., $Ni_{25}Ag_{13}$, Ni_8Ag_{30} and Ni_6Ag_{32}. In addition, $Ni_{13}Ag_{32}$ was the particularly stable stoichiometry of the size N = 45.

6.2 Results and Discussion

Like Cu–Ag, there are just a few selected sizes of Ni–Ag clusters which have been studied systematically. For a complete understanding of the properties of Ni_mAg_n clusters, we decided to determine and investigate the corresponding global minimum structures over a wide range of sizes, N = m+n = 2 to 60, and of all possible combinations of m and n. Again we performed more than 1800 time consuming calculations, and analyzed all the GM structures by using the methods explained in Sec. 3. The result of these analyses are presented in the following section. In the analyses, only some of the more interesting cluster sizes are selected for a more detailed discussion. These are N = 34, 38, 39, 55 and 60.

6.2.1 Structural Properties of Ni–Ag Nanoalloys

Structural Motifs

The structures that we find for the putative GM of Ni–Ag clusters are almost similar to those of Cu–Ag, i.e., they include mainly core–shell polyicosahedron (pIh), capped 5-fold pancakes (c-$cp5_{34}$) and 55-atom Mackay icosahedron (Ih_{55}). We can also see some differences, and the main one is the fact that the symmetric structures for Ni–Ag are not realized as often as in the Cu–Ag case. Structures of some selected Ni–Ag clusters are shown in Fig. 6.1. At small sizes, i.e., N < 13, the GM structures are completely similar to the Cu–Ag clusters, and the new atoms always place at the T sites. At N = 13, all the GM's have Ih_{13} structures. For N > 13, we find different variants of 13-atom icosahedron with extra atoms on the T sites over the surfaces of clusters. The global minima of all compositions of size N = 19 belong to the double icosahedron Ih_{19} category. At sizes N = 19 to 23, the Ih_{19} becomes the main part of all geometries for every stoichiometry. The third icosahedron forms at N = 23, for which we identify three interpenetrating Ih_{13}'s with many shared atoms. According to our results, almost all the GM structures of clusters with 27 to 33 atoms belong

to the pIh category. The first (incomplete) c-pc5_{34} structures are then found for the GM of some Ni–Ag clusters with 33 atoms. These are (7, 26), (10, 23), (23, 10), (24, 9) and (25, 8).

The complete c-pc5_{34} is the GM structure for the stoichimetries of Ni_mAg_n clusters with 34 atoms and m = 7 to 24. All these structures show some deviations from a perfect 5-fold pancake, which are due to the differences in Ni–Ni, Ni–Ag, and Ag–Ag bond-lengths. Nevertheless, many of these c-pc5_{34} have D_{5h} point group, e.g., Ni_7Ag_{27} and $Ni_{23}Ag_{11}$. There are also two exceptions among these stoichiometries which have non-symmetric pIh structures and include the $Ni_{15}Ag_{19}$ and $Ni_{22}Ag_{12}$ clusters. In both cases, some Ag atoms form islands over the Ni atoms. Our results for N = 34 are in agreement with those of Rapallo, who found the 5-fold pancake for a range of Ni–Ag clusters with m = 7-27 Ni atoms [133]. For 34 < N < 38, all structures are polyicosahedra and we do not find any symmetric geometries.

At N = 38, we find a symmetric structure for the (4, 34) cluster which has D_{2h} symmetry and is formed by six Ih_{13} icosahedra with a perfect core–shell ordering of atoms. All of the Ih_{13}'s share two Ag atoms and four of them have one Ni atom in their cores. Each of these Ih_{13}'s has ten common atoms with their two neighbors. Rapallo has also found this (uncapped) 6-fold pancake structure for the Ni–Ag clusters of the range m = 3–6 [133]. The structures of Ni-rich nanoalloys (m = 36 and 37) with 38 atoms are similar to those of pure Ni or Ag clusters, i.e., truncated octahedron (TO). On the contrary, other Ni-rich (m = 32–35) and also Ag-rich nanoalloys (m = 1 and 2) have 5-fold pancake geometries. In the pancake structures of compositions with m = 27–31, the displacement of some of the outer-shell atoms have completely changed the structures to pIh's. We find the polyicosahedron geometries also for the putative global minima of other stoichiometries of the size N = 38.

The c-pc5_{39} structure is the GM of just two Ag-rich clusters, i.e, Ni_1Ag_{38} and Ni_2Ag_{37}. But we find this for many Ni-rich stoichiometries of the size, which include those with m = 30, and 32–36. A 6-fold pancake (c-pc6_{40}) with a vacant site is formed for the $Ni_{26}Ag_{13}$ and $Ni_{28}Ag_{11}$ clusters. All other stoichiometries of size N = 39 have polyicosahedra structures.

Although for the putative GM of some clusters within the size range of N = 40 to 54, a part of the icosahedron Ih_{55} is formed in most of the cases but we should categorize them as pIh structures. Examples of these clusters with an incomplete

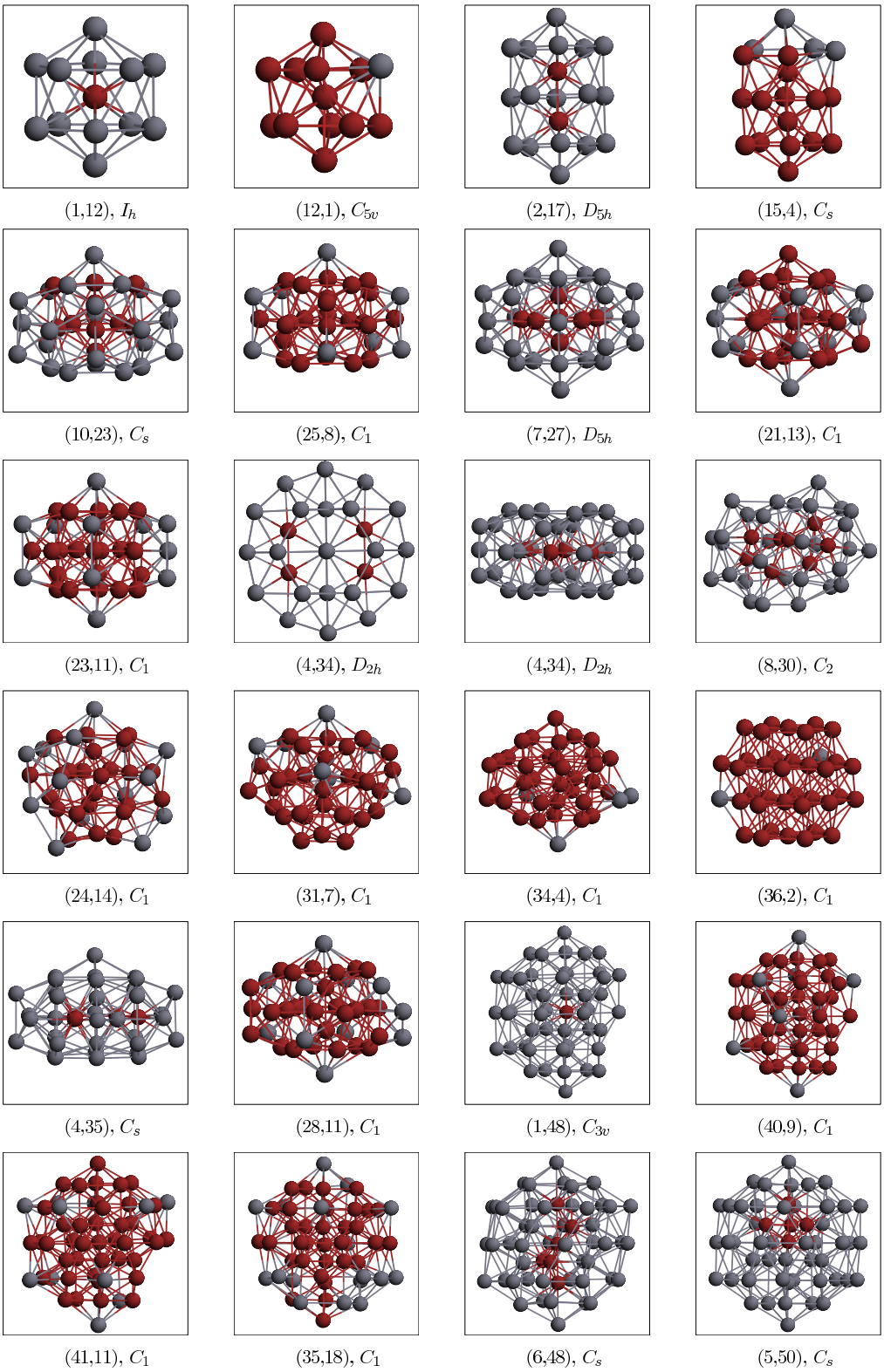

Figure 6.1: Structures of some selected Ni–Ag nanoclusters with selected compositions (m, n). Dark red and gray spheres are Ni and Ag atoms, respectively.

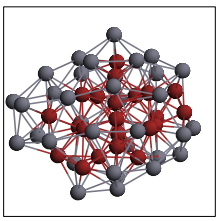

(22,33), C_1

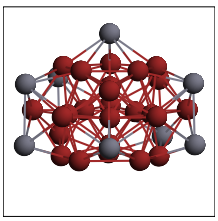

(25,8), C_1

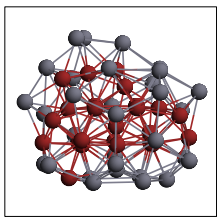

(24,31), C_1

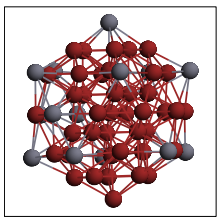

(41,14), C_1

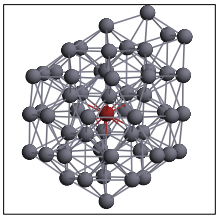

(1,57), C_{3v}

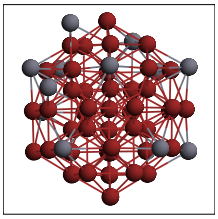

(45,12), C_1

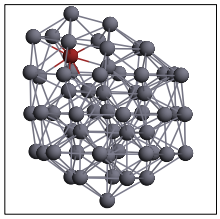

(1,58), C_{3v}

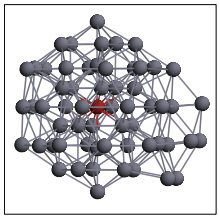

(1,59), C_s

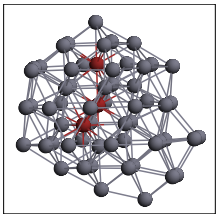

(3,57), C_1

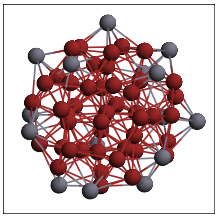

(45,15), C_1

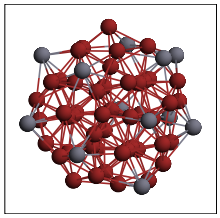

(48,12), C_1

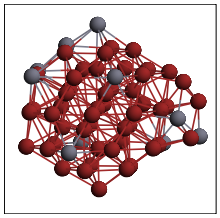

(50,10), C_1

6.1 (Continued)

Ih_{55} structure are the (1, 45), (1, 48), (40, 9), (41, 11), (35, 18) and (6, 48) stoichiometries (Fig. 6.1). We find the 55-atom icosahedron as the GM of Ni-rich (m = 36–55) and Ag-rich (m = 0–9) nanoalloys of size 55. The only exception is the m = 7, which has a pIh motif. Not surprisingly, all the symmetric geometries of Ih_{55} possess some deformations caused by differences in bond lengths. Clusters with a larger number of Ag atoms are generally more deformed, because Ag atoms take all the sites on the surface and therefore the deformation can not be compensated by other bonds around. For clusters of larger sizes, N > 55, which are also Ni- or Ag-rich, the GM structures are formed by 55-atom icosahedron with extra atoms outside the last shell of the Ih_{55}. Examples include $Ni_{45}Ag_{12}$, Ni_1Ag_{57}, Ni_1Ag_{58}, and Ni_1Ag_{59}. Other stoichiometries of these sizes take pIh motifs.

At small sizes of Ni-Ag nanoalloys, as previously stated, new atoms always sit on the T sites of the last shell of a cluster. The same way of growth also happens for the larger sizes. This indicates that the growth of Ni-Ag nanoalloys has a TIC/Polyicosahedral pattern [129].

Bond order Parameter And Radial Distances

We should employ the bond order parameter (see Sec. 3.4.2) to analyze the degree of mixing or segregation of atoms in the Ni–Ag nanoalloys. Fig. 6.2 shows bond order parameter versus the number of Ni atoms (m) for all the compositions of five selected sizes, i.e, N = 34, 38, 39, 55, and 60. The inset of each figure shows the corresponding number of Ni–Ni, Ni–Ag, and Ag–Ag bonds versus m. σ takes only positive values for all of the clusters. This implies that the segregation is the dominant ordering of the two types of atoms, and the structures are of the core–shell type.

The number of Ni–Ag bonds maximizes for the clusters with a comparable number of Ni and Ag atoms. Obviously, this minimizes the σ parameter. The $Ni_{16}Ag_{18}$ and $Ni_{17}Ag_{17}$ clusters have the lowest value of σ for N = 34. The lowest values of σ for N = 38, 39, 55, and 60 are found for asymmetric clusters, which are $Ni_{16}Ag_{22}$, $Ni_{17}Ag_{22}$, $Ni_{23}Ag_{32}$, and $Ni_{34}Ag_{26}$, respectively. It turns out that none of these clusters, except (17, 22), belong to the group of particularly stable ones.

According to Fig. 6.2, the number of Ag–Ag bonds decreases monotonically by replacing more Ag atoms with Ni ones. This number vanishes even when there is a considerable number of Ag atoms in the clusters. In contrast, when there are just

a few Ni atoms in a cluster, the corresponding number of Ni–Ni bonds is not zero. These suggest that a spatial separation of the Ag and Ni atoms happens in Ni–Ag nanoalloys, where Ni atoms always tend to stay close to each other and form a core, while Ag atoms are well-separated.

The ratio of average radial distances of atoms from the center of clusters can help us to identify the type of atoms which have segregated to the surfaces of clusters. Fig. 6.3 depicts this ratio for the average radial distances of Ni and Ag atoms in all Ni–Ag nanoalloys considered in the current study. The values of the ratio are almost always less than one and suggest that Ag atoms segregate to the outer sites of clusters, while Ni atoms place in the inner parts. These indicate the core–shell ordering of atoms in Ni–Ag nanoalloy structures, although the segregation may not be complete.

6.2.2 Energetic Properties of Ni–Ag Nanoalloys

Binding Energy

To analyze the energetic properties of Ni–Ag nanoalloys, first we discuss the binding energies per atom, i.e., $E_b = -\frac{E(m,n)}{N}$. E_b is shown in Fig. 6.4 as a function of (m, n). When keeping the stoichiometry (i.e., $\frac{m}{m+n}$) fixed, E_b increases. This can be seen by following straight lines that pass through $(0, 0)$ in Fig. 6.4, and it implies that larger clusters are more stable than the sum of two noninteracting fragments with the same stoichiometry. Fig. 6.4 also shows that clusters of a given size (i.e., N = m+n) generally have a larger binding energy, the larger the number, m, of Ni atoms is.

There are, however, interesting size-dependent details that are not visible in Fig. 6.4. Thus, in Fig. 6.5 we show E_b as a function of N with either m or n fixed. In both cases, the binding energies have local maxima for N = 13, 19, and 55. For these values the structures form complete icosahedra that have maximal close packing.

The bond order parameter shows that the number of Ni–Ni bonds for clusters with the same value of m stays almost constant, independent of the cluster size. This was interpreted as the formation of a Ni core and a shell of Ag atoms which covers it. Therefore [cf. Fig. 6.5a], the larger E_b for clusters with the larger value of Ni atoms can be related to the higher number of Ni–Ni bonds which are stronger than Ag–Ag or Ni–Ag bonds. This fact can also be recognized in Fig. 6.5b, where

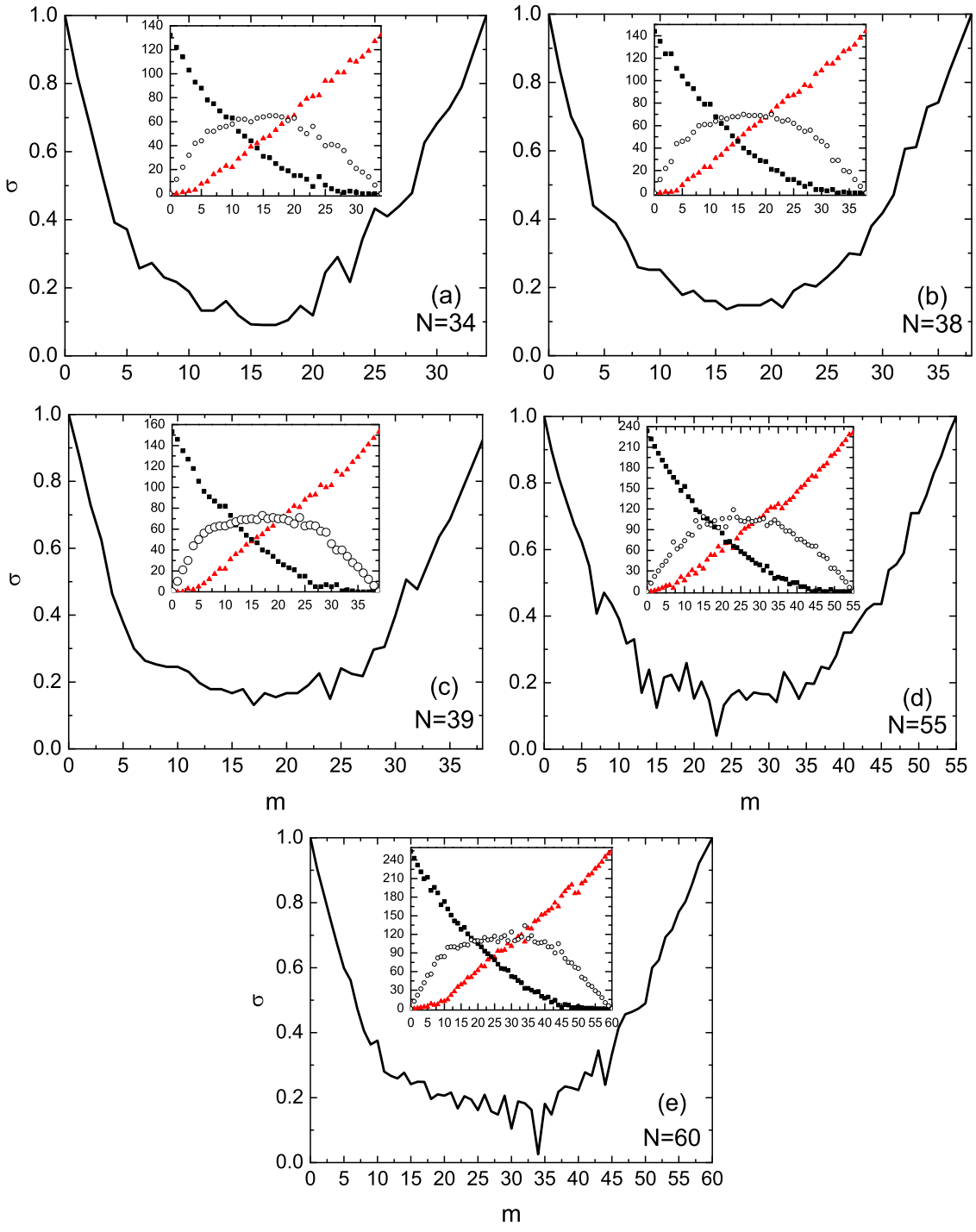

Figure 6.2: The bond order parameter as a function of m (number of Ni atoms) for the global minima of five selected sizes (N = 34, 38, 39, 55, and 60) of Ni–Ag clusters. The insets show the number of the three possible types of bonds vs m. Solid squares and triangles refer to the numbers of Ni–Ni and Ag–Ag bonds, respectively, whereas open circles are for the number of Ni–Ag bonds.

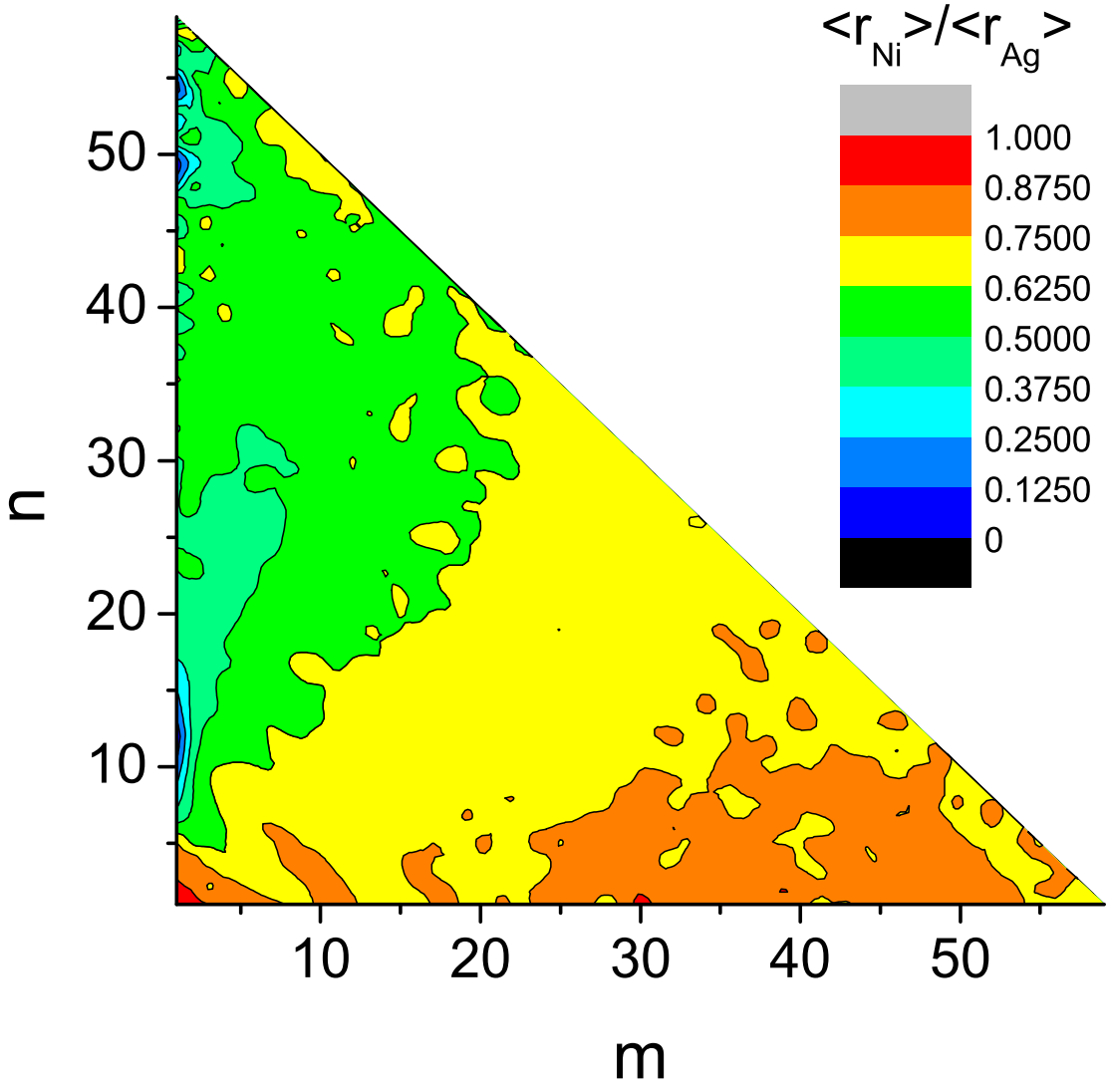

Figure 6.3: Ratio of the average radial distance of the Ni atoms to that of the Ag atoms in Ni_mAg_n clusters as a function of (m, n) for N = m+n from 2 to 60.

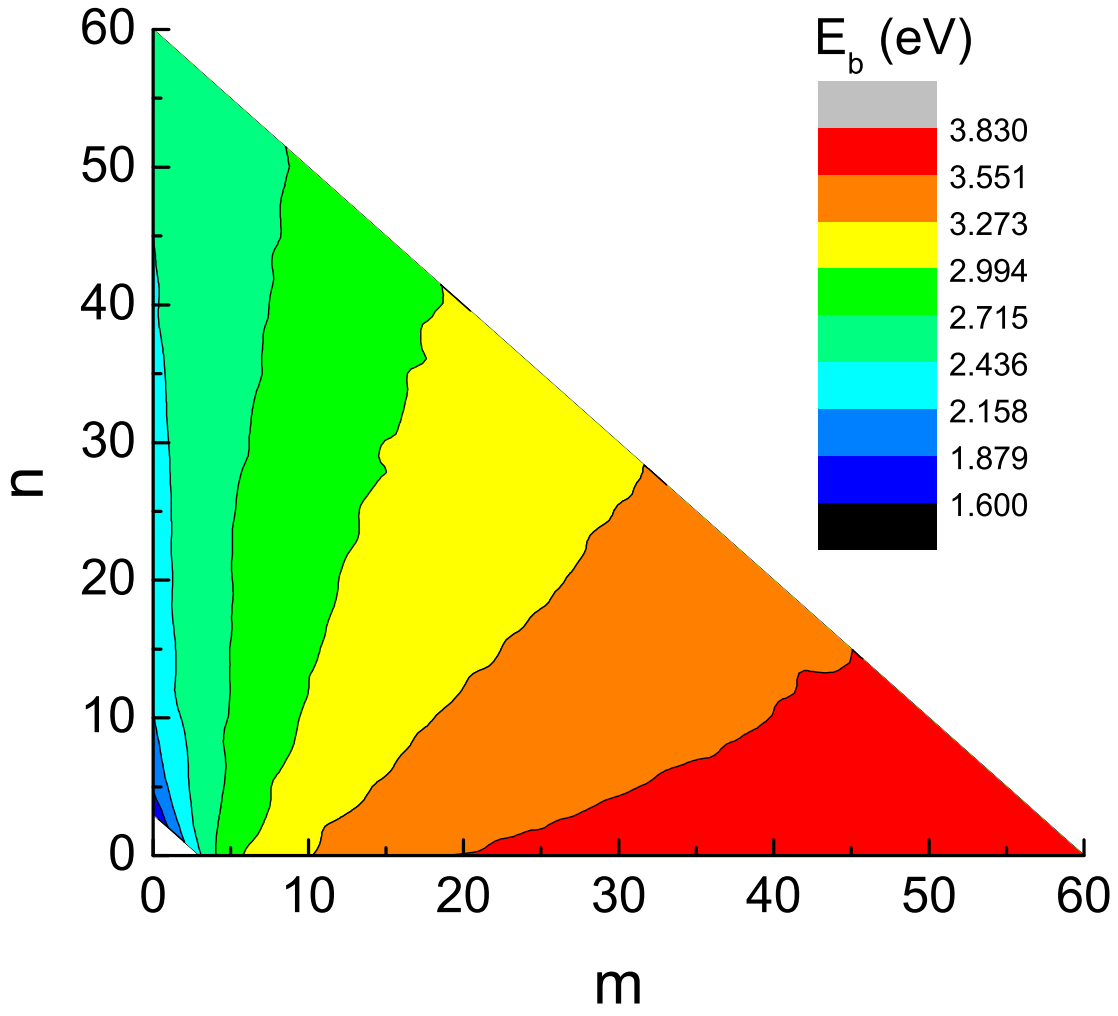

Figure 6.4: Binding energy per atom of Ni–Ag clusters for all compositions and sizes vs number of Ni (m) and Ag (n) atoms.

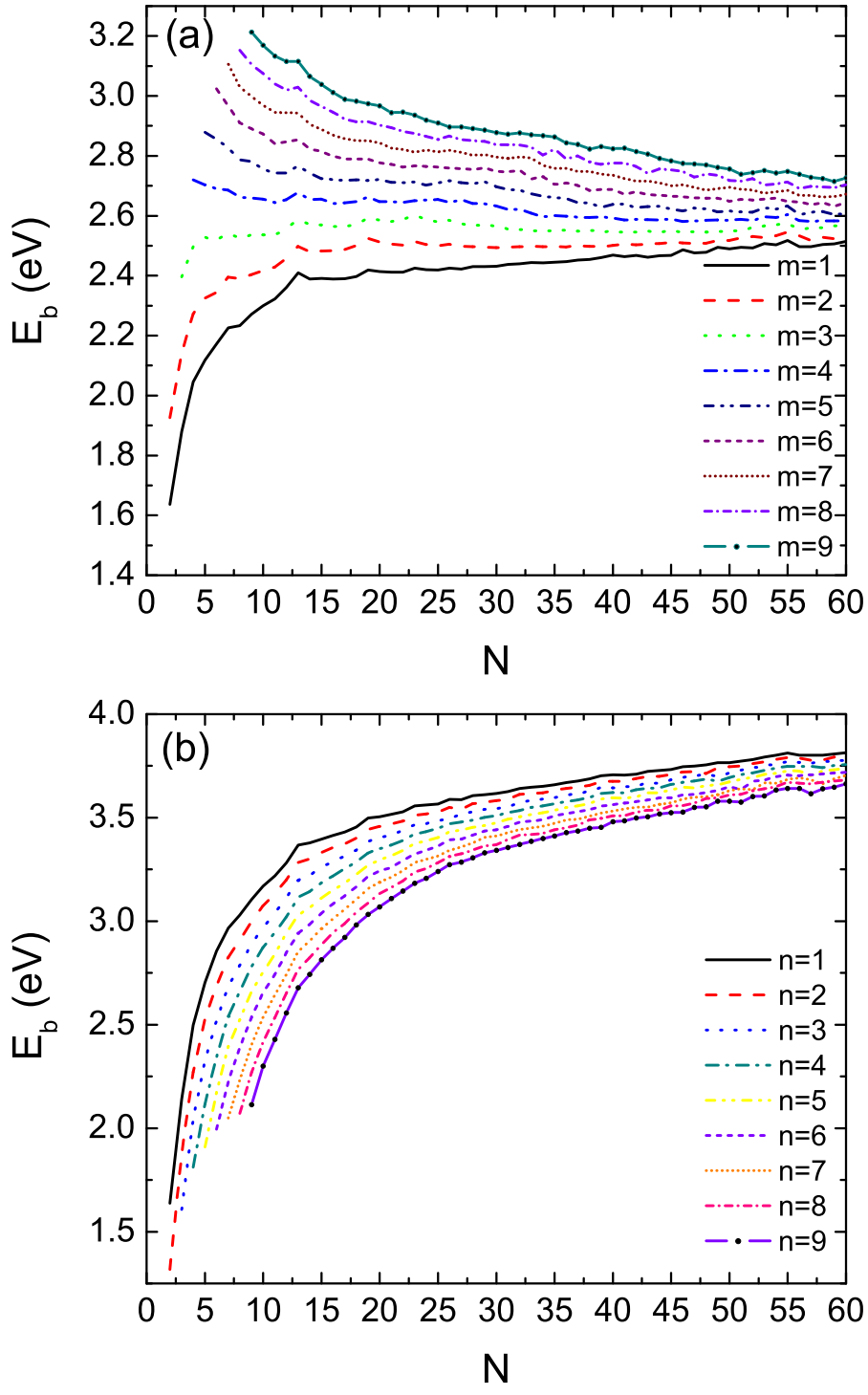

Figure 6.5: Binding Energy per atom of Ni-Ag clusters for some selected compositions vs total number of atoms (N).

the higher-lying curves belong to the structures with more Ni atoms.

In Fig. 6.5a we also see that for a fixed, but increasing, number of Ni atoms, m, E_b as a function of N changes overall behavior: for small m (i.e., $1 \leq m \leq 3$), E_b increases as a function of N, but for larger m ($m > 3$), it decreases. Furthermore, E_b is almost constant for clusters with $N > 10$ and $m = 3$ or 4. Such nonstandard behavior of the E_b plots for large m is explainable: For smaller N the average binding energy is determined mostly by the stronger Ni–Ni bonds, whereas for larger N the binding energy per atom, i.e., E_b, decreases because of the appearance of the weaker Ni–Ag and Ag–Ag bonds.

Stability Function

The unsmoothly varying binding energy suggests that particularly stable Ni–Ag clusters exist. We analyze the GM structures of Ni–Ag nanoalloys, by using the stability functions (Eqs. 3.6-3.10), to identify these stoichiometries. First, we notice that, with one exception, all of the Δ_2 functions determine the Ni_1Ag_{12} and Ni_2Ag_{17} clusters as the most stable stoichiometries of sizes N = 13 and 19, respectively. The exception for N = 13 is $Ni_{12}Ag_1$, given as the most stable cluster by ${}^{m}\Delta_2$ and ${}^{mn}\Delta_2^{(2)}$. For N = 19, the exception is the result of ${}^{mn}\Delta_2^{(2)}$ which indicates the $Ni_{18}Ag_1$ cluster.

The stability function determined by Eq. 3.6 is shown in Fig. 6.6 for five sizes of N = 34, 38, 39, 55, and 60 versus the number of Ni atoms (m). In this figure we find the c-pc5_{34} Ni_7Ag_{27} cluster to be the most stable composition for N = 34. Other noticeable magic clusters of this size are also c-pc5_{34} which include $Ni_{23}Ag_{11}$ and $Ni_{21}Ag_{13}$. All three of these pancake structures have D_{5h} point group. The enhanced stability of these structures is in agreement with other available studies [39, 72, 73, 133]. The Ni_4Ag_{34} cluster with the symmetric structure described before proves to be the most stable composition of size N = 38. Other magic compositions with 38 atoms, according to Fig. 6.6b, have disordered pIh structures and include those with m = 8, 13, 19, 24, and 31. The exception is for m = 34 which is a c-pc5_{39} with one vacant site.

The ${}^{N}\Delta_2$ function determines the c-pc6_{40} Ni_28Ag_{11} to be the most stable cluster of size N = 39 (Fig. 6.6c). The next cluster with an enhanced stability is (4, 35) with a structure similar to that of the (4, 34) but with one extra Ag atom placed along the symmetry axis. The other noticeable stable clusters with 39-atoms include pIh (4, 35), c-pc6_{40} (26, 11), c-pc5_{39} (32, 7).

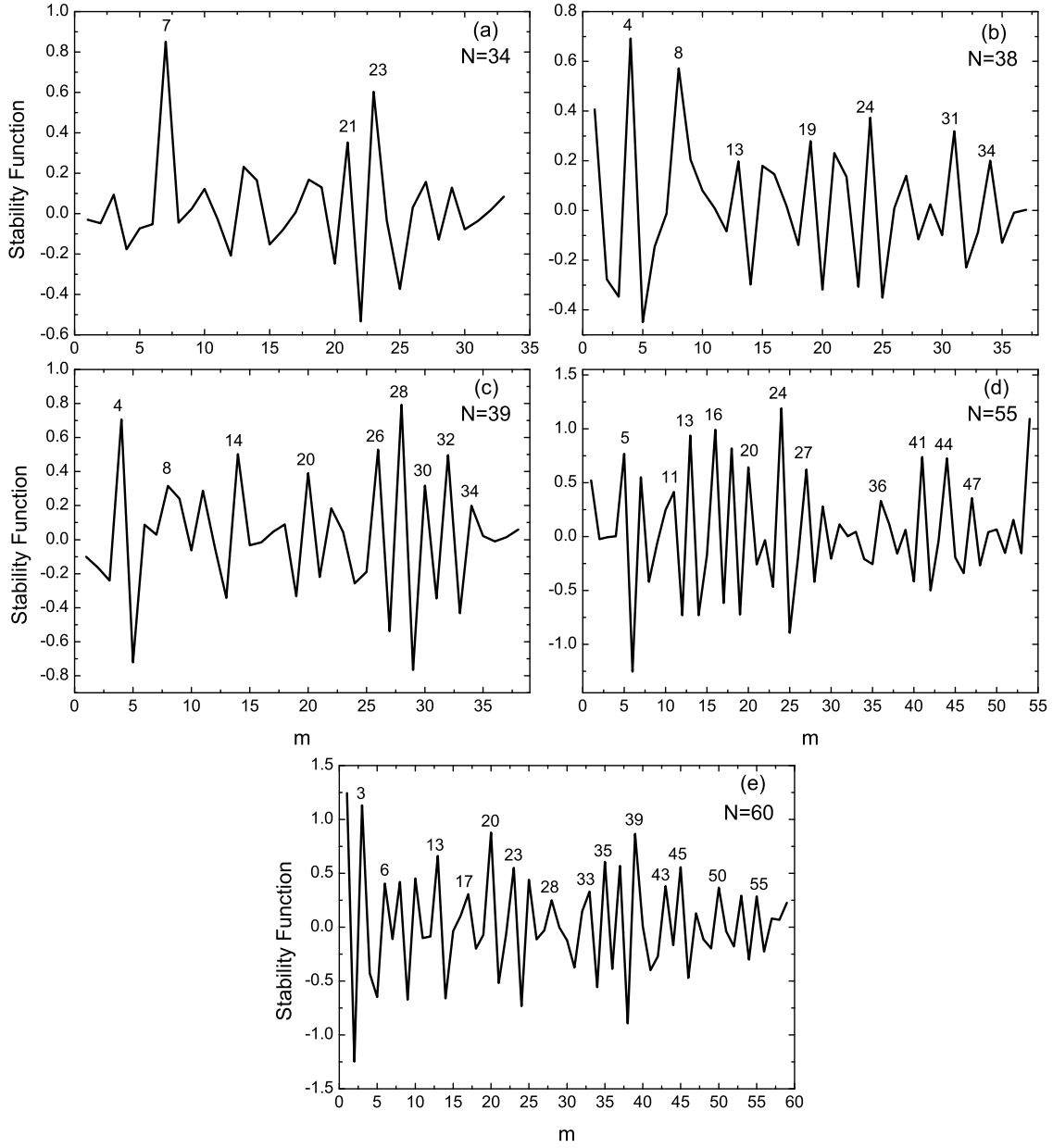

Figure 6.6: Stability function ${}^{N}\Delta_2$ for selected sizes of Ni–Ag nanoalloys vs number of Ni atoms (m).

For N = 55, ${}^{\mathrm{N}}\Delta_2$ determines the pIh $Ni_{24}Ag_{31}$ to be the most stable cluster of the size. According to Fig. 6.6d, other clusters with 55 atoms and of enhanced stabilities have the following compositions: (5, 55), (11, 44), (13, 42), (16, 39), (27, 28), (41, 14), and (44, 11). There is only one other available study for Ni–Ag nanoalloys of the size N = 55, in which the authors found $Ni_{19}Ag_{36}$ as the most stable cluster [86]. The most stable cluster for N = 60 is the GM of Ni_1Ag_{59} with a structure consisting of an Ih_{55} with one Ni atom at the center and five extra Ag atoms on the surface of the icosahedron (Fig. 6.1). This geometry has C_s point group. The following clusters are other more stable clusters of size N = 60 according to ${}^{\mathrm{N}}\Delta_2$: Ni_3Ag_{57}, $Ni_{20}Ag_{40}$, and $Ni_{39}Ag_{21}$.

If we compare the results of stability analyses of Cu–Ag clusters performed by using ${}^{\mathrm{N}}\Delta_2$ with those discussed above, then we find significant differences. Although for N = 60, the particularly stable Cu–Ag clusters are mainly with small values of m, for Ni–Ag they have many different values of m over the whole range of $0 < m < 60$. The number of different particularly stable clusters with 34 atoms is also significantly higher for Cu–Ag than for Ni–Ag. In a general trend, $|{}^{N}\Delta_2|$ has larger values for Ni–Ag than for Cu–Ag nanoalloys. This indicates that the larger similarity in the properties of Cu and Ag compared with Ni and Ag can reduce the values of stability function. All these suggest that more different stable stoichiometries may be produced for Cu–Ag than for Ni–Ag.

Obviously we can not calculate the stability functions defined by Eqs. 3.7–3.10 for the clusters with 60 atoms. Therefore, in Figs. 6.7–6.10, we show the values of these functions for the sizes N = 34, 38, 39, and 55. The most stable clusters of size the N = 34 determined by ${}^{\mathrm{m}}\Delta_2$ and ${}^{\mathrm{mn}}\Delta_2^{(1)}$ are two different stoichiometries, i.e., Ni_6Ag_{28} and $Ni_{10}Ag_{24}$, respectively (Figs. 6.8 and 6.9). The only compositions made stable by all of the stability functions are (21, 13), (23, 11), and (27, 7).

Also for N = 38, just three compositions have been determined to be magic clusters by all definitions of the stability functions. These are Ni_1Ag_{37}, $Ni_{24}Ag_{14}$, and $Ni_{34}Ag_4$. The ${}^{\mathrm{n}}\Delta_2$ and ${}^{\mathrm{mn}}\Delta_2^{(1)}$ functions determine the cluster with (8, 30) to be the most stable one, while ${}^{\mathrm{mn}}\Delta_2^{(2)}$ points to the (17, 21) cluster. Besides this cluster we find $Ni_{18}Ag_{20}$ and $Ni_{19}Ag_{19}$, which have very close values of the stability functions. The cluster with (19, 19) is also stable according to the ${}^{\mathrm{m}}\Delta_2$ function.

At N = 39, the results of the ${}^{\mathrm{m}}\Delta_2$ function defined by Eq. 3.8 are very different from those of other definitions. All of the stability functions, except ${}^{\mathrm{m}}\Delta_2$, give the

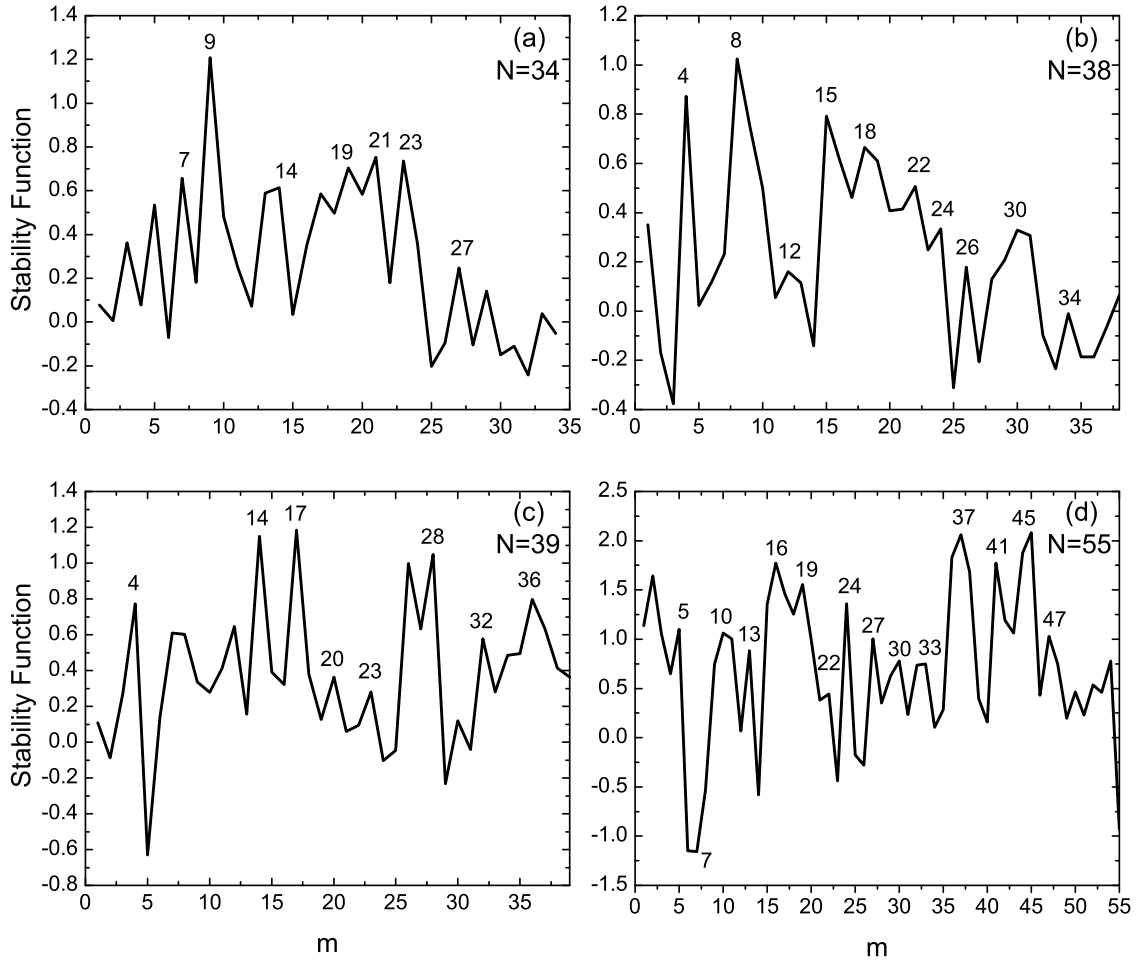

Figure 6.7: Stability function ${}^{n}\Delta_2$ for selected sizes of Ni–Ag nanoalloys vs number of Ni atoms (m).

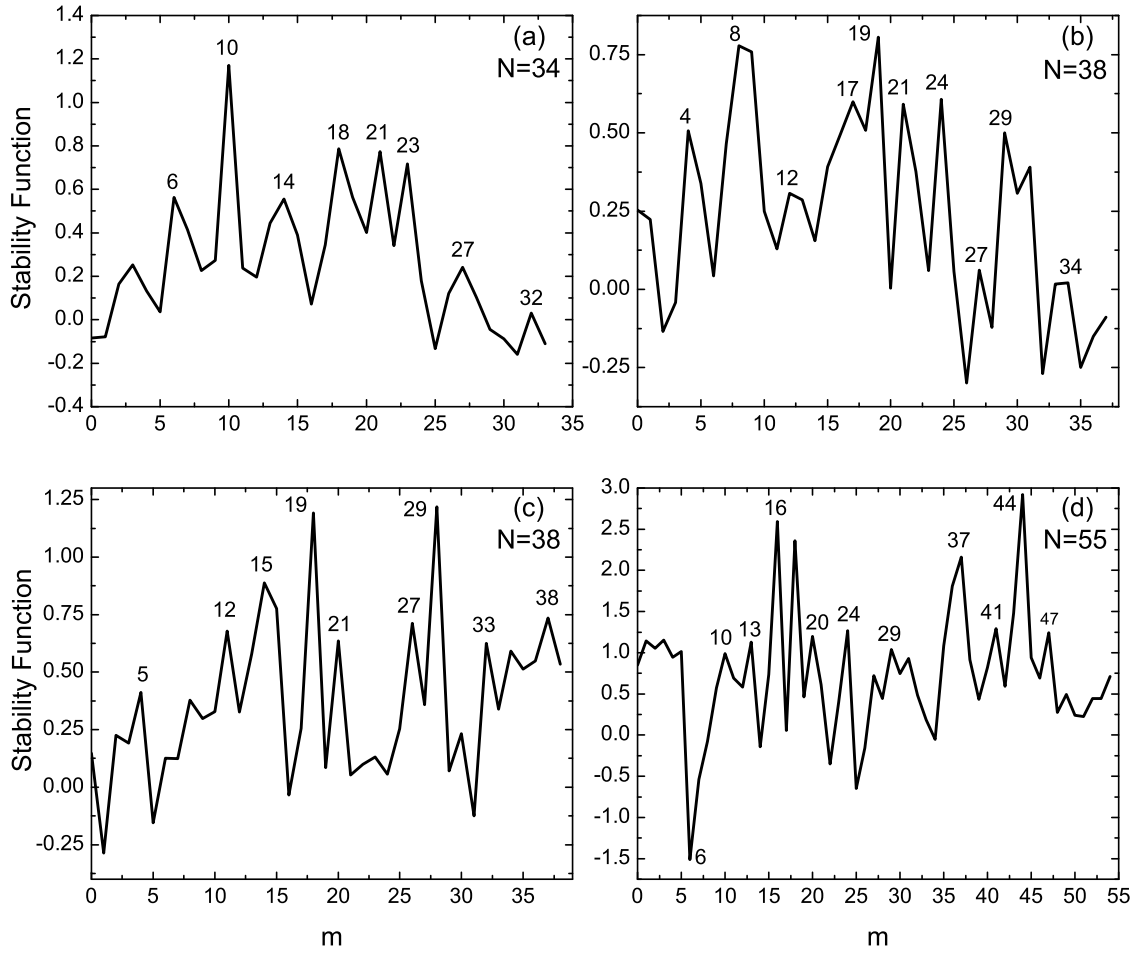

Figure 6.8: Stability function $^{m}\Delta_2$ for selected sizes of Ni–Ag nanoalloys vs number of Ni atoms (m).

clusters with (4, 35), (26, 13), and (28, 11) as the magic compositions. The pIh $Ni_{14}Ag_{35}$ has enhanced stability according to ${}^{N}\Delta_2$, ${}^{n}\Delta_2$, and ${}^{mn}\Delta_2^{(2)}$. The two latter functions also propose the $Ni_{17}Ag_{22}$ to be a magic cluster.

The differences in the results of Δ_2 functions are even more pronounced for N = 55. For this size, various compositions are suggested as stable clusters by different stability functions (Figs. 6.6–6.10). Even in this case we can find some clusters which have peaks of stability for many definitions of Δ_2 function. In the results of all definitions we notice the stability peaks for the clusters with (24, 31), (41, 14) and (47, 8). This is also the case for (13, 42) and (16, 39), if we exclude the ${}^{mn}\Delta_2^{(2)}$ function.

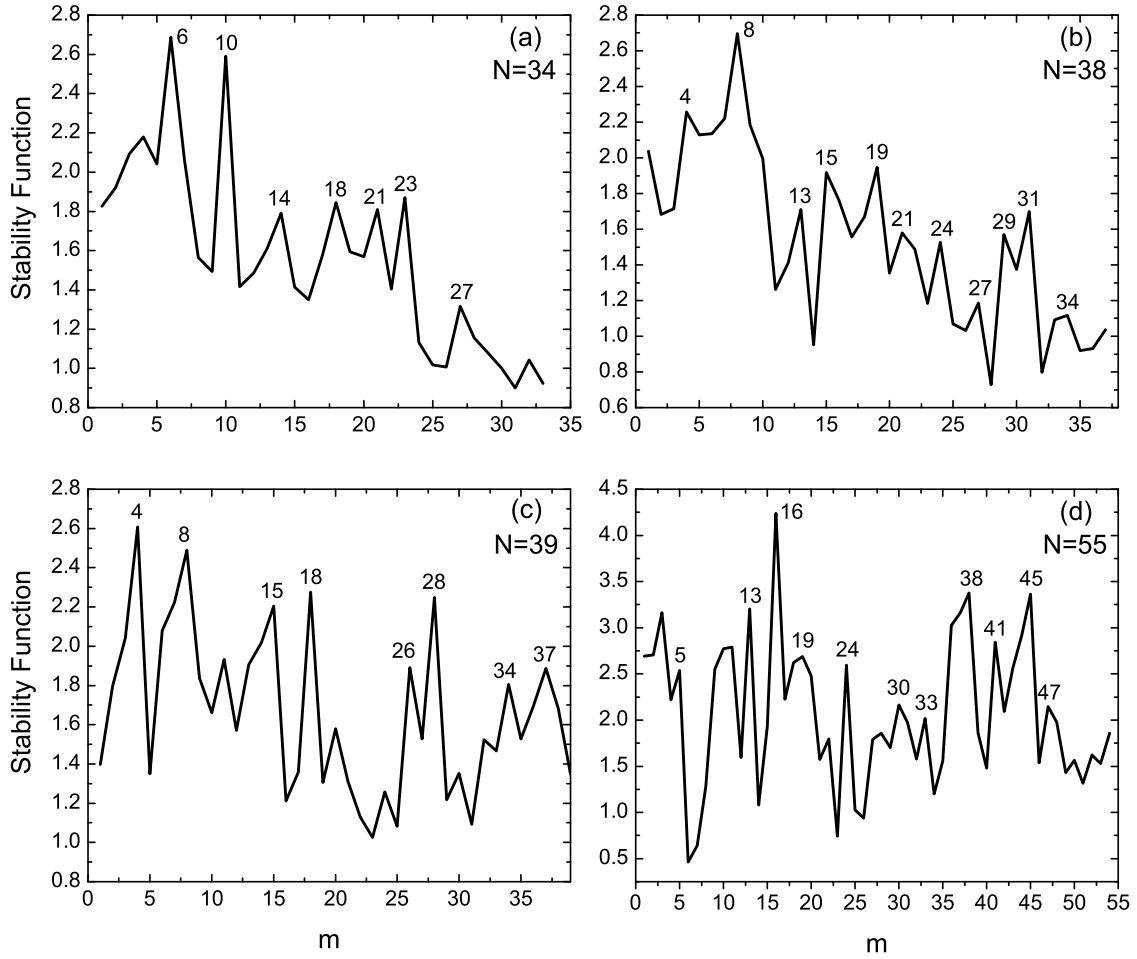

Figure 6.9: Stability function ${}^{mn}\Delta_2^{(1)}$ for selected sizes of Ni–Ag nanoalloys vs number of Ni atoms (m).

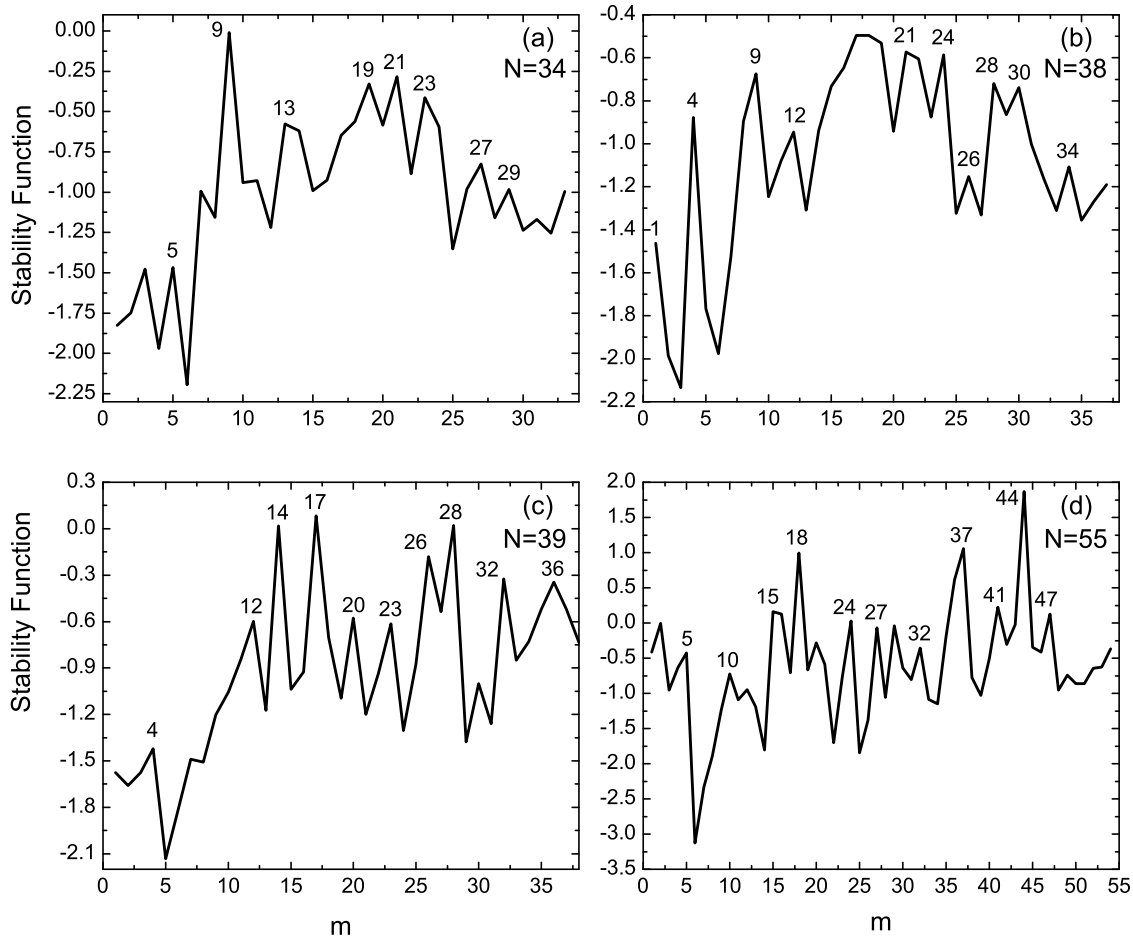

Figure 6.10: Stability function $^{mn}\Delta^{(}2)_2$ for selected sizes of Ni–Ag nanoalloys vs number of Ni atoms (m).

The comparison of the above results, for Ni–Ag, with the previous results on Cu–Ag clusters shows that for both systems the similarities are mainly between the results of the different stability functions for a system, rather than between the two different systems. Therefore, a difference between two types of nanoalloys can be identified by the stability function, although it is not found in the bond order parameters.

Excess Energy

We should also determine stable Ni-Ag clusters in comparison to all stoichiometries for a given size. For this we use the concept of the excess energy E_{exc} introduced in Sec. 3.4.1. E_{exc} can also indicate whether the mixing is the preferred ordering of atoms in a given nanoalloy. First, we show in Fig. 6.11 the excess energies per atom for all Ni–Ag clusters considered in our study. The negative values of E_{exc}/N for almost all sizes suggests that a degree of mixing is almost always preferred by Ni-Ag clusters. Here, we also find a certain range of compositions, i.e., m$\simeq$10 and n$\simeq$22, where the excess energies per atom are very negative and show that the clusters with these compositions are particularly stable in comparison to all other considered Ni–Ag clusters.

For a detailed analysis, Fig. 6.12 depicts the excess energies of five selected sizes of Ni–Ag nanoalloys versus the number of Ni atoms (m). These sizes include N = 34, 38, 39, 55, and 60. In all cases, E_{exc} decreases monotonically from zero, for a pure cluster, and after a minimum value again increases almost monotonically to zero. In spite of these monotonic changes, we find that sudden structural changes cause small deviations in the values of E_{exc} for some specific clusters, and specially for larger sizes like N = 55 and 60 (Fig. 6.12).

The minimum value of the excess energy for N = 34 corresponds to $Ni_{10}Ag_{24}$, while Ni_9Ag_{25} and Ni_7Ag_{27} also have very close values (Fig. 6.12a). The stability of these clusters was also given by the stability functions (Figs. 6.6–6.10). Although these three clusters have 5-fold pancake structures, the deformations have reduced the symmetries of the (9, 25) and (10, 24) clusters to C_2, while the cluster with (7, 27) has D_{5h} point group. The Ni–Ag clusters with (21, 13) and (23, 11) compositions have fivefold pancake geometries. This is also the case for (22, 12), but for this cluster two Ag atoms have left their sites and are placed outside Ni atoms. Therefore, we should correlate the sudden change of E_{exc} for (22, 12) to this structural change.

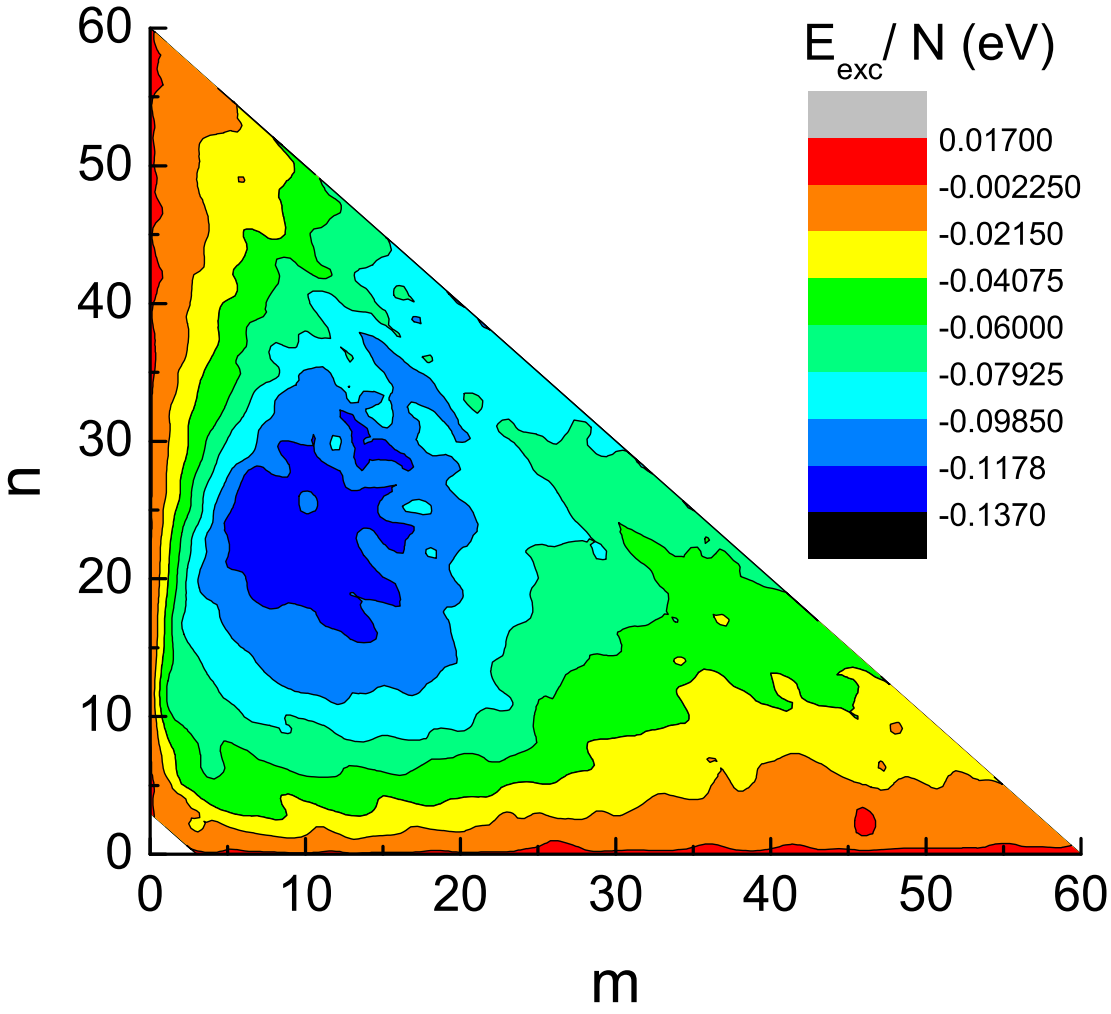

Figure 6.11: The excess energy per atom for Ni–Ag clusters as a function of (m, n) for all possible combinations of m and n, with N = m+n from 2 to 60.

The $Ni_{10}Ag_{28}$ cluster possesses the minimum value of the excess energy for N = 38. Next to it, we find Ni_9Ag_{29} which was predicted to be a stable composition by the ${}^{mn}\Delta_2^{(2)}$ function (Figs. 6.10 and 6.12b). These two clusters have pIh motifs made by a broken fivefold pancake structure in which some Ag atoms are displaced to the surface of the structure to cover more Ni atoms. In the excess energies of clusters of sizes N = 34 and 38, we see a plateau for m = 7–14 and 8–13, respectively (Fig. 6.12). In the first case, i.e., N = 34 and m = 7–14, all structures are 5-fold pancakes, and in the second one they are all polyicosahedra formed by a (partially) deformed 5-fold pancake with extra atoms attached to it.

For N = 39, E_{exc} of the Ni–Ag cluster with (14, 25) composition is the minimum. This is in agreement with the results of the stability functions where three definitions have determined this composition to be a magic cluster. The frequent deviations in the excess energies of clusters with N = 39 and m > 25 are the results of the interplay between different structural motifs, i.e., mainly the pIh's and also capped pancakes.

According to Fig. 6.12d, the E_{exc} of clusters with N = 55 atoms has a minimum for $Ni_{18}Ag_{37}$ which is just 0.011 eV higher than $Ni_{16}Ag_{39}$. Both of these clusters have Ih_{55} geometries. We notice that the excess energies of all clusters of this size which consist of m = 15 to 25 Ni atoms are very low. But they also oscillate frequently while they are all (different forms of) polyicosahedral motifs. To explain the pronounced change in the excess energy of $Ni_{23}Ag_{32}$ which is a disordered pIh, we have to look at the structures of the $Ni_{22}Ag_{33}$ and $Ni_{24}Ag_{31}$ clusters. Each structure has a 5-fold pancake core in which the atoms from the caps have left their sites to form an Ih_{13}, together with the atoms of the last shell. Fig. 6.12e shows that E_{exc} of the $Ni_{20}Ag_{40}$ cluster becomes the minimum value for the size N = 60. This cluster has a truncated Ih_{55} with five extra atoms on the surface.

Generally, the excess energy is lowest for the Ag-rich compositions of Ni–Ag clusters. The same behavior was also found for Cu–Ag. This is especially noticeable for the clusters of smaller sizes like N = 34, 38, and 39. In spite of this common trend in both types of nanoalloys, we notice that the smooth change of E_{exc} of Cu–Ag clusters over a wide range of m for N = 55 and 60 is not seen for Ni–Ag clusters. It can be considered an effect of the closer similarity between Cu and Ag rather than Ni and Ag.

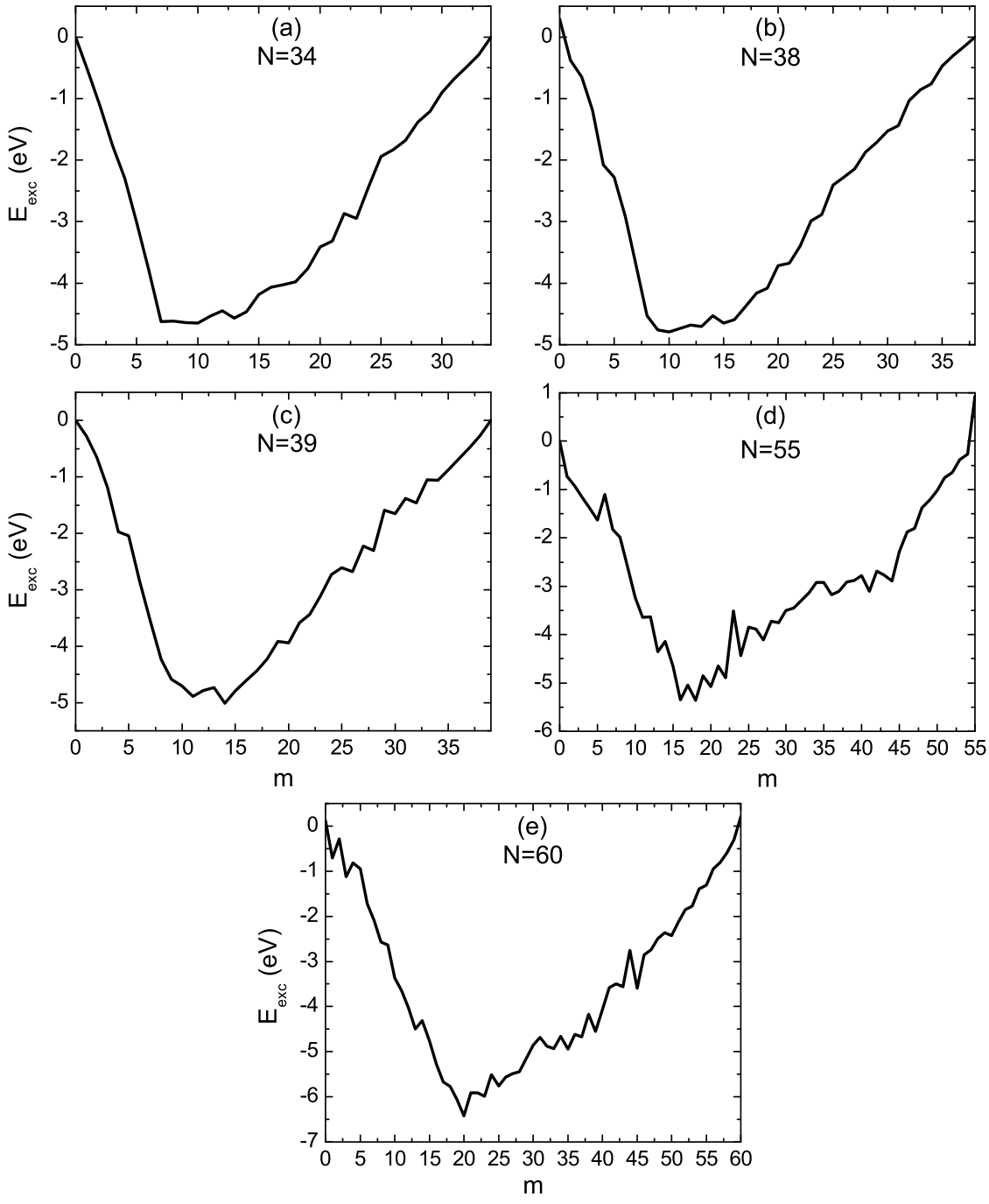

Figure 6.12: The excess energy of the Ni–Ag nanoalloys for five selected sizes (N = 34, 38, 39, 55, and 60) vs number of Ni atoms (m).

Isomers Energy Difference

We have also investigated the thermal stability of Ni-Ag clusters by calculating the energy differences of the first and second lowest-lying isomers (see Sec. 3.4.1). The results are shown in Fig. 6.13 for all stoichiometries of five selected sizes, i.e., N = 34, 38, 39, 55, and 60. According to Figs. 6.13a and 6.13b, many of the magic clusters of sizes 34 and 38 also have large energy gaps with respect to their second isomers and are therefore thermally stable. Despite this similarity in the results, there are also some differences. A noticeable difference is the stability of the $Ni_{28}Ag_6$ and $Ni_{25}Ag_{13}$ clusters, which was not given by the stability functions. The lowest energy isomer of the first clusters is a fragment of a 6-fold pancake, and that of the next(second) isomer is an non-symmetric pIh. Both lowest-lying isomers of the $Ni_{25}Ag_{13}$ cluster are two different polyicosahedra. We find other differences for those clusters of sizes 34 and 38 which are stable according to the stability functions but they are not thermally stable clusters. For instance, the first and second isomers of the cluster with (6, 28) composition have almost the same energies, while both ${}^{\mathrm{m}}\Delta_2$ and ${}^{\mathrm{mn}}\Delta_2^{(1)}$ determined the first isomer as a magic cluster. The effect of the surface energies becomes clear when we look at the structures of these two isomers. The second isomer has a 5-fold pancake geometry, whereas the first one is a nonsymmetric pIh with a perfect core-shell structure.

The first isomers of many magic Ni–Ag clusters with 38 atoms (Figs. 6.6–6.10) are not stable according to their small energy gaps with the corresponding following isomers (Fig. 6.13). These include the (9, 29), (12, 26), (18, 20), (24, 14), and (26, 12) clusters. We find both isomers of all these clusters, except (24, 14), to be homotops. For the (24, 14) cluster, the structures of the two isomers are completely different.

Our results for the clusters with 39 atoms show that many clusters, often defined as stable by the stability functions, also have enhanced thermal stabilities. Examples are clusters with m = 4, 8, 17, 26, and 28. Both isomers of the first three clusters have different pIh structures. For the (26, 13) cluster, the first isomer is a capped 6-fold 40-atom pancake with some vacant sites and the second one is a pIh. For $Ni_{28}Ag11$ both isomers are c-pc6_{40}, but the vacant site has a different place in each case. Additionally, we find the (31, 8) cluster stable, whereas it does not have peak for any definitions of the Δ_2 functions (Fig. 6.13c). The lowest-lying isomers of this cluster both have disordered polyicosahedra motifs.

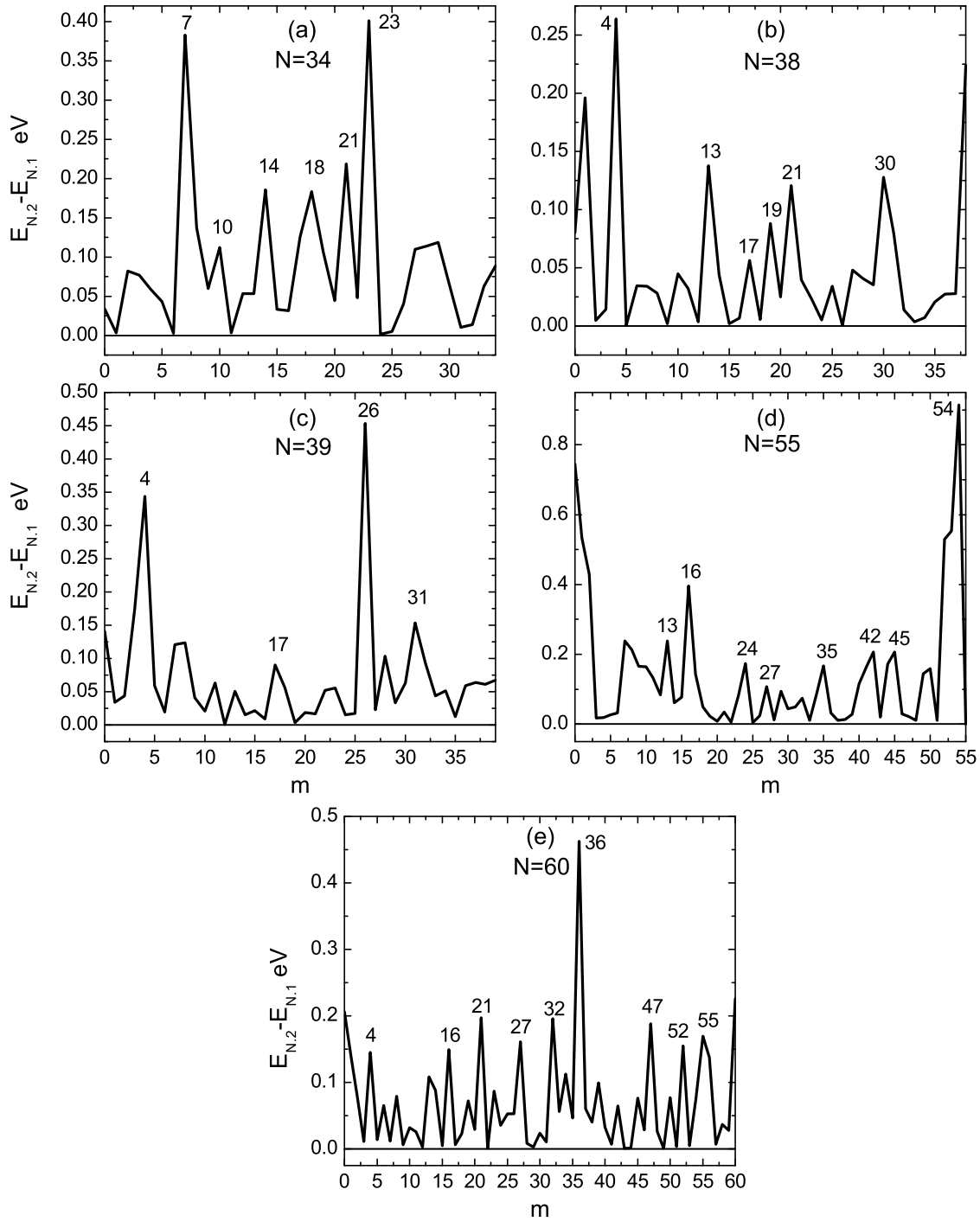

Figure 6.13: Energy differences between the two lowest-lying (first and second) stable isomers for five selected sizes of Ni–Ag nanoalloys vs number of Ni atoms (m).

For N = 55, the stable clusters determined by the stability functions and also the isomers energy differences are (7, 48), (13, 42), (16, 39), (24, 31), (45, 10), and (54, 1). However, we can also see the following differences between the results of these stability measures. First we find that the isomers energy differences of $Ni_{35}Ag_{20}$ and $Ni_{42}Ag_{13}$ point to the stability of these two clusters, whereas they do not have peaks in the stability function graphs (Fig. 6.13d). The first and second isomers of $Ni_{35}Ag_{20}$ have different pIh structures, and those of $Ni_{42}Ag_{13}$ are Ih_{55} motifs. But in the second isomer of the latter cluster an Ag atom from a vertex site is displaced to a T site over the last icosahedron shell. There are also some 55-atom Ni–Ag clusters, such as those with m = 3, 20, 33, and 52, which have enhanced stabilities according to Figs. 6.6–6.10, but are not thermally stable.

We can compare the thermal stability of size N = 60 just to the results of ${}^{N}\Delta_2$. Considering the common stable clusters found for other sizes by the stability functions and also the isomers energy differences, the latter measure can help here to predict other possible stable clusters of this size. Among these types of clusters with high peaks in Fig. 6.13d, the cluster with (36, 24) shows to be very stable. The structure of both its first and second isomers are pIh's consisting of an Ih55 with high degrees of deformations. Other stable clusters of this size include those with m = 4, 16, 21, 27, 47, and 52 Ni atoms.

To summerize the results of stability analyses of the Ni–Ag nanoalloys, table 6.1 lists all of the most stable clusters determined by different stability criteria, i.e., the stability functions (Eqs. 3.6–3.10), the isomers energy differences, and also the excess energy (Eq. 3.11).

According to table 6.1, different criteria often give similar, but not identical, results, although in many cases quite different results occur. However, we should consider that the table lists only the most stable clusters. Thus, even a small change in the relative stability is one source for the differences in the table. In spite of this, we find in the table that both Ni_2Ag_5, and $Ni_{14}Ag_{33}$ clusters meet six of the stability criteria, while Ni_5Ag_1, Ni_2Ag_{17} and $Ni_{17}Ag_{24}$, are stable in accord with five out of seven stability measures. There are seventeen Ni–Ag clusters, i.e., Ni_2Ag_6, Ni_1Ag_8, Ni_1Ag_9, Ni_1Ag_{11}, Ni_1Ag_{12}, Ni_1Ag_{13}, Ni_1Ag_{14}, Ni_1Ag_{15}, Ni_9Ag_{13}, Ni_3Ag_{20}, Ni_4Ag_{23}, Ni_5Ag_{24}, $Ni_{16}Ag_{24}$, $Ni_{11}Ag_{31}$, $Ni_{15}Ag_{29}$, $Ni_{35}Ag_{18}$ and $Ni_{45}Ag_{12}$, that match four stability conditions. And finally, the fifteen clusters which satisfy at least three stability criteria are Ni_1Ag_{10}, $Ni_{12}Ag_1$, Ni_5Ag_{15}, $Ni_{17}Ag_{11}$, $Ni_{14}Ag_{16}$, Ni_6Ag_{26},

N	$^{N}\Delta_2$	$^{n}\Delta_2$	$^{m}\Delta_2$	$^{mn}\Delta_2^{(1)}$	$^{mn}\Delta_2^{(2)}$	$E_{N,2}$-$E_{N,1}$	E_{exc}	N	$^{N}\Delta_2$	$^{n}\Delta_2$	$^{m}\Delta_2$	$^{mn}\Delta_2^{(1)}$	$^{mn}\Delta_2^{(2)}$	$E_{N,2}$-$E_{N,1}$	E_{exc}
2							(1, 1)	32	(12, 20)	(6, 26)	(24, 8)	(6, 26)	(30, 2)	(6, 26)	(7, 25)
3	(1, 2)	(2, 1)	(2, 1)	(2, 1)	(2, 1)		(1, 2)	33	(6, 27)	(24, 9)	(25, 8)	(4, 29)	(23, 10)	(7, 26)	(10, 23)
4	(1, 3)	(3, 1)	(3, 1)	(1, 3)	(3, 1)		(2, 2)	34	(7, 27)	(9, 25)	(10, 24)	(6, 28)	(9, 25)	(23, 11)	(10, 24)
5	(3, 2)	(3, 2)	(3, 2)	(3, 2)	(3, 2)		(3, 2)	35	(7, 28)	(7, 28)	(8, 27)	(7, 28)	(9, 26)	(33, 2)	(9, 26)
6	(3, 3)	(5, 1)	(5, 1)	(5, 1)	(5, 1)	(5, 1)	(3, 3)	36	(9, 27)	(11, 25)	(6, 30)	(5, 31)	(21, 15)	(9, 27)	(12, 24)
7	(2, 5)	(2, 5)	(2, 5)	(2, 5)	(2, 5)	(1, 6)	(2, 5)	37	(13, 24)	(11, 26)	(10, 27)	(2, 35)	(10, 27)	(9, 28)	(10, 27)
8	(2, 6)	(2, 6)	(4, 4)	(2, 6)	(6, 2)	(2, 6)	(4, 4)	38	(4, 34)	(8, 30)	(19, 19)	(8, 30)	(17, 21)	(4, 34)	(10, 28)
9	(1, 8)	(1, 8)	(5, 4)	(1, 8)	(5, 4)	(1, 8)	(4, 5)	39	(28, 11)	(17, 22)	(28, 11)	(4, 35)	(17, 22)	(26, 13)	(14, 25)
10	(1, 9)	(1, 9)	(6, 4)	(1, 9)	(8, 2)	(1, 9)	(4, 6)	40	(16, 24)	(11, 29)	(16, 24)	(16, 24)	(31, 9)	(39, 1)	(16, 24)
11	(1, 10)	(1, 10)	(8, 3)	(1, 10)	(7, 4)	(8, 3)	(4, 7)	41	(17, 24)	(11, 30)	(17, 24)	(17, 24)	(11, 30)	(17, 24)	(17, 24)
12	(1, 11)	(1, 11)	(7, 5)	(1, 11)	(7, 5)	(1, 11)	(4, 8)	42	(11, 31)	(14, 28)	(11, 31)	(11, 31)	(14, 28)	(14, 28)	(11, 31)
13	(1, 12)	(1, 12)	(12, 1)	(1, 12)	(12, 1)	(12, 1)	(1, 12)	43	(16, 27)	(13, 30)	(21, 22)	(13, 30)	(20, 23)	(40, 3)	(13, 30)
14	(1, 13)	(1, 13)	(5, 9)	(1, 13)	(13, 1)	(1, 13)	(5, 9)	44	(15, 29)	(12, 32)	(15, 29)	(12, 32)	(15, 29)	(11, 33)	(15, 29)
15	(1, 14)	(1, 14)	(4, 11)	(1, 14)	(14, 1)	(1, 14)	(4, 11)	45	(30, 15)	(15, 30)	(14, 31)	(15, 30)	(14, 31)	(30, 15)	(15, 30)
16	(1, 15)	(1, 15)	(8, 8)	(1, 15)	(14, 2)	(1, 15)	(6, 10)	46	(11, 35)	(1, 45)	(1, 45)	(1, 45)	(21, 25)	(11, 35)	(17, 29)
17	(2, 15)	(2, 15)	(4, 13)	(1, 16)	(16, 1)	(4, 13)	(5, 12)	47	(14, 33)	(14, 33)	(14, 33)	(14, 33)	(14, 33)	(19, 28)	(14, 33)
18	(2, 16)	(2, 16)	(5, 13)	(1, 17)	(9, 9)	(1, 17)	(6, 12)	48	(17, 31)	(17, 31)	(20, 28)	(10, 38)	(20, 28)	(44, 4)	(17, 31)
19	(2, 17)	(2, 17)	(2, 17)	(2, 17)	(18, 1)	(2, 17)	(4, 15)	49	(1, 48)	(40, 9)	(26, 23)	(8, 41)	(1, 48)	(41, 8)	(16, 33)
20	(2, 18)	(2, 18)	(5, 15)	(1, 19)	(9, 11)	(5, 15)	(5, 15)	50	(7, 43)	(30, 20)	(31, 19)	(30, 20)	(31, 19)	(32, 18)	(20, 30)
21	(2, 19)	(5, 16)	(11, 10)	(1, 20)	(11, 10)	(2, 19)	(8, 13)	51	(29, 22)	(29, 22)	(12, 39)	(12, 39)	(23, 28)	(11, 40)	(16, 35)
22	(3, 19)	(3, 19)	(9, 13)	(1, 21)	(9, 13)	(9, 13)	(9, 13)	52	(23, 29)	(15, 37)	(41, 11)	(11, 41)	(40, 12)	(32, 20)	(18, 34)
23	(3, 20)	(3, 20)	(10, 13)	(3, 20)	(22, 1)	(3, 20)	(7, 16)	53	(12, 41)	(35, 18)	(35, 18)	(35, 18)	(35, 18)	(44, 9)	(18, 35)
24	(3, 21)	(7, 17)	(18, 6)	(1, 23)	(23, 1)	(3, 21)	(7, 17)	54	(17, 37)	(22, 32)	(6, 48)	(6, 48)	(22, 32)	(45, 9)	(22, 32)
25	(4, 21)	(3, 22)	(10, 15)	(2, 23)	(15, 10)	(4, 21)	(10, 15)	55	(24, 31)	(45, 10)	(44, 11)	(16, 39)	(44, 11)	(54, 1)	(18, 37)
26	(5, 21)	(24, 2)	(17, 9)	(2, 24)	(24, 2)	(6, 20)	(7, 19)	56	(17, 39)	(15, 41)	(17, 39)	(14, 42)	(15, 41)	(18, 38)	(17, 39)
27	(4, 23)	(5, 22)	(4, 23)	(4, 23)	(23, 4)	(4, 23)	(7, 20)	57	(15, 42)	(45, 12)	(45, 12)	(45, 12)	(45, 12)	(46, 11)	(18, 39)
28	(5, 23)	(17, 11)	(13, 15)	(1, 27)	(17, 11)	(17, 11)	(8, 20)	58	(1, 57)	(17, 41)	(16, 42)	(20, 38)	(16, 42)	(1, 57)	(20, 38)
29	(5, 24)	(5, 24)	(22, 7)	(5, 24)	(16, 13)	(5, 24)	(8, 21)	59	(21, 38)	(1, 58)	(44, 15)	(1, 58)	(51, 8)	(24, 35)	(21, 38)
30	(10, 20)	(14, 16)	(14, 16)	(3, 27)	(14, 16)	(12, 18)	(10, 20)	60	(1, 59)					(36, 24)	(20, 40)
31	(6, 25)	(12, 19)	(13, 18)	(3, 28)	(22, 9)	(27, 4)	(10, 21)								

Table 6.1: The most stable compositions, (m, n), for Ni–Ag nanoalloys within the size range of N = 2 to 60. These compositions are defined by all of the proposed stability criteria, i.e., the stability functions (Eqs. 3.6–3.10) as well as the first and second isomers energy difference, and the excess energy (Eq. 3.11).

Ni_7Ag_{28}, $Ni_{10}Ag_{27}$, $Ni_{14}Ag_{28}$, $Ni_{13}Ag_{30}$, $Ni_{15}Ag_{30}$, Ni_1Ag_{45}, $Ni_{17}Ag_{31}$, $Ni_{22}Ag_{32}$ and $Ni_{17}Ag_{39}$.

Mixing Energy and Coefficient

We should also calculate the mixing coefficients and mixing energies of Ni–Ag nanoalloys to study the structural ordering of atoms and the effects of mixing on the structural energies.

Fig. 6.14 depicts the mixing coefficient M and the mixing energy E_{mix} per atom for all Ni_mAg_n clusters with every possible combination of m and n for N = m+n from 2 to 60. We find that M increases positively and E_{mix} increases negatively as more Ni atoms are substituted for Ag atoms. An interpretation for this effect is

the stabilizing effect of Ni atoms when they are introduced to the Ag-rich clusters, while the opposite case can not be concluded here, i.e., Ni-rich clusters do not become stabilized by substituting Ni with Ag atoms. This can be explained by the stronger Ni–Ni and weaker Ag–Ag bonds, when we compare them with the Ag–Ni bonds. The large and negative values of E_{mix} are also the result of preference for some degrees of mixing in the Ni–Ag clusters. In comparison, the mixing coefficients and energies of Ni–Ag and Cu–Ag clusters have totally different behaviors with respect to the changes in the stoichiometries, although the corresponding structures are very similar. Additionally, the values of M and E_{mix}/N for Ni–Ag clusters are much larger (cf. Figs. 5.14 and 5.14). Therefore, these quantities are not helpful in the structural analyses and comparison of two different nanoalloys, and they just give information on the corresponding energetic properties. The large differences between the mixing coefficients and energies of Ni–Ag and Cu–Ag clusters are in agreement with the fact that Ag atoms are more similar to Cu atoms in energetic properties rather than to Ni.

Comparison of Cu–Ag and Ni–Ag Nanoalloys

In many parts of the above discussions, we have compared the properties of the Cu–Ag and Ni–Ag clusters. But we should also compare both structural and energetical properties of these clusters more quantitatively.

For a structural comparison, we employ the similarity function (Eq. 3.14) and calculate it for each pair of Cu_mAg_n and Ni_mAg_n clusters with the same values of m and n. Fig. 6.15 shows the results versus m and n for all clusters considered in our studies. The similarity function of Cu–Ag and Ni–Ag clusters is mainly more than 80%, and only in a few cases drops between 70% and 80%. These high values of similarity function are in agreement with the structural motifs that we found for these clusters. According to Fig. 6.15 the low values belong to the stoichiometries with a comparable number of Ag and Ni/Cu atoms. For these types of clusters, the global minimum structures have mainly disordered pIh structures for which the determination of the similarities is sometimes not trivial, and requires more precise mathematical tools.

For a quantitative comparison of a given property of Cu-Ag and Ni-Ag nanoalloys such as Z, we consider its average values for both systems and calculate the following

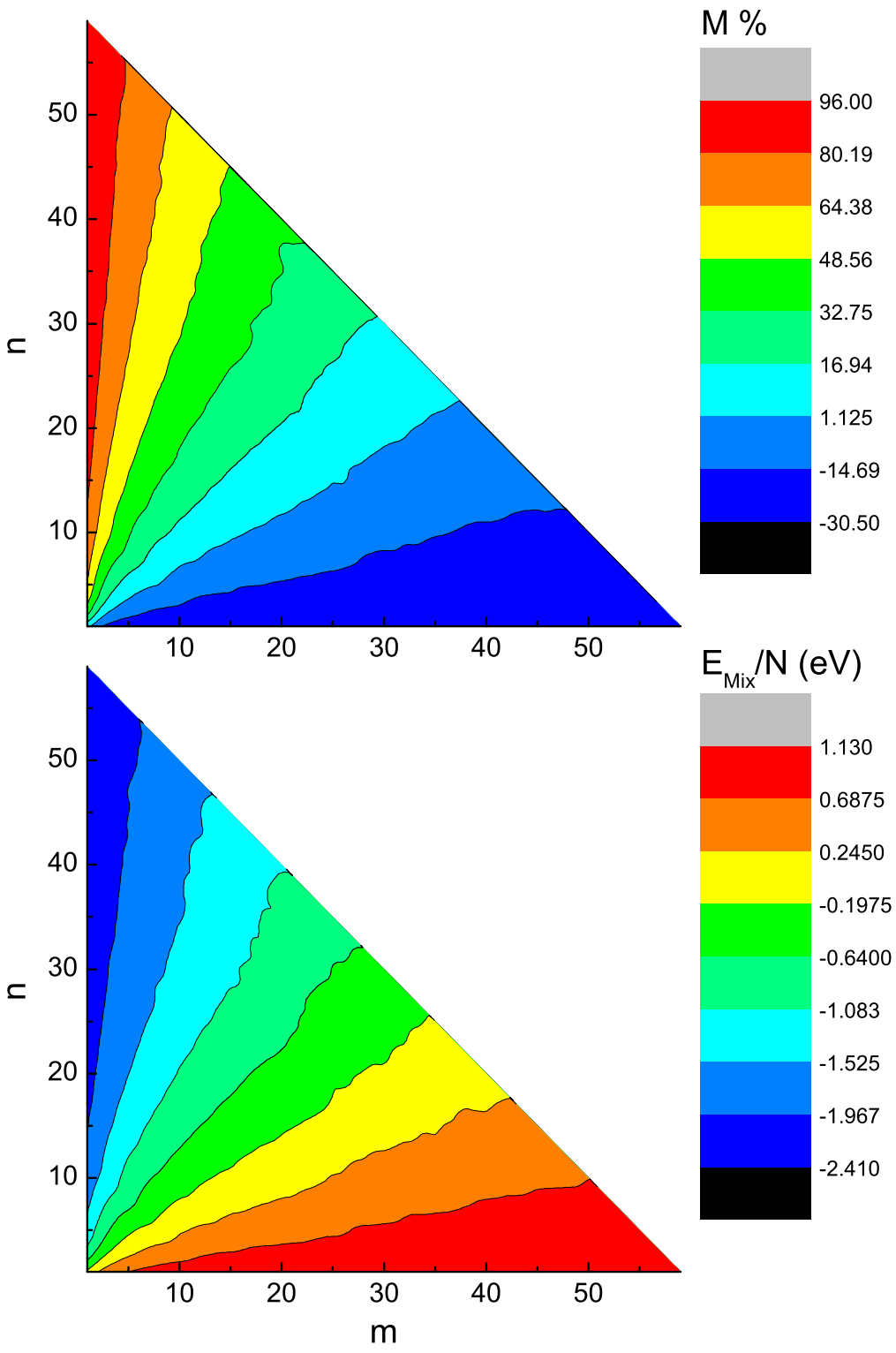

Figure 6.14: The mixing coefficient (upper panel) and mixing energy (lower panel) for Ni–Ag clusters vs number of Ni (m) and Ag (n) atoms for N = m+n from 2 to 60.

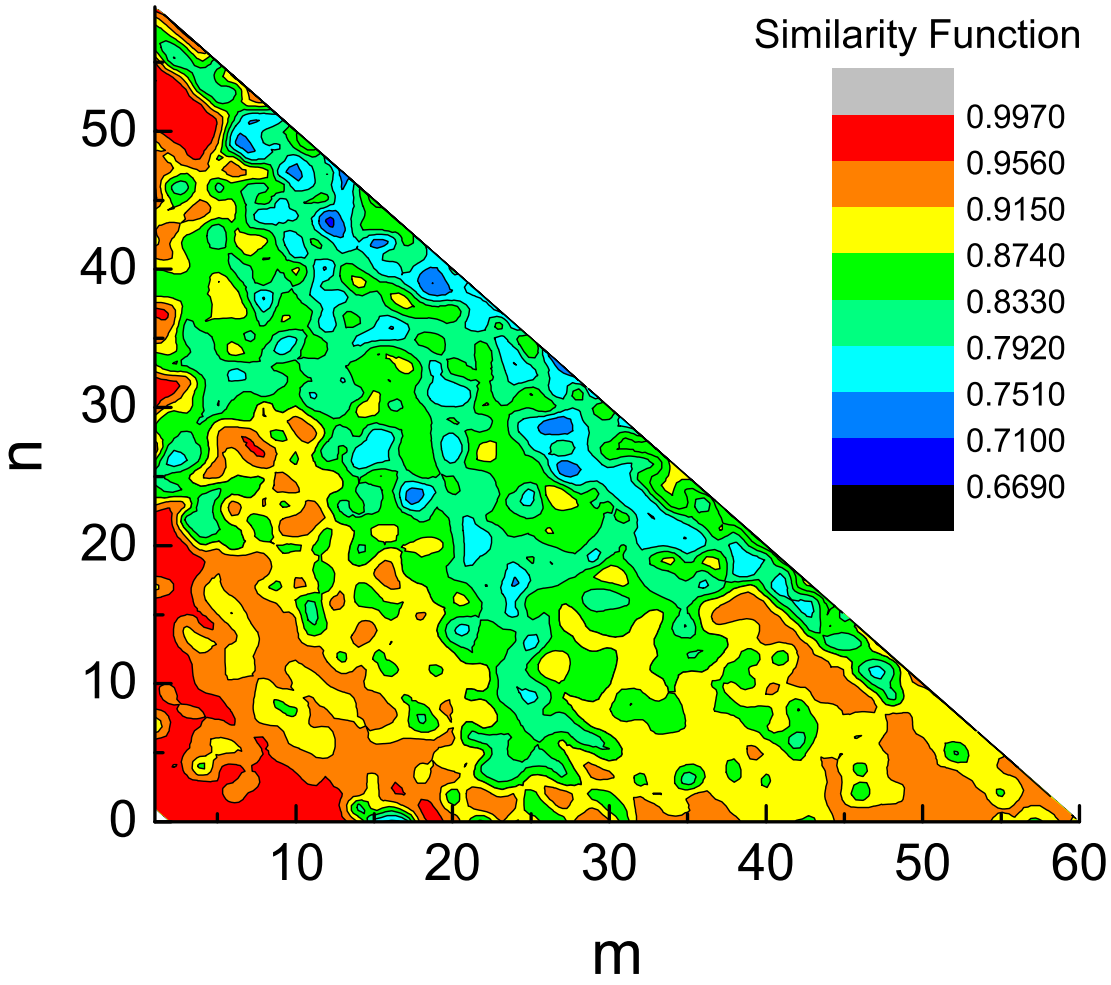

Figure 6.15: Similarity function between the Ni_mAg_n and Cu_mAg_n clusters as a function of (m, n) for N = m+n from 2 to 60. Clusters with the same values of (m, n) are compared to each other.

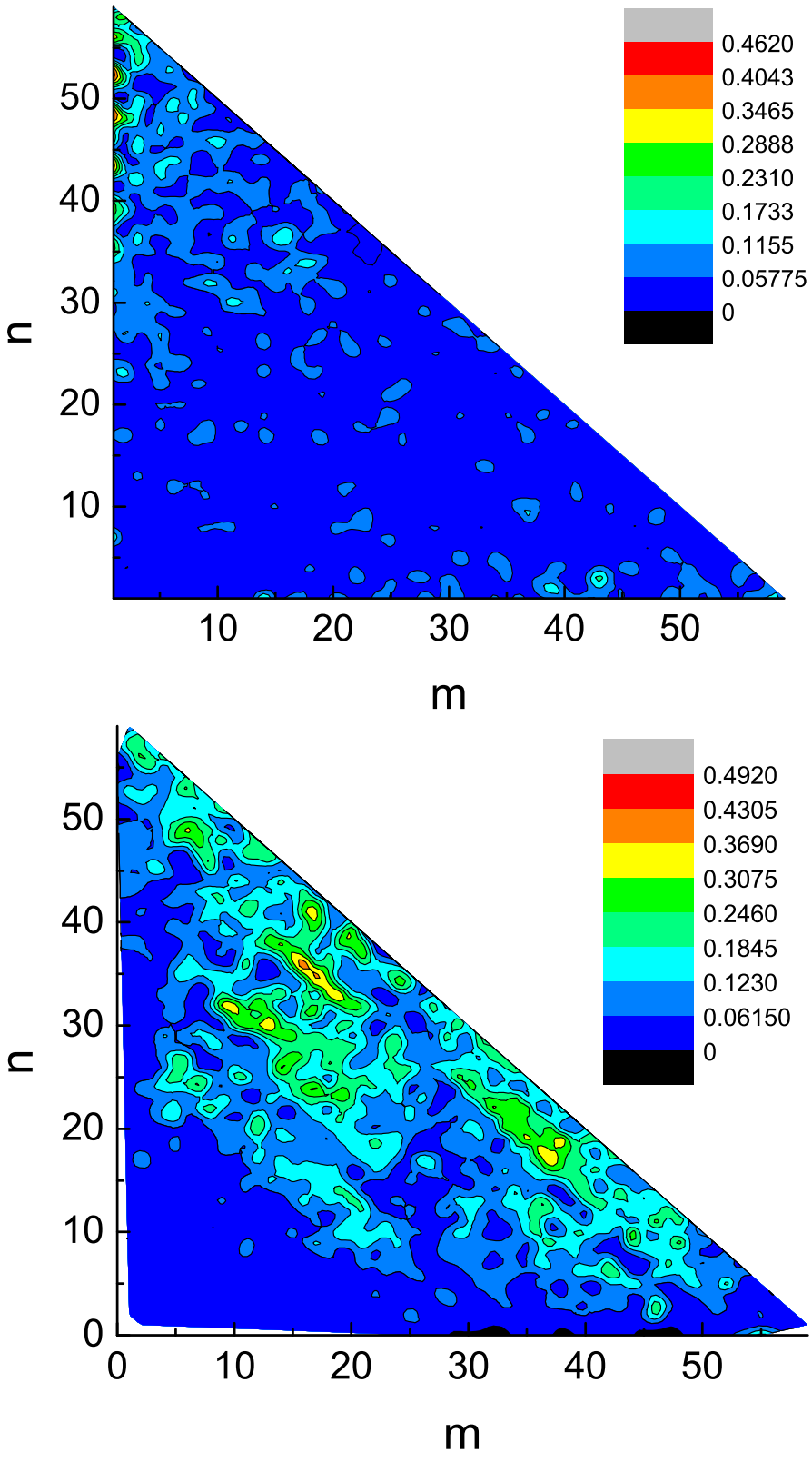

Figure 6.16: The comparison quantity, D(m, n), for (upper panel) the ratio of the average radial distances (Eq. 5.3), and (lower panel) the excess energy per atom (Eq. 3.11) of Cu_mAg_n and Ni_mAg_n clusters with N = m+n ranging from 2 to 60.

quantity

$$\mathrm{D(m,n)} = \log\left(1 + \left|\frac{\mathrm{Z_{NiAg}(m,n)}}{\langle \mathrm{Z_{NiAg}} \rangle} - \frac{\mathrm{Z_{CuAg}(m,n)}}{\langle \mathrm{Z_{CuAg}} \rangle}\right|\right). \tag{6.1}$$

D(m, n) should become zero if the property Z of both clusters has similar dependence on the stoichiometries. But, when Z has a material-specific dependence on the (m, n), then the values of D should increase.

We determine D(m, n) for the ratio of the average radial distances of the Cu–Ag and Ni–Ag clusters (Eq. 5.3) to compare the structural properties, and for the excess energy per atom (Eq. 3.11) for an energetic properties comparison. The results are shown in Fig. 6.16. The close similarity of Cu–Ag and Ni–Ag clusters is obviously seen in the very low values of D(m, n) for the ratio of the average radial distances. This quantity is mostly between 0 and 0.057, but in very few cases, i.e., for some Ag-rich clusters, becomes less than 0.46. This suggests, however, that although the atomic properties of Cu and Ag (such as atomic radii, surface energies, and cohesive energies) are closer to each other than those of Ni and Ag, they can barely be identified in the structural properties of nanoalloys made of these atoms.

In the lower panel of Fig. 6.16, the energetic properties of the Cu–Ag and Ni–Ag clusters prove to be less similar, as the values of D(m, n) increase for the excess energies of these two systems. This is also in accord with distinct mixing energies and coefficients of these clusters.

Chapter 7

Conclusions and Outlook

The aim of this work was to investigate the energetic and structural properties of Ag, and Ag-based alloyed clusters. The selected nanoalloys were Cu-Ag and Ni-Ag. To this end, we first determined all the global minimum structures of Ag clusters with N = 2 to 100 atoms. For the Cu_mAg_n and Ni_mAg_n nanoalloys we did the same for every possible combination of m and n with N = m+n from 2 to 60. To make this exhaustive research more feasible, we used the EAM potential to calculate all atom-atom interactions, and combined it with the basin-hopping (BH) algorithm for global optimization. As the output, we obtained long listings of total energies and structures as functions of clusters' stoichiometries. Then we used different theoretical tools to obtain an insight in to the properties of these clusters.

For Ag clusters, our results for the GM structures included icosahedra, decahedra, and *fcc* truncated octahedra which are in agreement with other experimental and theoretical studies [5, 60, 107, 120]. These structures suggested the icosahedral growth for the Ag clusters but with islands of decahedra and *fcc* truncated octahedra. Moreover, the sequence of the stable clusters and the way that new atoms were added to the clusters showed that there is a competition between the MIC/Polyicosahedral and TIC growth pattern for different ranges of sizes. We compared the GM of Ag_N clusters with those of Ni_N and Cu_N by using the similarity function, and found that structures of Ag clusters more resemble those of Cu than Ni clusters.

The structural comparison of the GM of Ag clusters, determined by different model potentials, emphasized the effects of the type of potentials used in calculations. We have also investigated the stability of Ag clusters by using the well known stability function and the isomers energy differences. The magic sizes that

we found also include those with symmetric geometries such as 13- and 19-atom icosahedron, *fcc* truncated octahedron with 38 atoms, 55-atom Mackay icosahedron, and Decahedron with 75 atoms.

Our results for the global minimum of both Cu–Ag and Ni–Ag clusters are in agreement with the very few available studies. The corresponding global minima have different structures such as icosahedra, polyicosahedra, 5-fold and 6-fold pancakes, and even *fcc* truncated octahedra, which were identified for some few clusters of size N = 38. We employed various measures to determine the ordering of atoms in Ag-based nanoalloys. The results revealed that in both cases the Ag atoms form the shell of the structures and cover the Cu or Ni cores. This tendency even proved to prevent the formation of symmetric geometries in favor of core–shell structures. The segregation of Ag atoms to the surfaces of the structures was suggested by the ratio of the average radial distances and the bond order parameter. As we have performed the first systematic studies for the Cu–Ag and Ni–Ag clusters over a wide range of sizes and compositions, we were able to identify their growth pattern. Our results proposed that the growth for both types of bimetallic clusters is based on TIC/Polyicosahedral, where new atoms are added to the T sites over the last shell of atoms and the structures are mainly different types of polyicosahedra [129].

The determination of the most stable structures of nanoalloys proved to be a non-trivial task, as there are different definitions for the stability functions. Even in these cases, we could find some clusters in which a cluster was determined of enhanced stabilities by different definitions. For example, in agreement with other studies, we found Cu_7Ag_{27} and Ni_7Ag_{27} to be the most stable clusters with 34 atoms [39, 72, 73, 133, 134]. Additionally, we calculated the excess energies and the energy differences between the first and second isomers of both Cu–Ag and Ni–Ag nanoalloys and determined the stable clusters according to these two measures. An overview of the results of all the stability criteria suggested that for the both types of nanoalloys the Ag-rich clusters are more stable in many cases.

We also compared the structural and energetical properties of Cu–Ag and Ni–Ag nanoalloys. The results showed that although the properties of Ag atoms are closer to those of Cu than Ni atoms, the structures of the Cu–Ag and Ni–Ag nanoalloys of the same sizes and compositions are quite similar. On the other hand, the differences are noticed when we compare the energetical properties of these nanoalloys. For instance, we found that the excess energies and especially mixing energies of these

two nanoalloys are very different.

As a further step, we should employ other precise methods like density functional theory to explore our large database of nanoclusters for more physical and chemical properties. This is along the lines of the two step method proposed by Ferrando et al. [73]. In these further studies one should first reoptimize the structures and then try to determine the corresponding physical properties like optical or magnetic, or the heat capacity.

Bibliography

[1] R. Ferrando, J. Jellinek, and R. L. Johnstom, *Chem. Rev.* **108**, 845 (2008).

[2] G. Barcaro, A. Fortunelli, G. Rossi, F. Nita, and R. Ferrando, *J. Phys. Chem. B* **110**, 23197 (2006).

[3] V. G. Grigoryan, D. Alamanova, and M. Springborg, *Phys. Rev. B* **73**, 115415 (2006).

[4] V. G. Grigoryan and M. Springborg, *Phys. Rev. B* **70**, 205415 (2004).

[5] D. Alamanova, V. G. Grigoryan, and M. Springborg, *J. Phys. Chem. C* **111**, 12577 (2007).

[6] J. A. Alonso, *Structure and Properties of Atomic Nanoclusters*, Imperial College Press: London, 2005.

[7] F. Baletto and R. Ferrando, *Rev. Mod. Phys.* **77**, 371 (2005).

[8] V. Vijayakrishnan, A. Chainani, D. Sarma, and C. N. R. Rao, *J. Phys. Chem.* **96**, 8679 (1992).

[9] R. L. Johnstom, *Atomic and Molecular Clusters*, Taylor and Francis: London, 2002.

[10] W. Krätschmer, L. D. Lamb, K. Fostiropoulos, and D. R. Huffman, *Nature* **347**, 354 (1990).

[11] R. L. Johnston, *Philos. Trans. of the R. Soc. London A* **356**, 211 (1998).

[12] E. Roduner, *Nanoscopic Materials:Size-Dependent Phenomena*, The Royal Society of Chemistry, 2006.

[13] F. H. Stillinger and T. A. Weber, *Phys. Rev. A* **25**, 978 (1982).

[14] C. J. Tsai and K. D. Jordan, *J. Chem. Phys.* **99**, 6957 (1993).

[15] F. H. Stillinger, *Phys. Rev. E* **59**, 48 (1999).

[16] J. P. K. Doye and D. J. Wales, *J. Chem. Phys.* **116**, 3777 (2002).

[17] J. P. K. Doye, M. A. Miller, and D. J. Wales, *J. Chem. Phys.* **111**, 8417 (1999).

[18] M. R. Hoare and J. McInnes, *Faraday Discuss. Chem. Soc.* **61**, 12 (1976).

[19] J. P. K. Doye and D. J. Wales, *J. Chem. Phys.* **102**, 9659 (1995).

[20] A. L. Mackay, *Acta Crystallographica* **15**, 916 (1962).

[21] T. P. Martin, *Phys. Rep.* **273**, 199 (1996).

[22] J. Farges, M. F. de Feraudy, B. Raoult, and G. Torchet, *J. Chem. Phys.* **84**, 3491 (1986).

[23] D. Reinhard, B. D. Hall, P. Berthoud, S. Valkealahti, and R. Monot, *Phys. Rev. Lett.* **79**, 1459 (1997).

[24] D. Reinhard, B. D. Hall, P. Berthoud, S. Valkealahti, and R. Monot, *Phys. Rev. B* **58**, 4917 (1998).

[25] T. P. Martin, T. Bergmann, H. Göhlich, and T. Lange, *Zeitschrift für Physik D Atoms, Molecules and Clusters* **19**, 25 (1991).

[26] T. P. Martin, *Solid State Ionics* **131**, 3 (2000).

[27] J. Zhao, Y. Luo, and G. Wang, *Eur. Phys. J. D* **14**, 309 (2001).

[28] J. Jellinek, *Theory of Atomic and Molecular Clusters, With a Glimpse at Experiments*, Springer-Verlag Berlin Heidelberg, 1999.

[29] P. Jain, I. H. ElSayed, and M. A. El-Sayed, *Nano Today* **2**, 18 (2007).

[30] M. P. Andrews and S. C. O'Brien, *The Journal of Physical Chemistry* **96**, 8233 (1992).

[31] S. Sao-Joao, S. Giorgio, J. M. Penisson, C. Chapon, S. Bourgeois, and C. Henry, *The Journal of Physical Chemistry B* **109**, 342 (2005).

[32] U. A. Paulus, A. Wokaun, G. G. Scherer, T. J. Schmidt, V. Stamenkovic, V. Radmilovic, N. M. Markovic, and R. N. Ross, *The Journal of Physical Chemistry B* **106**, 4181 (2002).

[33] G. Schmid, A. Lehnert, J. O. Malm, and J. O. Bovin, *Angew. Chem., Int. Ed. Engl.* **30**, 874 (1991).

[34] J. H. Hodak, A. Henglein, M. Giersig, and G. V. Hartland, *J. Phys. Chem. B* **104**, 11708 (2000).

[35] J. P. Wilcoxon and P. P. Provencio, *J. Am. Chem. Soc.* **126**, 6402 (2004).

[36] K. Sumiyama, K. Suzuki, S. A. Makhlouf, K. Wakoh, T. Kamiyama, S. Yamamuro, T. J. Konno, Y. F. Xu, M. Sakurai, and T. Hihara, *J. Non-Cryst. Solids* **192**, 539 (1995).

[37] N. L. Rosi and C. A. Mirkin, *Chem. Rev.* **105**, 1547 (2005).

[38] J. Jellinek and E. B. Krissinel, *Chem. Phys. Lett.* **258**, 283 (1996).

[39] G. Rossi, A. Rapallo, C. Mottet, A. Fortunelli, F. Baletto, and R. Ferrando, *Phys. Rev. Lett.* **93**, 105503 (2004).

[40] M. S. Nashner, A. I. Frenkel, D. Somerville, C. W. Hills, J. R. Shapley, and R. G. Nuzzo, *J. Am. Chem. Soc.* **120**, 8093 (1998).

[41] Y. Yang, J. Shi, G. Kawamura, and M. Nogami, *Scripta Materialia* **58**, 862 (2008).

[42] M. M. noz Navia, J. Dorantes-Dávila, D. Zitoun, C. Amiens, N. Jaouen, A. Rogalev, M. Respaud, and G. M. Pastor, *Appl. Phys. Lett.* **95**, 233107 (2009).

[43] J. Jellinek, *Faraday Discuss.* **138**, 11 (2008).

[44] M. C. Fromen, J. Morillo, M. J. Casanove, and P. Lecante, *Europhys. Lett.* **73**, 885 (2006).

[45] D. Cheng, W. Wang, and S. Huang, *J. Phys. Chem. B* **110**, 16193 (2006).

[46] D. Ferrer, A. Torres-Castro, X. Gao, S. Sepúlveda-Guzmán, U. Ortiz-Méndez, and M. José-Yacamán, *Nano Letters* **7**, 1701 (2007).

[47] T. H. Lee and R. M. Dickson, *Proceedings of the National Academy of Sciences* **100**, 3043 (2003).

[48] T. H. Lee, J. I. Gonzalez, J. Zheng, and R. M. Dickson, *Accounts of Chemical Research* **38**, 534 (2005).

[49] H. C. Yeh, J. Sharma, J. J. Han, J. S. Martinez, and J. H. Werner, *Nano Letters* **10**, 3106 (2010).

[50] K. Shimizu, Y. Miyamoto, and A. Satsuma, *Journal of Catalysis* **270**, 86 (2010).

[51] G. Ganteför, M. Gausa, K. H. Meiwes-Broer, and H. O. Lutz, *J. Chem. Soc., Faraday Trans.* **86**, 2483 (1990).

[52] I. Katakuse, T. Ichihara, Y. Fujita, T. Matsuo, T. Sakurai, and H. Matsuda, *Int. J Mass Spectrom. Ion Processes* **67**, 229 (1985).

[53] I. Katakuse, T. Ichihara, Y. Fujita, T. Matsuo, and T. S. H. Matsuda, *Int. J. Mass Spectrom. Ion Processes* **74**, 33 (1986).

[54] C. L. Pettiette, S. H. Yang, M. J. Craycraft, J. Conceicao, R. T. Laaksonen, O. Cheshnovsky, and R. E. Smalley, *J. Chem. Phys.* **88**, 5377 (1988).

[55] O. Cheshnovsky, K. J. Taylor, J. Conceicao, and R. E. Smalley, *Phys. Rev. Lett.* **64**, 1785 (1990).

[56] C. Massobrio, A. Pasquarello, and R. Car, *Chem. Phys. Lett.* **238**, 215 (1995).

[57] T. L. Haslett, K. A. Bosnick, and M. Moskovits, *J. Chem. Phys.* **108**, 3453 (1998).

[58] J. A. Howard, R. Sutcliffe, and B. Mile, *Surface Science* **156**, 214 (1985).

[59] X. Xing, R. M. Danell, I. L. Garzón, K. Michaelian, M. N. Blom, M. M. Burns, and J. H. Parks, *Phys. Rev. B* **72**, 081405 (2005).

[60] M. N. Blom, D. Schooss, J. Stairs, and M. M. Kappes, *J. Chem. Phys.* **124**, 244308 (2006).

[61] H. Handschuh, C.-Y. Cha, P. S. Bechthold, G. Ganteför, and W. Eberhardt, *J. Chem. Phys.* **102**, 6406 (1995).

[62] M. N. Huda and A. K. Ray, *Phys. Rev. A* **67**, 013201 (2003).

[63] M. Huda and A. Ray, *Eur. Phys. J. D* **22**, 217 (2003).

[64] V. Bonačić-Koutecký, L. Češpiva, P. Fantucci, and J. Koutecký, *J. Chem. Phys.* **98**, 7981 (1993).

[65] V. Bonačić-Koutecký, J. Pittner, M. Boiron, and P. Fantucci, *J. Chem. Phys.* **110**, 3876 (1999).

[66] V. Bonačić-Koutecky, V. Veyret, and R. Mitrić, *J. Chem. Phys.* **115**, 10450 (2001).

[67] J. Belloni, M. Mostafavi, H. Remita, J. L. Marignier, and M. O. Delcourt, *New. J. Chem.* **22**, 1239 (1998).

[68] A. Henglein and R. Tausch-Treml, *J. Colloid Interface Sci.* **80**, 84 (1981).

[69] C. Langlois, D. Alloyeau, Y. L. Bouar, A. Loiseau, T. Oikawa, C. Mottet, and C. Ricolleau, *Faraday Discuss.* **138**, 375 (2008).

[70] M. Cazayous, C. Langlois, T. Oikawa, C. Ricolleau, and A. Sacuto, *Phys. Rev. B* **73**, 113402 (2006).

[71] E. Janssens, S. Neukermans, X. Wang, N. Veldeman, R. E. Silverans, and P. Lievens, *Eur. Phys. J. D* **34**, 23 (2005).

[72] R. Ferrando, A. Fortunelli, and G. Rossi, *Phys. Rev. B* **72**, 085449 (2005).

[73] R. Ferrando, A. Fortunelli, and R. L. Johnston, *Phys. Chem. Chem. Phys.* **10**, 640 (2008).

[74] M. A. Ortigoza and T. S. Rahman, *Phys. Rev. B* **77**, 195404 (2008).

[75] Z. Y. Jiang, K. H. Lee, S. T. Li, and S. Y. Chu, *Phys. Rev. B* **73**, 235423 (2006).

[76] D. Bochicchio and R. Ferrando, *Nano Lett.* **10**, 4211 (2010).

[77] M. Gaudry, J. Lermé, E. Cottancin, M. Pellarin, B. Prével, M. Treilleux, P. Mélinon, J. L. Rousset, and M. Broyer, *Eur. Phys. J. D* **16**, 201 (2001).

[78] H. Portales, L. Saviot, E. Duval, M. Gaudry, E. Cottancin, M. Pellarin, J. Lermé, and M. Broyer, *Phys. Rev. B* **65**, 165422 (2002).

[79] M. Gaudry, E. Cottancin, M. Pellarin, J. Lermé, L. Arnaud, J. R. Huntzinger, J. L. Vialle, M. Broyer, J. L. Rousset, M. Treilleux, and P. Mélinon, *Phys. Rev. B* **67**, 155409 (2003).

[80] M. Harb, F. Rabilloud, and D. Simon, *J. Chem. Phys.* **131**, 174302 (2009).

[81] C. C. Lee and D. H. Chen, *Nanotechnology* **17**, 3094 (2006).

[82] T. B. Massalski, J. L. Murray, L. H. Bernett, and H. Baker, *Binary Alloy Phase Diagrams*, American Society for Metals; Metals Park: OH, 1986.

[83] F. Calvo, E. Cottancin, and M. Broyer, *Phys. Rev. B* **77**, 121406 (2008).

[84] O. Proux, R. J. Regnard, I. Manzini, C. Revenant, B. Rodmacq, and J. Mimault, *Eur. Phys. J. AP* **9**, 115 (2000).

[85] M. Harb, F. Rabilloud, and D. Simon, *J. Phys. Chem. A* **111**, 7726 (2007).

[86] F. Baletto, C. Mottet, A. Rapallo, G. Rossi, and R. Ferrando, *Surface Science* **566**, 192 (2004).

[87] R. P. Gupta, *Phys. Rev. B* **23**, 6265 (1981).

[88] V. Rosato, M. Guillope, and B. Legrand, *Philos. Mag. A* **59**, 321 (1989).

[89] F. Ercolessi, M. Parrinello, and E. Tosatti, *Philos. Mag. A* **58**, 213 (1988).

[90] A. P. Sutton and J. Chen, *Philos. Mag. Lett.* **61**, 139 (1990).

[91] K. W. Jacobsen, J. K. Norskov, and M. J. Puska, *Phys. Rev. B* **35**, 7423 (1987).

[92] M. S. Daw and M. I. Baskes, *Phys. Rev. Lett.* **50**, 1285 (1983).

[93] M. S. Daw and M. I. Baskes, *Phys. Rev. B* **29**, 6443 (1984).

[94] M. J. Stott and E. Zaremba, *Phys. Rev. B* **22**, 1564 (1980).

[95] S. M. Foiles, M. I. Baskes, and M. S. Daw, *Phys. Rev. B* **33**, 7983 (1986).

[96] M. S. Daw, S. Foiles, and M. I. Baskes, *Mat. Sci. Rep.* **9**, 251 (1993).

[97] T. V. Hoof and M. Hou, *Phys. Rev. B* **72**, 115434 (2005).

[98] B. Medasani, Y. H. Park, and I. Vasiliev, *Phys. Rev. B* **75**, 235436 (2007).

[99] D. N. Tafen and L. J. Lewis, *Phys. Rev. B* **77**, 075429 (2008).

[100] E. Hristova, Y. Dong, V. G. Grigoryan, and M. Springborg, *J. Phys. Chem. A* **112**, 7905 (2008).

[101] Z. Li and H. A. Scheraga, *Proceedings of the National Academy of Sciences* **84**, 6611 (1987).

[102] C. Baysal and H. Meirovitch, *J. Chem. Phys.* **105**, 7868 (1996).

[103] D. J. Wales and H. A. Scheraga, *Science* **285**, 1368 (1999).

[104] J. P. K. Doye and D. J. Wales, *J. Chem. Phys.* **105**, 8428 (1996).

[105] D. J. Wales and J. P. K. Doye, *J. Phys Chem. A* **101**, 5111 (1997).

[106] D. J. Wales, *Energy Landscapes:Applications to Clusters, Biomolecules and Glasses*, Cambridge University Press, 2004.

[107] J. P. K. Doye and D. J. Wales, *New J. Chem.* **22**, 733 (1998).

[108] J. P. K. Doye and L. Meyer, *Phys. Rev. Lett.* **95**, 063401 (2005).

[109] E. Hristova, V. G. Grigoryan, and M. Springborg, *J. Chem. Phys.* **128**, 244513 (2008).

[110] L. J. Munro, A. Tharrington, and K. D. Jordan, *Comput. Phys. Comm.* **145**, 1 (2002).

[111] F. Calvo and E. Yurtsever, *Phys. Rev. B* **70**, 045423 (2004).

[112] K. Clemenger, *Phys. Rev. B* **32**, 1359 (1985).

[113] I. A. Solovýov, A. V. Solovýov, and W. Greiner, *Phys. Rev. Lett.* **90**, 053401 (2003).

[114] W. de Heer, W. Knight, M. Chou, and M. Cohen, *Solid State Physics: Advances in Research and Applications* **40**, 93 (1987).

[115] G. Rossi, R. Ferrando, A. Rapallo, A. Fortunelli, B. C. Curley, L. D. Lloyd, and R. L. Johnston, *J. Chem. Phys.* **122**, 194309 (2005).

[116] F. Pittaway, L. O. Paz-Borbon, R. L. Johnston, H. Arslan, C. Mottet, G. Barcaro, and A. Fortunelli, *J. Phys. Chem. C* **113**, 9141 (2009).

[117] J. C. Idrobo, S. Öğüt, and J. Jellinek, *Phys. Rev. B* **72**, 085445 (2005).

[118] M. Yang, K. A. Jackson, and J. Jellinek, *J. Chem. Phys.* **125**, 144308 (2006).

[119] H. M. Lee, M. Ge, B. R. Sahu, P. Tarakeshwar, and K. S. Kim, *J. Phys. Chem. B* **107**, 9994 (2003).

[120] K. Michaelian, N. Rendón, and I. L. Garzón, *Phys. Rev. B* **60**, 2000 (1999).

[121] X. Shao, X. Liu, and W. Cai, *J. Chem. Theo. and Comput.* **1**, 762 (2005).

[122] F. Baletto, C. Mottet, and R. Ferrando, *Phys. Rev. Lett.* **84**, 5544 (2000).

[123] V. Beutel, H.-G. Kramer, G. L. Bhale, M. Kuhn, K. Weyers, and W. Demtroder, *J. Chem. Phys.* **98**, 2699 (1993).

[124] B. Simard, P. A. Hackett, A. M. James, and P. R. R. Langridge-Smith, *Chem. Phys. Lett.* **186**, 415 (1991).

[125] H. Häkkinen, M. Moseler, O. Kostko, N. Morgner, M. A. Hoffmann, and B. v. Issendorff, *Phys. Rev. Lett.* **93**, 093401 (2004).

[126] J. P. K. Doye, D. J. Wales, and R. S. Berry, *J. Chem. Phys.* **103**, 4234 (1995).

[127] V. G. Grigoryan, D. Alamanova, and M. Springborg, *Eur. Phys. J. D* **34**, 187 (2005).

[128] J. M. Montejano-Carrizales, M. P. I. niguez, J. A. Alonso, and M. J. López, *Phys. Rev. B* **54**, 5961 (1996).

[129] J. A. Alonso, *Chem. Rev.* **100**, 637 (2000).

[130] I. A. Harris, R. S. Kidwell, and J. A. Northby, *Phys. Rev. Lett.* **53**, 2390 (1984).

[131] M. W. Sung, R. Kawai, and J. H. Weare, *Phys. Rev. Lett.* **73**, 3552 (1994).

[132] T. Martin, T. Bergmann, H. Göhlich, and T. Lange, *Chem. Phys. Lett.* **176**, 343 (1991).

[133] A. Rapallo, G. Rossi, R. Ferrando, A. Fortunelli, B. C. Curley, L. D. Lloyd, G. M. Tarbuck, and R. L. Johnston, *J. Chem. Phys.* **122**, 194308 (2005).

[134] S. Nuñez and R. L. Johnston, *J. Phys. Chem. C* **114**, 13255 (2010).

[135] L. O. Paz-Borbón, T. V. Mortimer-Jones, R. L. Johnston, A. Posada-Amarillas, G. Barcaro, and A. Fortunelli, *Phys. Chem. Chem. Phys.* **9**, 5202 (2007).

[136] A. Logsdail, L. O. Paz-Borbon, and R. L. Johnston, *J. Comput. Theor. Nanosci.* **6**, 857 (2009).

[137] F. Baletto, C. Mottet, and R. Ferrando, *Eur. Phys. J. D* **24**, 233 (2003).

[138] F. Baletto, C. Mottet, and R. Ferrando, *Phys. Rev. B* **66**, 155420 (2002).

[139] F. Baletto, C. Mottet, and R. Ferrando, *Phys. Rev. Lett.* **90**, 135504 (2003).

[140] F. Lequien, J. Creuze, F. Berthier, and B. Legrand, *J. Chem. Phys.* **125**, 094707 (2006).

[141] V. Moreno, J. Creuze, F. Berthier, C. Mottet, G. Tréglia, and B. Legrand, *Surface Science* **600**, 5011 (2006).

[142] F. Lequien, J. Creuze, F. Berthier, I. Braems, and B. Legrand, *Phys. Rev. B* **78**, 075414 (2008).

[143] M. Molayem, V. G. Grigoryan, and M. Springborg, *J. Phys. Chem. C* **115**, 7179 (2010).